



OPTIMISATION OF IONOSPHERIC SCINTILLATION MODEL USED IN RADIO OCCULTATION

Marta Boryczko
Tomasz Dziendziel

This thesis is presented as part of Degree of
Master of Science in Electrical Engineering

Blekinge Institute of Technology
March 2016

Blekinge Institute of Technology
Department of Applied Signal Processing
Supervisor: Prof. Mats Pettersson
Examiner: Dr. Sven Johansson

Abstract

This thesis is executed in cooperation with RUAG Space AB, which specializes in highly reliable on-board satellite equipment. The thesis focuses on the effect, which disturbs the amplitude and phase of a Global Positioning System (GPS) signal, called scintillation effect. It has a substantial impact on a GPS signal, during Radio Occultation (RO). RO is a method of analysis of a refracted signal which passes through the atmosphere. RO can be used for measuring climate change and for weather forecasting. By retrieving the bending angle of a GPS signal, three basic parameters of the Earth's atmosphere can be obtained at different heights: temperature, pressure and humidity. As the scintillation effect causes prominent errors in the bending angle calculations, it is crucial to provide possibly the most precise mathematical model, which allows to conceive proper ionospheric corrections. In this thesis, the model using Rytov approach is implemented and optimised with different optimisation functions. It is shown that the scintillation model can be optimized, which may contribute to a more accurate retrieval of the atmospheric profiles.

Keywords: Global Positioning System, ionospheric scintillation, optimization, Radio Occultation

Acknowledgments

We would like to express our gratitude to our supervisor prof. Mats Pettersson for guidance and engagement during the working process on the thesis project. We are very thankful for all the suggestions and valuable support, which allowed to accomplished the thesis.

Furthermore we would like to thank Anders Carlström from RUAG Space AB for thorough comments and remarks, which were essential to understand the subject matter. We are very grateful for the time, dedicated to our thesis.

Table of contents

Abstract	I
Acknowledgments	III
Table of contents	V
List of figures	VII
List of tables	IX
List of abbreviations	XI
1. Introduction.....	1
1.1 RUAG Space	2
1.2 Problem statement.....	2
1.3 Scope of the thesis	3
1.4 Division of work	3
1.5 Outline of the thesis	4
2. Background and related works.....	5
2.1 Background.....	5
2.2 Related Works	7
3. Ionospheric scintillation in Radio Occultation.....	9
3.1 Input data description	9
3.1.1 Transforming data for analysis	9
3.2 Scintillation detection.....	10
3.3 Scintillation modelling.....	11
3.3.1 Amplitude modelling	11
3.3.2 Phase Modelling	14
3.4 Model implementation	15
3.5 Model verification	17
4. Optimization of the scintillation model.....	26
4.1 Optimization functions overview	26
4.2 Obtained results	27
4.3 Comparative analysis of the results	39
4.4 Optimization based on further GRAS data	41
4.4.1 Distinction of the final parameters	52
5. Conclusions.....	61
6. Future work	62
Reference list.....	63

List of figures

Figure 1.1. Example of the scintillation effect on a signal.....	2
Figure 2.1. GPS Radio Occultation concept.....	6
Figure 2.2. Radio Occultation atmospheric profiles retrieval	6
Figure 3.1. L1 frequency scintillation events of the signal amplitude.....	12
Figure 3.2. L1 frequency scintillation events of the signals phase	14
Figure 3.3. Log-amplitude PSD of the scintillation models	16
Figure 3.4. Phase PSD of the scintillation models	17
Figure 3.5. Amplitude first scintillation event [1-150] and model cases comparison.....	18
Figure 3.6. Amplitude second scintillation event [650-900] and model cases comparison.....	19
Figure 3.7. Amplitude third scintillation event [1300-1500] and model cases comparison	20
Figure 3.8. Phase first scintillation event [1-150] and model cases comparison	21
Figure 3.9. Phase second scintillation event [650-900] and model cases comparison.....	22
Figure 3.10. Phase third scintillation event [1300-1500] and model cases comparison	23
Figure 4.1. Optimization of the amplitude model for the first scintillation using lsqcrvefit.....	28
Figure 4.2. Optimization of the phase model for the first scintillation using lsqcrvefit.....	29
Figure 4.3. Optimization of the amplitude model for the second scintillation using lsqcrvefit	30
Figure 4.4. Optimization of the phase model for the second scintillation using lsqcrvefit	31
Figure 4.5. Optimization of the amplitude model for the third scintillation using lsqcrvefit	32
Figure 4.6. Optimization of the amplitude model for the second scintillation using fminsearch	33
Figure 4.7. Optimization of the amplitude model for the third scintillation using fminsearch	34
Figure 4.8. Optimization of the phase model for the third scintillation using fminsearch	35
Figure 4.9. Optimization of the phase model for the first scintillation using fminunc	36
Figure 4.10. Optimization of the amplitude model for the third scintillation using fminunc.....	37
Figure 4.11. Optimization of the phase model for the third scintillation using fminunc.....	38
Figure 4.12. Optimization of the amplitude model from 2014/03/17 at 00:06 UTC	44
Figure 4.13. Optimization of the phase model from 2014/03/15 at 04:15 UTC	45
Figure 4.14. Optimization of the phase model from 2014/03/16 at 20:42 UTC.....	46
Figure 4.15. Optimization of the amplitude model from 2014/03/19 at 06:15 UTC	47
Figure 4.16. Optimization of the phase model from 2014/03/19 at 21:21 UTC.....	48
Figure 4.17. Optimization of the amplitude model from 2014/03/21 at 03:51 UTC	49
Figure 4.18. Optimization of the phase model from 2014/03/21 at 03:51 UTC.....	50
Figure 4.19. Optimization of the amplitude model from 2014/03/21 at 22:21 UTC	51
Figure 4.20. Optimization of the phase model from 2014/03/24 at 11:15 UTC.....	52
Figure 4.21. $T\chi$ parameter histogram and normal density function for amplitude.....	53
Figure 4.22. $f_0\chi$ parameter histogram and normal density function for amplitude.....	54
Figure 4.23. $p\chi$ parameter histogram and normal density function for amplitude.....	55
Figure 4.24. $T\phi$ parameter histogram and normal density function for phase.....	56
Figure 4.25. $f_0\phi$ parameter histogram and normal density function for phase.....	57
Figure 4.26. $p\phi$ parameter histogram and normal density function for phase.....	58

List of tables

Table 3.1. Sets of parameters for the model provided by RUAG [4].....	16
Table 3.2. MSE comparison of the amplitude models	24
Table 3.3. MSE comparison of the phase models	24
Table 4.1. Parameters for the amplitude model for the first scintillation using lsqcurvefit.....	27
Table 4.2. Parameters for the phase model for the first scintillation using lsqcurvefit.....	28
Table 4.3. Parameters for the amplitude model for the second scintillation using lsqcurvefit.....	29
Table 4.4. Parameters for the phase model for the second scintillation using lsqcurvefit.....	30
Table 4.5. Parameters for the amplitude model for the third scintillation using lsqcurvefit	31
Table 4.6. Parameters for the amplitude model for the second scintillation using fminsearch.....	33
Table 4.7. Parameters for the amplitude model for the third scintillation using fminsearch	34
Table 4.8. Parameters for the phase model for the third scintillation using fminsearch	35
Table 4.9. Parameters for the phase model for the first scintillation using fminunc	36
Table 4.10. Parameters for the amplitude model for the third scintillation using fminunc	37
Table 4.11. Parameters for the phase model for the third scintillation using fminunc	38
Table 4.12. MSE obtained after optimization for the first amplitude scintillation event.	39
Table 4.13. MSE obtained after optimization for the second amplitude scintillation event.	39
Table 4.14. MSE obtained after optimization the third amplitude scintillation event.	39
Table 4.15. MSE obtained after optimization for the first phase scintillation event.	40
Table 4.16. MSE obtained after optimization for the second phase scintillation event.	40
Table 4.17. MSE obtained after optimization for the third phase scintillation event.....	41
Table 4.18. Optimization results using lsqcurvefit for further amplitude scintillation events	42
Table 4.19. Optimization results using lsqcurvefit for further phase scintillation events	42
Table 4.20. Optimization results for the amplitude from 2014/03/17 at 00:06 UTC	43
Table 4.21. Optimization results for the phase from 2014/03/15 at 04:15 UTC	44
Table 4.22. Optimization results for the phase from 2014/03/16 at 20:42 UTC	45
Table 4.23. Optimization results for the amplitude from 2014/03/19 at 06:15 UTC	46
Table 4.24. Optimization results for the phase from 2014/03/19 at 21:21 UTC	47
Table 4.25. Optimization results for the amplitude from 2014/03/21 at 03:51 UTC	48
Table 4.26. Optimization results for the phase from 2014/03/21 at 03:51 UTC	49
Table 4.27. Optimization results for the amplitude from 2014/03/21 at 22:21 UTC	50
Table 4.28. Optimization results for the phase from 2014/03/24 at 11:15 UTC	51
Table 4.29. Verification process of the final results for the amplitude.....	59
Table 4.30. Verification process of the final results for the phase	60
Table 5.1. Resulting set of parameters for the amplitude	61
Table 5.2. Resulting set of parameters for the phase	61

List of abbreviations

C/A	Course/Acquisition
EUMETSAT	European Organization for the Exploitation of Meteorological Satellites
FFT	Fast Fourier Transform
GISM	Global Ionospheric Scintillation Model
GNSS	Global Navigation Satellites System
GPS	Global Positioning System
GRAS	GNSS Receiver for Atmospheric Sounding
LEO	Low Earth Orbit
MEO	Medium Earth Orbit
MetOp	Meteorological Operational
MSE	Mean Square Error
PEM	Parabolic Equation Method
PSD	Power Spectral Density
RO	Radio Occultation
WBMOD	Wide Band Model

1. Introduction

Nowadays climate on the Earth is rapidly changing, which results in an increased number of life threatening weather anomalies on the planet. Therefore weather forecasting based on accurate measurements is desirable. Especially now, when the climate changing becomes more and more visible and dangerous, due to extended human activity, there is a need to measure these changes and predict the weather with highly reliable methods. There are many procedures to acquire an accurate weather report. One of the relatively new approach to collect data is the Radio Occultation (RO) method. It consists of a common physics law regarding signal refractivity. Global Positioning System (GPS) satellite sends the signal to Low Earth Orbit (LEO) satellite. When it passes through the Earth's atmosphere the signal is refracted with a certain angle. LEO satellite retrieves the bended signal on two frequencies L1 and L2 while ascending or descending. By analyzing the refractivity of a signal it is possible to calculate temperature, humidity and pressure of a certain area of the globe. However when the signal travels through the atmosphere it might get disrupted. One of the signal distortions occurs in the ionosphere. The irregularities in the density of free moving electrons in the ionosphere can cause amplitude and phase variations of the signal, called scintillation effect. These fluctuations may lead to inaccurate measurements and navigation errors [1]. If the signal is free from any distortions, the characteristic itself would be flat around the amplitude value. In the Figure 1.1 example of an amplitude and phase scintillation can be seen, which cause rapid and random fluctuations in the signal. It is generated by using a simulator from [2] for the value of the amplitude equal to 4.

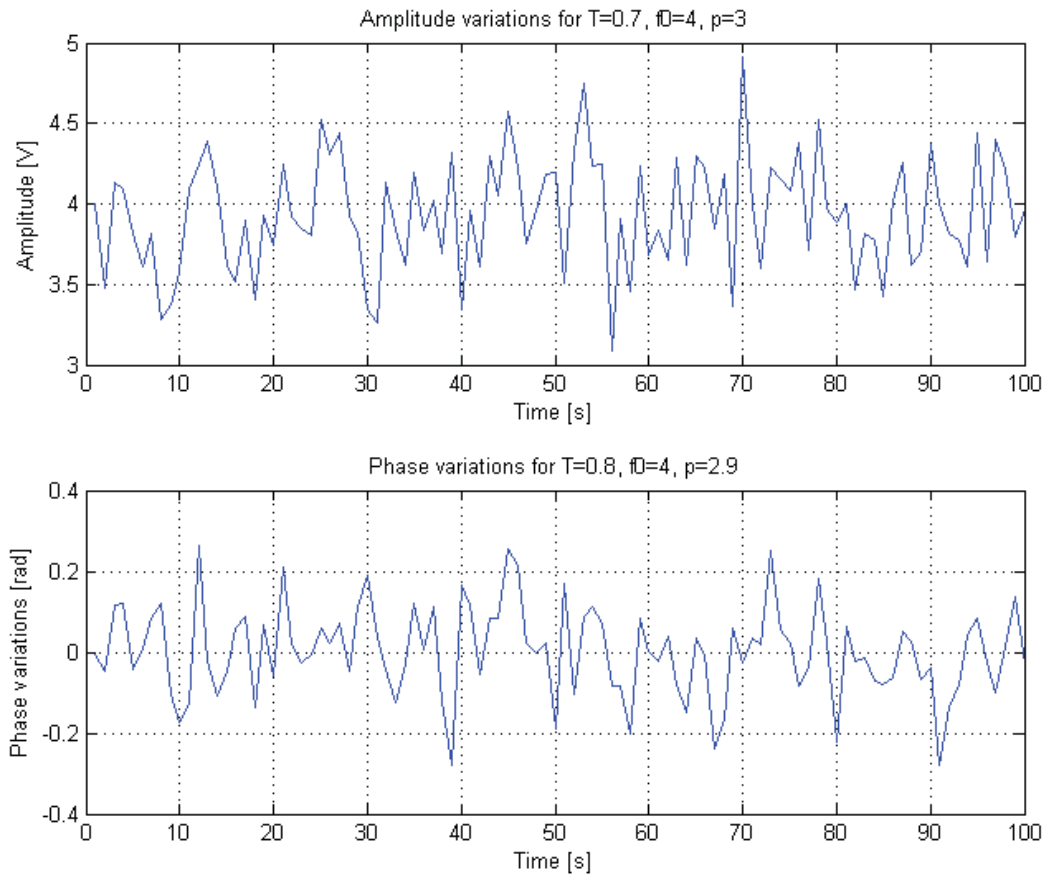


Figure 1.1. Example of the scintillation effect on a signal

1.1 RUAG Space

RUAG Space is a company specialized in producing advanced on-board satellite equipment, including systems, antennas, electronics and adapters. RUAG Space AB is a part of RUAG group and provides advanced space equipment as a Europe leader in space industry. The location for design and manufacture of digital electronics, microwave electronics and antennas is situated in Gothenburg, Sweden.

The thesis is executed in cooperation with RUAG Space AB in Gothenburg, Sweden. The company has provided all the necessary documentation and real data measurements to accomplish the project.

1.2 Problem statement

This thesis focus on the scintillation effect on the GPS signal transmitted from GPS satellites. As the scintillation effect causes prominent errors in the bending angle calculations, it is crucial to provide possibly the most precise mathematical model, which allows to conceive proper ionospheric corrections. Complexity of the problem is high due to constant changes of the electron density in the ionosphere, which emerge in random variations of amplitude and

phase. The main objective of the thesis is to conduct an optimization of the Rytov model, used to derive power spectra for amplitude and phase scintillation [3]. The problem is connected to the fact that the parameters are not well known for the RO geometry and they need to be estimated using real RO measurements. This would provide a realistic model, to be used for testing the tracking performance of RO instruments under development. To perform the optimization, mathematical model of scintillation effect should first be implemented. Implementation, verification and optimization of the model are conducted in Matlab software. There are many methods and functions that can be used to optimize the model. Each method is based on different approaches and algorithms, which may give wide range of results. It is intended to implement various methods of optimization, that could give possibly the best results and verify how much they differ from the previous parameters. This thesis aims to validate this hypothesis and provide an optimized scintillation model, which will contribute to a more accurate retrieval of the atmospheric profiles.

1.3 Scope of the thesis

First part of the thesis contains the mathematical model implementation of the ionosphere scintillation. Research made by RUAG in [4] provides the foundation for the implementation of the model and its further optimization. The model is developed using Rytov approach, based on expressions of the power spectrum for amplitude and phase of the signal. Any different approaches are not the part of the project. Analysis of the signal is conducted separately for an amplitude and phase, considering only the L1 signal. To get a realistic model in Matlab software, proper model parameters should be selected. The main part of this thesis is based on refinement of the model parameters, obtained before, with respect to real data measurements. To improve the results, three optimisation methods were applied, including *lsqcurvefit*, *fminsearch* and *fminunc*, which are part of Matlab Optimisation Toolbox.

1.4 Division of work

The thesis project was accomplished by two students due to high complexity of the problem. Tomasz Dziendziel was responsible for implementation of the amplitude model and optimizing the scintillation model with *lsqcurvefit* and *fminsearch* methods. Marta Boryczko performed the optimization process using *fminunc* function along with complete phase modelling. All the theoretical aspects including literature studying were executed equally for better understanding of the subject matter. Also the verification of the model and comparison of different optimization methods were performed together to obtain the proper optimization method for further data analysis.

1.5 Outline of the thesis

In chapter 2 background and related works are presented. Background indicates specifications of the problem i.e. Radio Occultation, Ionosphere Scintillation and its connections with GPS System. Also the main approach used to provide the mathematical model is described. Chapter 3 refers to the RO scintillation modelling. The subsequent chapters include description of the measurement data, modelling, implementation and verification of the model, executed in Matlab Software. Chapter 4 presents different methods of optimization, used to obtain more accurate parameters of the model. Thereafter the obtained results are analysed and the most suitable parameters of the model are indicated. In the end of the thesis summarizing conclusions are presented.

2. Background and related works

2.1 Background

The Global Navigation Satellite System (GNSS) is used to pinpoint the location of an electronic receiver on the earth surface, using time signals transmitted from the satellites. Currently few GNSS are used around the world, i.e. Global Positioning system (GPS) developed in the USA, Russian Global Navigation Satellite System (GLONASS) or Chinese BeiDou Navigation Satellite System, which is not operational [5].

GPS system currently uses 31 satellites which orbits the Earth in Medium Earth Orbit (MEO) at the altitude of 20200 km. In any time at least four of them are visible from any point, which is necessary to determine the location of GPS receiver. GPS system is able to find the position of the receiver by using method called trilateration. According to trilateration process, an approximate position can be found with only three satellites, but four satellites or more improves the accuracy and evaluates more precise coordinates. To calculate the distance from the satellite, GPS receiver analyses the radio signal and measures the travelling time of the signal. To obtain the time, very specific and accurate atomic clock is applied in the satellite. To perform the measurements, clocks in the receiver and the satellite have to be synchronized. Every small difference may generate huge calculation errors. Because of the receiver clock inaccuracy, fourth satellite is provided, which allows the receiver to synchronize its internal clock with the one in the satellite [6].

Today GPS satellites are not only used for positioning. There are many new applications of GPS signals and one of them will be described in this thesis. Radio Occultation (RO) is a modern technique of measuring weather profiles. At first RO was used to retrieve valuable atmospheric information about other planet. For example satellites Mariner IV and V used RO to measure the weather on Mars and Venus. It was conducted by NASA and Stanford University teams. In 1995 RO was applied to measure weather conditions on earth. It used GPS satellites and a receiver in LEO [7]. Weather measurement by RO has a lot of advantages. First of all, due to high number of GPS satellites orbiting the planet, measurements are very accurate and stable. Moreover data can be retrieved from above the oceans and land, with a high coverage. The other advantage of using RO is economic efficiency, as low-cost sensors are applied [8]. The procedure of obtaining the atmospheric properties is connected to refraction of the signal. GPS receiver are stationed on LEO while the transmitter, GPS or GNSS satellite, is located on the other side of the globe on MEO. It is illustrated in the Fig. 2.1. The LEO satellites are based up to 2000 km above the earth and can travel with high velocity. These satellites can round the earth in nearly 90 minutes. For MEO satellites it takes around 12 hours to fully travel around the globe.

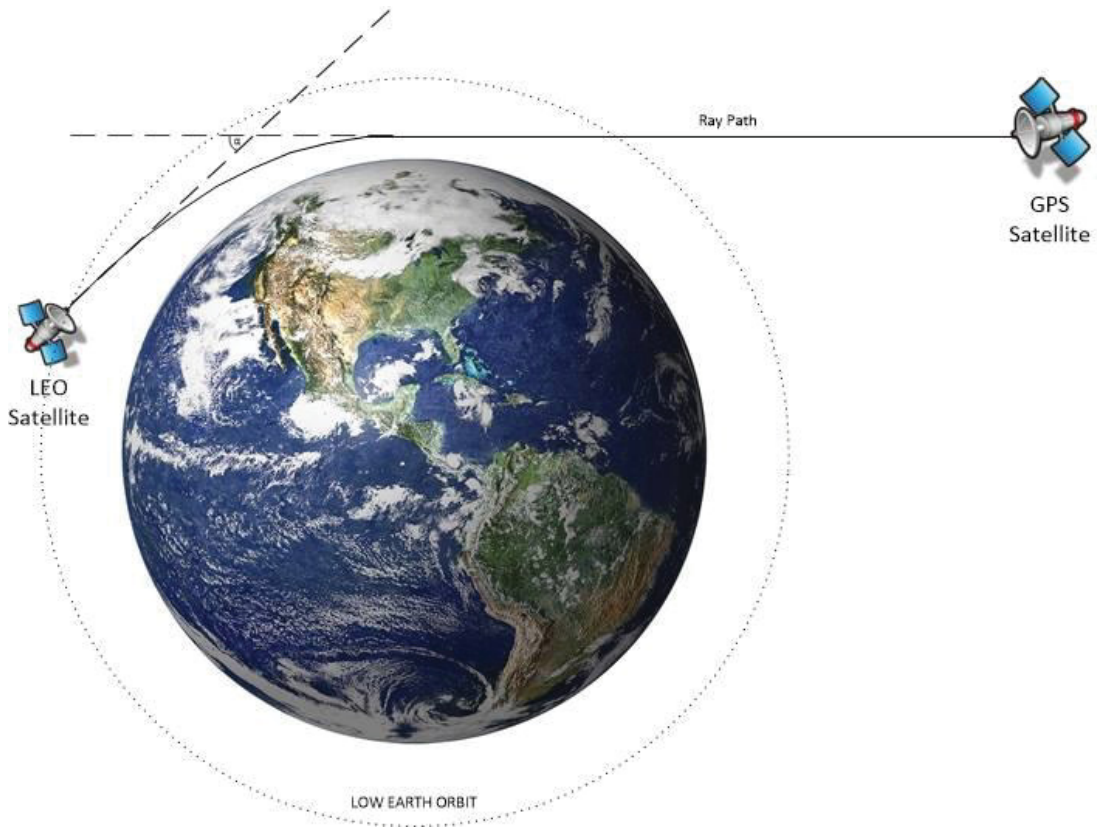


Figure 2.1. GPS Radio Occultation concept

The satellite transmits the signal to the receiver. At certain point it passes through the atmosphere. Atmospheric properties i.e. humidity, temperature and pressure, especially in the troposphere, cause the signal to bend with a certain angle [9]. Due to the Doppler's Shift the signal frequency is changing. Since altitude has a direct influence on the atmospheric parameters, LEO receiver ascends and descends to collect data from different part of the atmosphere. By computing the Doppler's frequency, the bending angle can be retrieved for further calculations. The signal contains number of errors and an ionospheric correction has to be applied in order to calculate the correct refraction of the signal. At the end, atmosphere properties are derived from the refractive profile [10], [11]. The process of receiving the vertical profiles of temperature, humidity an pressure is shown on the Fig. 2.2 [10].

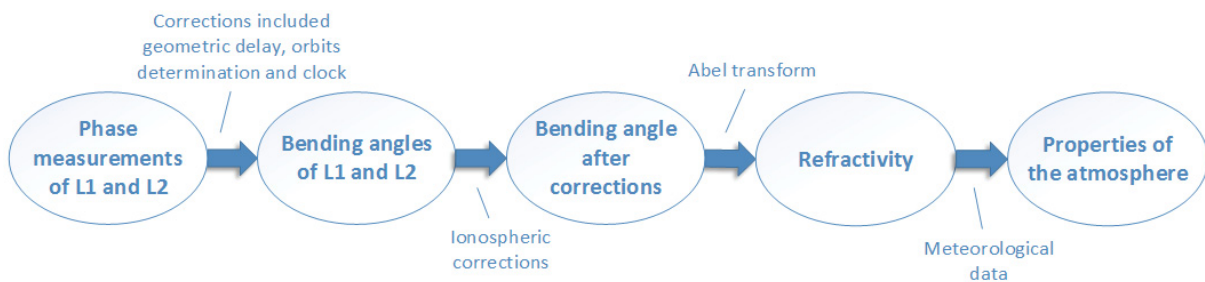


Figure 2.2. Radio Occultation atmospheric profiles retrieval

The scintillation issue arises in the higher parts of the atmosphere. Ionosphere is a part of atmosphere from 70 up to 750 km, where high irregularities in the density of free moving electrons occur. Region between 250 and 400 km is called F-Region and it is a part of the ionosphere, where the electrons concentration reaches its peak. This specific surrounding is the result of solar radiation caused by the sun. In different sun activity levels, the density of the ions may vary. Solar flares on the surface of the sun are common cause of higher density of electrons. They can be observed during high sun activity. These irregularities are causing many problems in navigation as well as in RO. GPS signal which passes through the ionosphere during scintillation events emerges rapid amplitude and phase fluctuations. This is called the Scintillation Effect. Scintillations are most likely to appear near the equatorial regions, as well as the high latitudes, predominantly in the evening. Low latitudes have stronger impact on the signal amplitude whereas phase of the signal is more presumable to be affected in polar regions. Scintillated signal have disrupted parameters which may cause undesirable results. At worst case they may cause a receiver to lose the GPS signal tracking. In most cases scintillations cause the RO measurements to be inaccurate. GPS satellites transmit the signal on two frequencies, L1 and L2, to get a correction for scintillation effect. However the influence of the scintillation effect is still visible and may cause disturbances in the signal. Due to adequate model of scintillations, negative effect can be reduced or even removed. As a result, the receiver of atmospheric sounding should be able to manage the worst scintillation case [12], [13].

There are several existing approaches, which mathematically describe the scintillation effect. Each theory considers different aspects of this phenomena. The first introduced theory, Phase Screen Theory describes irregular screens, which change only the phase of the signal. Rytov theory focuses on singular scattering effect of scintillation, affects the amplitude of the signal. On the other hand Parabolic Equation Method (PEM) was derived for strong scintillations and considers the multi-scattering effect of scintillation [3].

In this thesis simplified version of the Rytov approach was implemented and its parameters were optimized. This theory aimed for weak and moderately strong scintillations of a signal. Power spectrum of the electron density irregularities, thickness of the irregularity layer, distance from the layer to the receiver and scanning velocity are the essential variables, required to obtain the Rytov solution. Based on these parameters, power spectrum of the phase and log-amplitude variations can be derived. Those properties allow to calculate the scintillation index which is the normalized variance of the intensity of a signal, needed to describe the disturbing effect of scintillation [14].

2.2 Related Works

General description of the scintillation was revealed in [15]. Authors of this paper explained the scintillation and how it affects transmitted signals, as well as parameters of this phenomena. They also explore the difference between Global Ionospheric Scintillation Model

(GISM) and Wide Band Model (WBMOD). The WBMOD model focuses on the ionospheric irregularities. This model consists of the power law phase screen and contains parameters such as spectral strength, spectral slope and scintillation indices. Several methods describing scintillation effect are presented in the literature. Phase Screen, Parabolic Equation Method and Rytov methods are discussed by Yeh and Liu in [3]. These theories were the fundamentals on which many based their scintillation models. Analytical scintillation models were thoroughly described and compared by Priyadarshi in [14]. One of the scintillation effect model, which consider and simplify Rytov weak scatter theory, is the power law phase screen model proposed by Rino in [16]. It presents scintillation modelling with power spectral density of the signal phase and amplitude, which helps in further analysis. Correct modelling allows to apply proper ionospheric corrections to the signal.

All equations demanded to create the model of scintillation are proposed in the RUAG Space document [4]. The model is based on inverse power law presented by Rino. It defines few worst scenarios of scintillation in which the receiver will continue to work properly.

3. Ionospheric scintillation in Radio Occultation

3.1 Input data description

Input data used in the thesis are obtained from the Meteorological Operational satellite programme (MetOp). It consists of three satellites managed by the European Organization for the Exploitation of Meteorological Satellites (EUMETSAT). The first satellite in the series, MetOp-A was launched in 2006. In 2012 second satellite, MetOp-B was added to the first satellite and even more detailed observation could then be provided. Third satellite is planned to be launched in 2018. Satellites are equipped with GRAS instrument. GRAS is a GNSS receiver for atmospheric sounding, which receives high quality radio signal from satellites. It provides over 600 RO measurements each day. Operational meteorology and climate monitoring requirements of the instruments are included in [17]. Specification and performance of the instrument are presented in [18]. GRAS consists of three antennas with high gain and wide coverage. Each antenna has a capability to track two occultation at the same time [18], [19].

In order to analyze the scintillation events, proper data from the MetOp GRAS measurements were retrieved. The data used in the thesis was preprocessed by RUAG. It was divided into few stages of refinement and packed into Matlab structures for further analysis. From Level 1, where binary data of the measurements are stored, to Level 3 structures which consist of more sorted and refined data. In this thesis Level 3 files are used to obtain desired results of spectrum analysis. All necessary variables are shown below [20].

IMT_CA - Time variable for combined carrier phase [s],

PCA_CA - Combined carrier phase values for C/A- code [m],

IMT_IQ - Time variable for values quadrature components,

I_CA - In-phase component of the correlation amplitude for the C/A-code,

Q_CA - Quadrature component of the correlation amplitude for the C/A-code.

These variables are used to calculate the total phase and amplitude scintillation.

3.1.1 Transforming data for analysis

In order to obtain the power spectra of amplitude and phase, the data are preprocessed. Power Spectral Density (PSD) is a distribution of signal's power throughout its frequency [21]. To calculate the PSD of a log-amplitude, firstly it needs to be created from in-phase and quadrant components of C/A code, which are retrieved from the measurements. The log-amplitude signal z has the form shown in the equation below.

$$z(t) = 130 + 10 \times \log_{10}(I_{CA}^2 + Q_{CA}^2) \quad (3.1)$$

The next step of the process is calculation of the Fast Fourier Transform from the log-amplitude signal with a proper window.

$$Z(f) = FFT\{z(t) \times w(t)\} \quad (3.2)$$

Where:

$w(t)$ – window function.

Applying the window is necessary to minimize the spectral leakage connected to the discontinuities [22]. In these cases, hamming window is used. The signal is then multiplied by a scaling factor, which consists of the sampling frequency and window length. PSD can be also retrieved using a Matlab function *periodogram*. Calculations are made for different time segments, which consist of a particular scintillation event.

Transformation process of phase measurements is different and more complex than for the amplitude. Before retrieving the phase PSD, the background phase must be subtracted from the total phase of the C/A code. It can be done in few steps.

Firstly, a fifth order polynomial is fitted directly to the total phase of the signal. Different polynomial orders were checked to find the best possible fitting and to assure feasibly the highest accuracy of the results. The fitting process was made by two Matlab functions, *polyfit* and *polyval*. The first function fits a polynomial in the phase measurements, while the second evaluates this particular polynomial on the specific time period.

The next step is to subtract the total phase, *PCA_CA*, which is one of the variables stored in the Level 3 measurement structure, with the fitted polynomial. It behaves as a high-pass filter which allows to distinguish short-term variations in the specific time segment.

After that the FFT with a window can be applied to the signal in the same manner as in the amplitude. As in the case of amplitude, all the calculations are made for each individual scintillation event. Because of the low values of the phase, logarithmic scale is exploited on both axis.

3.2 Scintillation detection

To detect and categorize the scintillation effect, two important indices can be distinguished. S_4 index is a dimensionless value used to identify the strength of amplitude scintillation. It is defined as ratio of the standard deviation of the signal power to the mean signal power computed over a period of time [4].

$$S_4 = \sqrt{\frac{\langle I^2 \rangle - \langle I \rangle^2}{\langle I \rangle^2}} \quad (3.3)$$

Where:

I - intensity of the signal.

Based on experimental tests it is assumed that scintillation effect on signal amplitude occurs when S_4 index is higher than 0,12. When the S_4 index is higher than threshold but lower than the value of 0,3 it is qualified as a weak scintillation. Values greater than 0,3 and smaller than 0,6 indicate moderate level of scintillation. All the values higher than 0,6 are considered as a strong scintillation [23].

To define the strength of the phase scintillation, the root mean square (RMS) of the phase variations, σ_ϕ is used [4].

$$\sigma_\phi = \sqrt{\langle \phi \rangle^2} \quad (3.4)$$

Where:

ϕ – phase variations.

If the σ_ϕ is greater than 0,1 rad, which corresponds to $\sim 6^\circ$, scintillation effect on signal phase occurs. A σ_ϕ higher than ~ 1 rad denotes strong phase scintillation. To classify the part of the signal as a scintillation event, its indices must last above the threshold at least 30 seconds [24], [25].

3.3 Scintillation modelling

3.3.1 Amplitude modelling

To analyze the scintillation events occurring in the amplitude of the GPS signal, a mathematical model has been created. These events are random and they can appear in different parts of the signal causing fluctuation in its amplitude (Fig. 3.1).

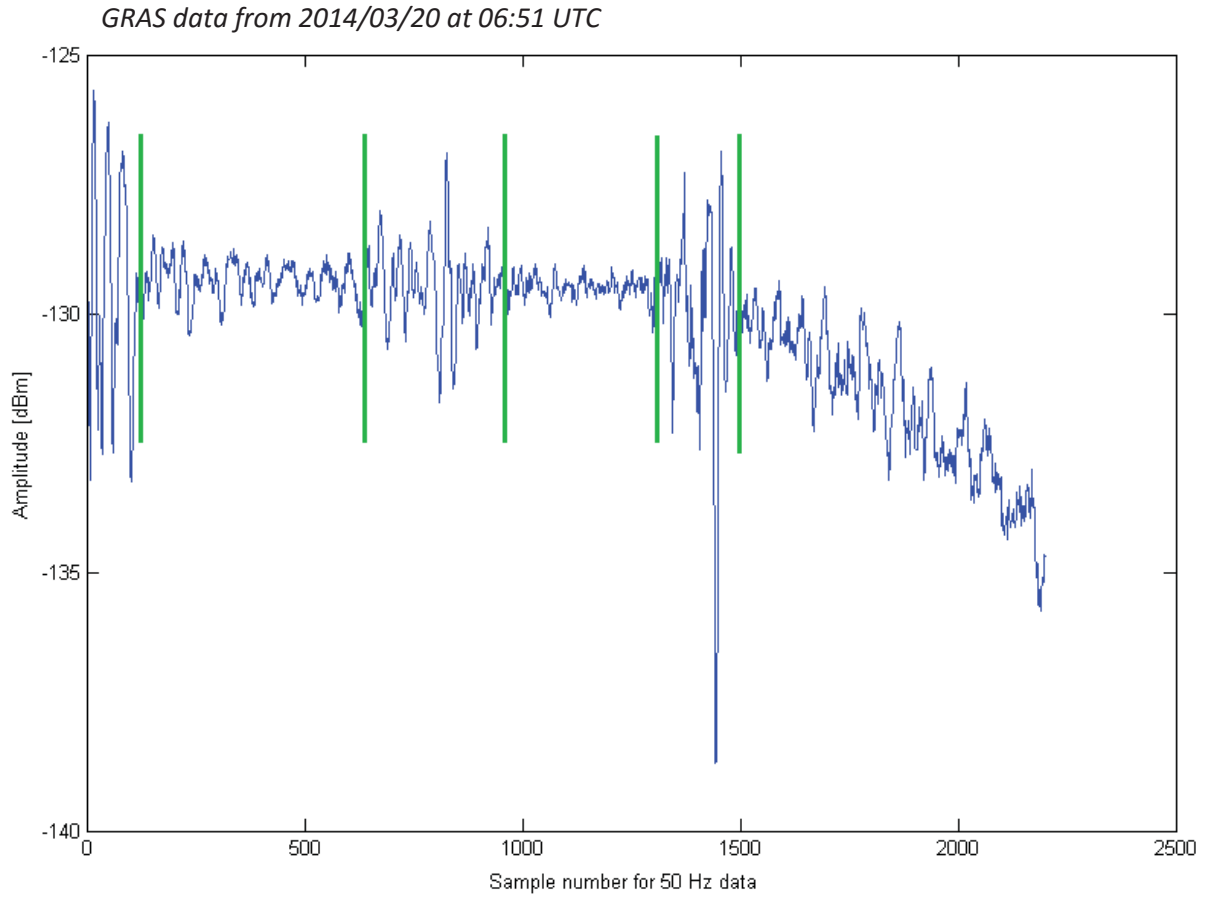


Figure 3.1. L1 frequency scintillation events of the signal amplitude

In the figure above three possible scintillation events can be seen. First scintillation occurs between 1 and 150 sample, where the sample rate is 50 Hz. The second between 650 and 900. The last scintillation of the amplitude can be seen from 1300 to 1500 sample. Mentioned intervals were additionally distinguished on the figure using green lines. Equations of the power spectrum of the log-amplitude defined by Rytov can be seen below [3].

$$S_{\chi}(f) = \frac{\pi r_e \lambda L}{U} \int_{-\infty}^{\infty} \left\{ 1 - \frac{2k}{q^2 L} \sin\left(\frac{q^2 L}{2k}\right) \times \cos\left(\frac{q^2}{k}(z - L/2)\right) \right\} \times S_{\Delta N}\left(\frac{f}{U}, \kappa_y, 0\right) d\kappa_y \quad (3.5)$$

Where the power of electron density irregularities is:

$$S_{\Delta N}(\kappa_x, \kappa_y, 0) = \frac{\eta \sigma_{\Delta N}^2 \Gamma\left(\frac{p}{2}\right)}{\pi^{2/3} \Gamma\left[\frac{p-3}{2}\right] \kappa_0^3} \times \left(1 + \frac{\eta^2 \kappa_x^2 + \kappa_y^2}{\kappa_0^2} \right)^{-p/2} \quad (3.6)$$

and

$$q^2 = \frac{f^2}{U^2} + \kappa_y^2 \quad (3.7)$$

Where:

U – scanning velocity,

f – signal frequency,

L – thickness of the irregularity layer,

z – distance between the layer and the receiver,

r_e – classical electron radius,

λ – radio wavelength,

k – radio wavenumber,

κ_0 – outer scale wave number,

κ_y – vertical wave number,

η – anisotropy factor,

$\sigma_{\Delta N}$ – RMS variations of the electron density irregularities,

p – spectral slope,

$\Gamma(x)$ – gamma function.

Rytov approach can be applied for weak and moderately strong scintillation. It allows to retrieve power spectra of amplitude and phase in frequency domain. Power Spectrum Density is desirable in order to compare the mathematical model to real data measurements. However this model is far more complex compared to its simplified version, which has been implemented in this project. Due to less number of parameters and less complexity it is more convenient to proceed with. The simplified model of scintillation power spectrum of log-amplitude is shown below [16].

$$S_x(f) = \frac{T_x}{(f_{0x}^4 + f^4)^{p_x/4}} \quad (3.8)$$

Where:

T_x – is the magnitude of the Power Spectral Density,

f_{0x} – is the roll-off frequency,

p_x – is the spectral slope of PSD.

The power spectrum of log-amplitude can be used to retrieve the normalized value, which describes scintillation in terms of signal disturbances. The scintillation index S_4 is used to classify how strong the modelled scintillation is [3].

$$S_4 = 2\sqrt{\langle \chi^2 \rangle} = 2 \sqrt{\int_{-\infty}^{\infty} S_\chi(f) df} \quad (3.9)$$

Where:

χ - log-amplitude,

S_χ – power spectrum of the log-amplitude

3.3.2 Phase Modelling

Modelling the phase of signal scintillation is similar to the amplitude scintillation modelling. Phase variations during a scintillation event are much lower and occur in same time segments. Figure 3.2 shows possible phase scintillation events origin from the same measurement sample as in the previous figure but the variation of the signal phase can be observed in the same interval as in the amplitude.

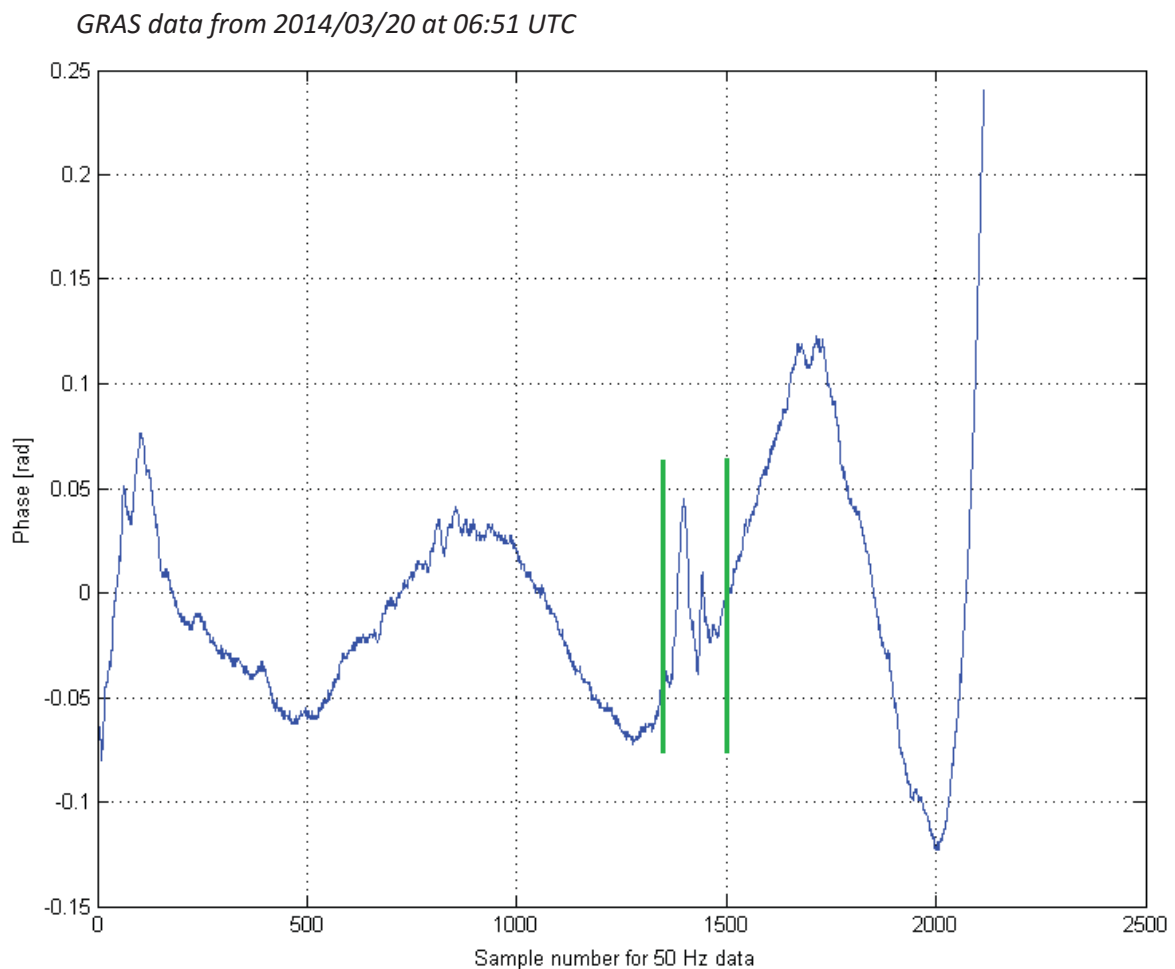


Figure 3.2. L1 frequency scintillation events of the signals phase

As it can be seen in the Fig. 3.2 scintillation events occur in the same time intervals as in the amplitude described before. The highest phase variations of the signal are visible from 1300 to 1500 sample. If there were no scintillation in the signal, the characteristic would present much smoother, without rapid fluctuations in comparison to the one in the Fig. 3.2.

Rytov solution for the phase scintillation model, which is the power spectrum of phase variations is [3]:

$$S_{\phi}(f) = \frac{\pi r_e \lambda L}{U} \int_{-\infty}^{\infty} \left\{ 1 + \frac{2k}{q^2 L} \sin\left(\frac{q^2 L}{2k}\right) \times \cos\left(\frac{q^2}{k}(z - L/2)\right) \right\} \times S_{\Delta N}\left(\frac{f}{U}, \kappa_{y,0}\right) d\kappa_y \quad (3.10)$$

Respectively the simplified model that retrieve the PSD of the phase has the form [16]:

$$S_{\phi}(f) = \frac{T_{\phi}}{(f_{0\phi}^2 + f^2)^{p_{\phi}/2}} \quad (3.11)$$

Where:

T_{ϕ} - is the magnitude of the phase PSD,

$f_{0\phi}$ - is the roll-off frequency,

p_{ϕ} - is the spectral slope of phase PSD.

3.4 Model implementation

In order to verify the scintillation model, firstly it was implemented in the Matlab software. Equations 3.8 and 3.11 are applied as a functions with three parameters. The model executes for different values of frequency. In previous studies conducted by RUAG, three cases were defined, as worst possible scintillations [4]. They were obtained for the Rytov solution with the spectral density equal to 1 Hz. For each case, parameters for the simplified model has been estimated. With every set of values, scintillation index and RMS of phase variation were calculated. The Scintillation index ranges between 0 and 1. All values of the cases parameters are shown in the Table 3.1.

	T_χ	$f_{0\chi}$	p_χ	S_4	T_ϕ	$f_{0\phi}$	p_ϕ	σ_ϕ
Case 1	0.05	1	3	0.8	0.02	0.1	2.9	1.9
Case 2	0.7	4	3	0.7	0.8	4	2.9	0.37
Case 3	0.17	1.5	2.7	1	0.17	0.34	2.6	1.6

Table 3.1. Sets of parameters for the model provided by RUAG [4]

Figure 3.3 presents the PSD of the log amplitude for each case from the table 3.1. Models represent a particular case of an ionospheric scintillation event.

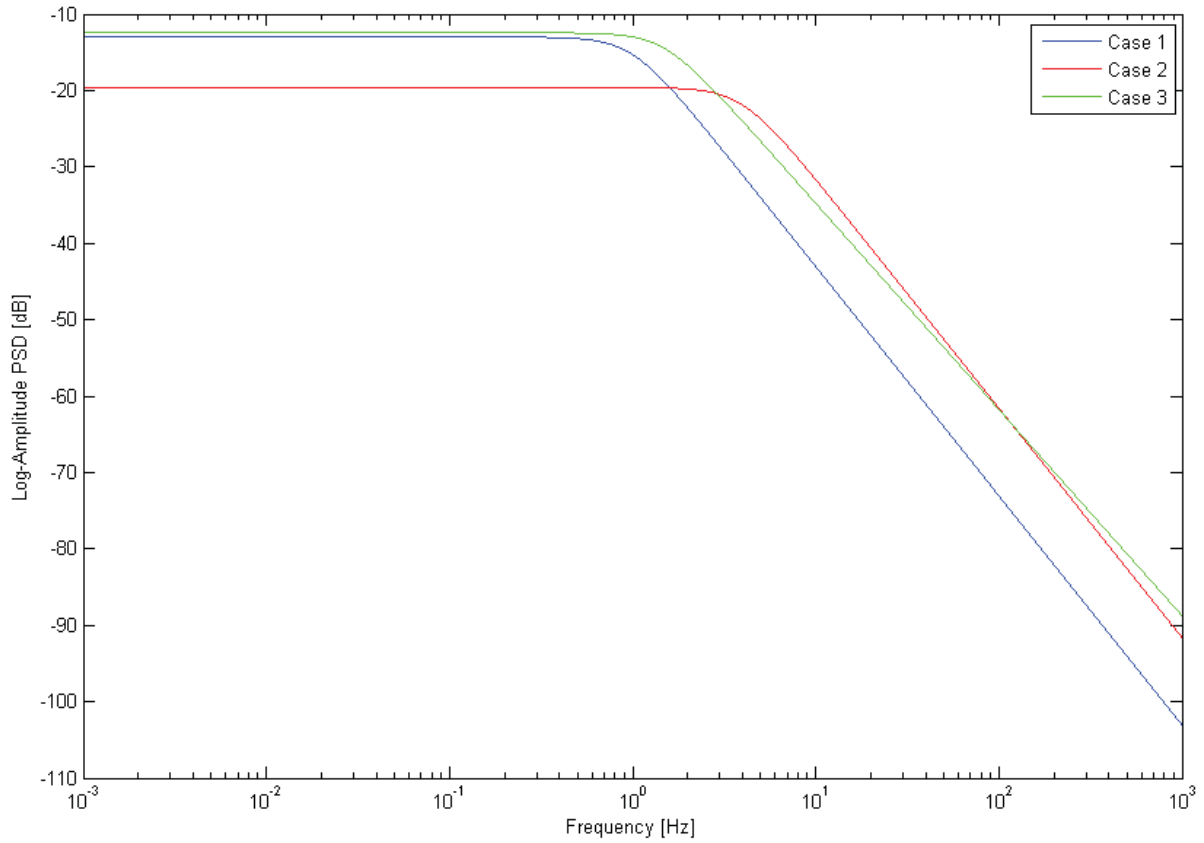


Figure 3.3. Log-amplitude PSD of the scintillation models

The phase PSD of these cases are shown in the Figure 3.4.

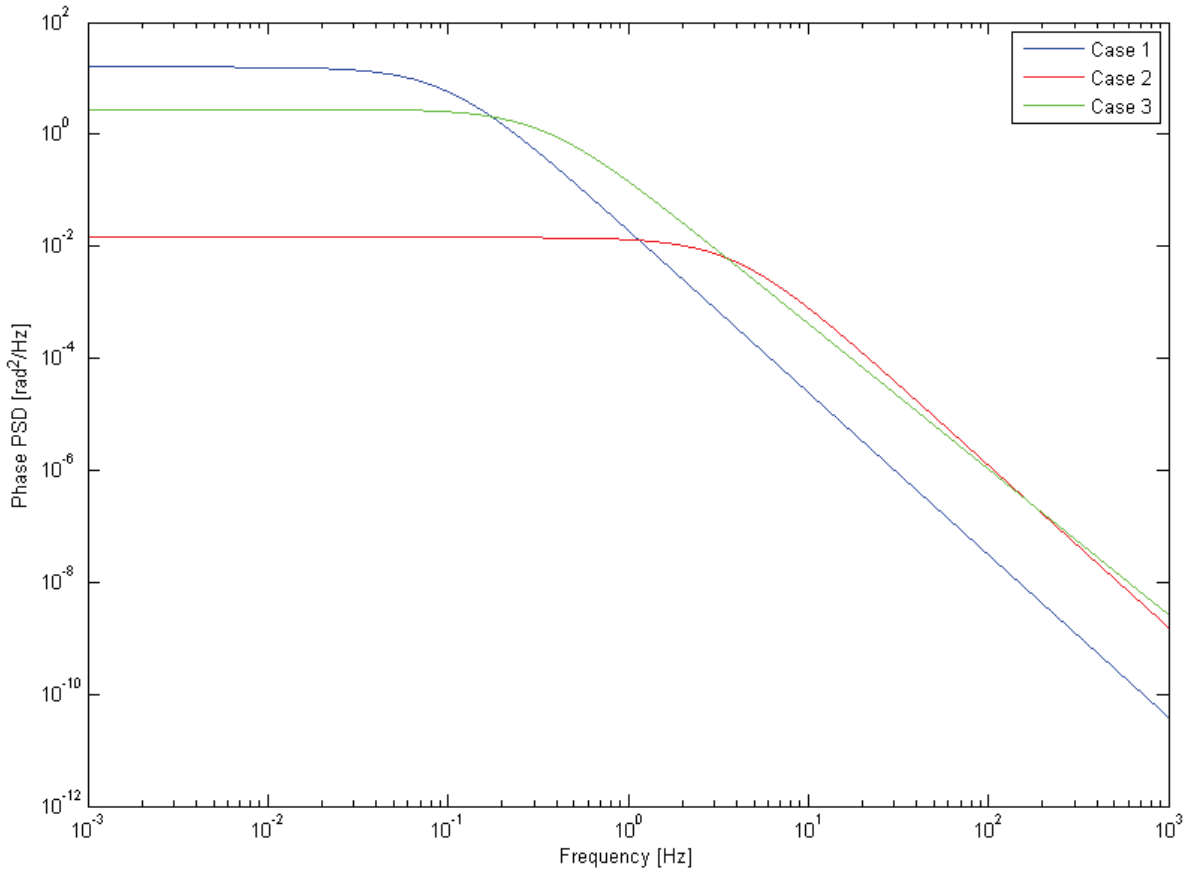


Figure 3.4. Phase PSD of the scintillation models

Amplitude models with various set of parameters introduced by RUAG differ from each other regarding the slope, roll-off frequency and magnitude, which is more visible for case 2. However, in the phase models all these three coefficient varies, resulting in completely different models. The most important factors which imply how they reflect the real data measurements, will be discovered in the next subchapter.

All characteristics of the model, as well as measurements are presented in a dB scale rather than linear scale. Values which are retrieved in the measurements are very high and analysis conducted in linear scale would be imprecise.

3.5 Model verification

To verify the performance of the implemented models, described in the previous section, they were compared with the particular scintillation events. GRAS data from 2014/03/20 at 06:51 UTC were used for comparison, where three scintillations events were visible, showed in the Fig. 3.1. Range from 1 to 150 sample denotes the first scintillation, 650-900 sample second scintillation, and 1300-1500 third scintillation. The amplitude PSD are plotted in logarithmic scale and are shown below (Fig. 3.5-3.7).

GRAS data from 2014/03/20 at 06:51 UTC

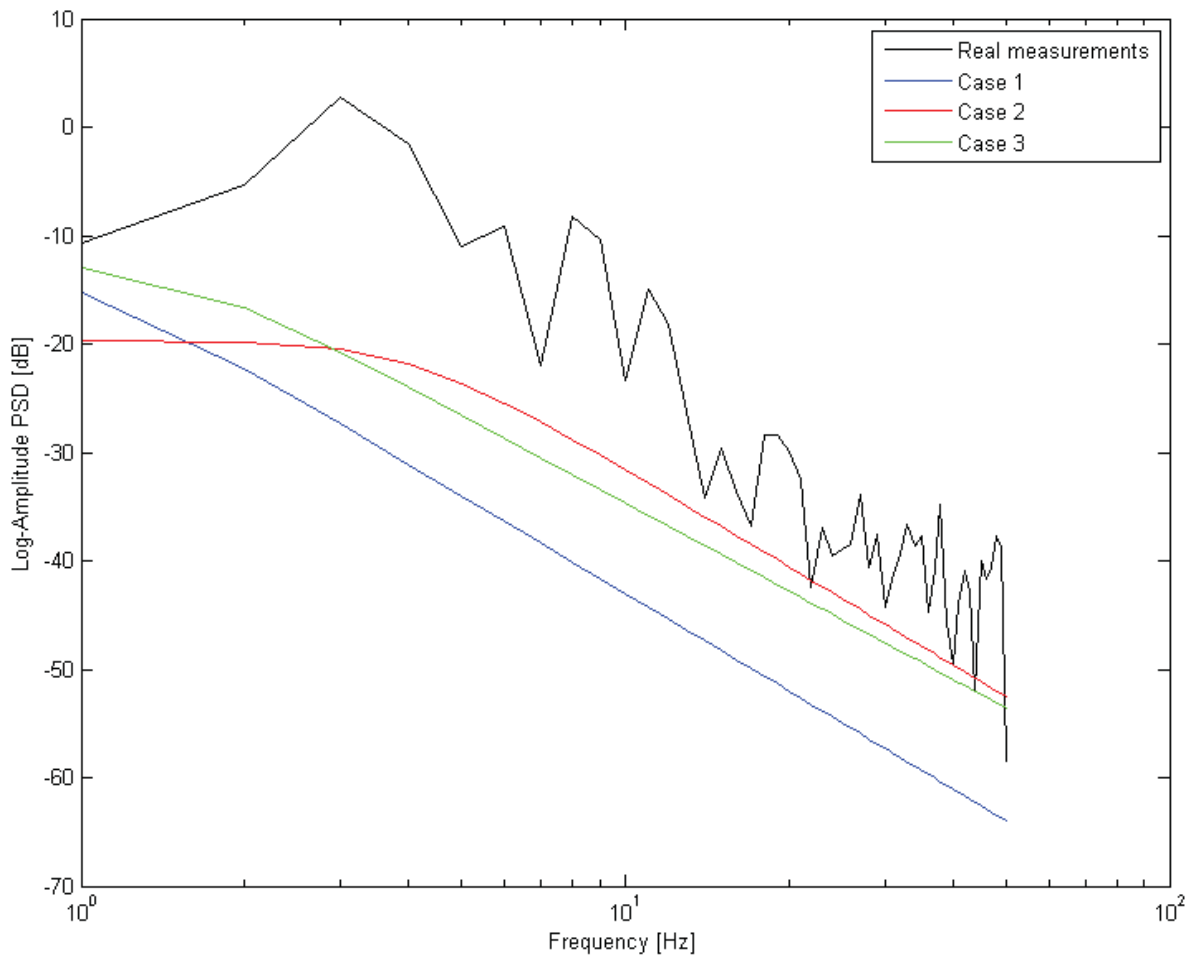


Figure 3.5. Amplitude first scintillation event [1-150] and model cases comparison

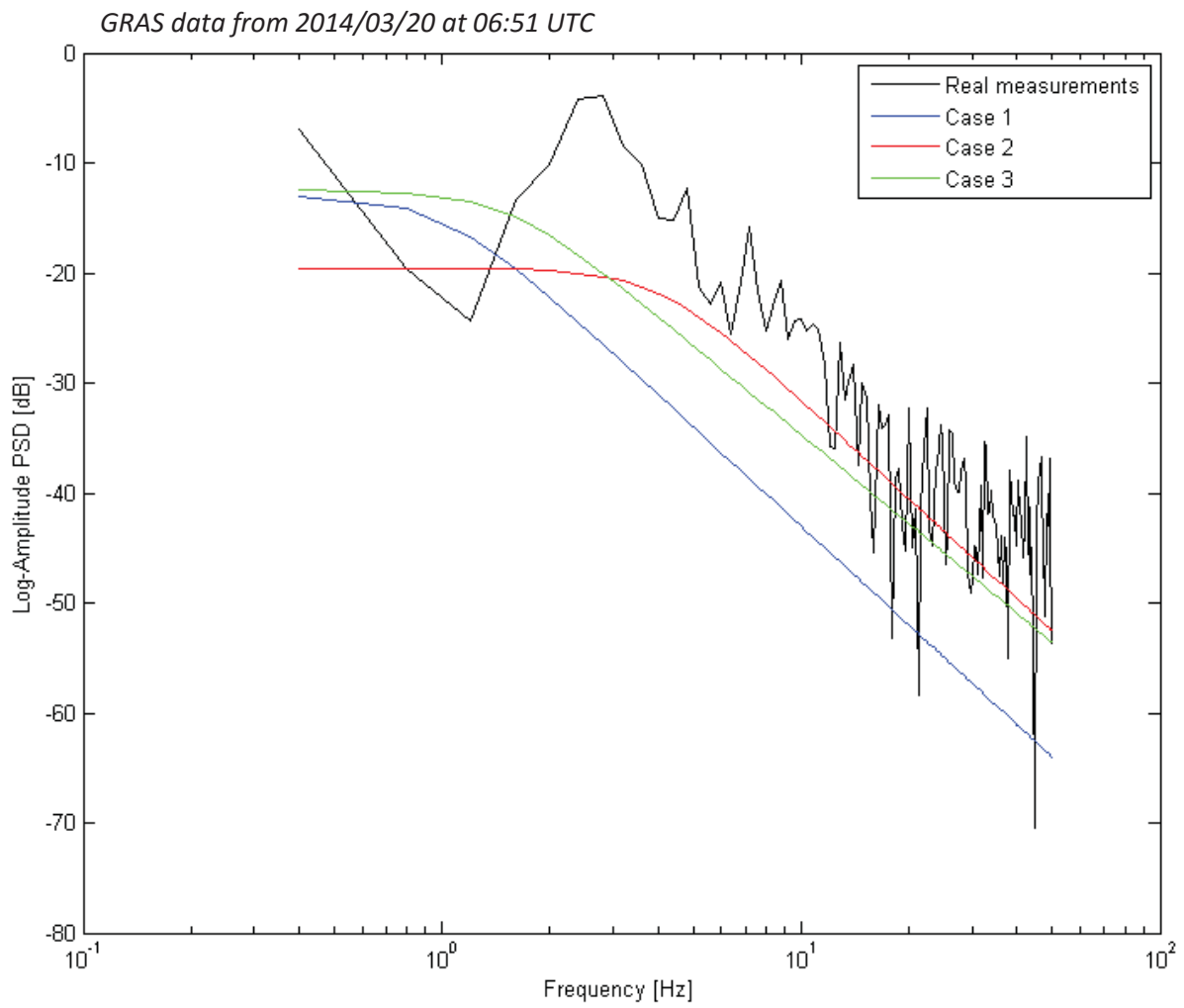


Figure 3.6. Amplitude second scintillation event [650-900] and model cases comparison

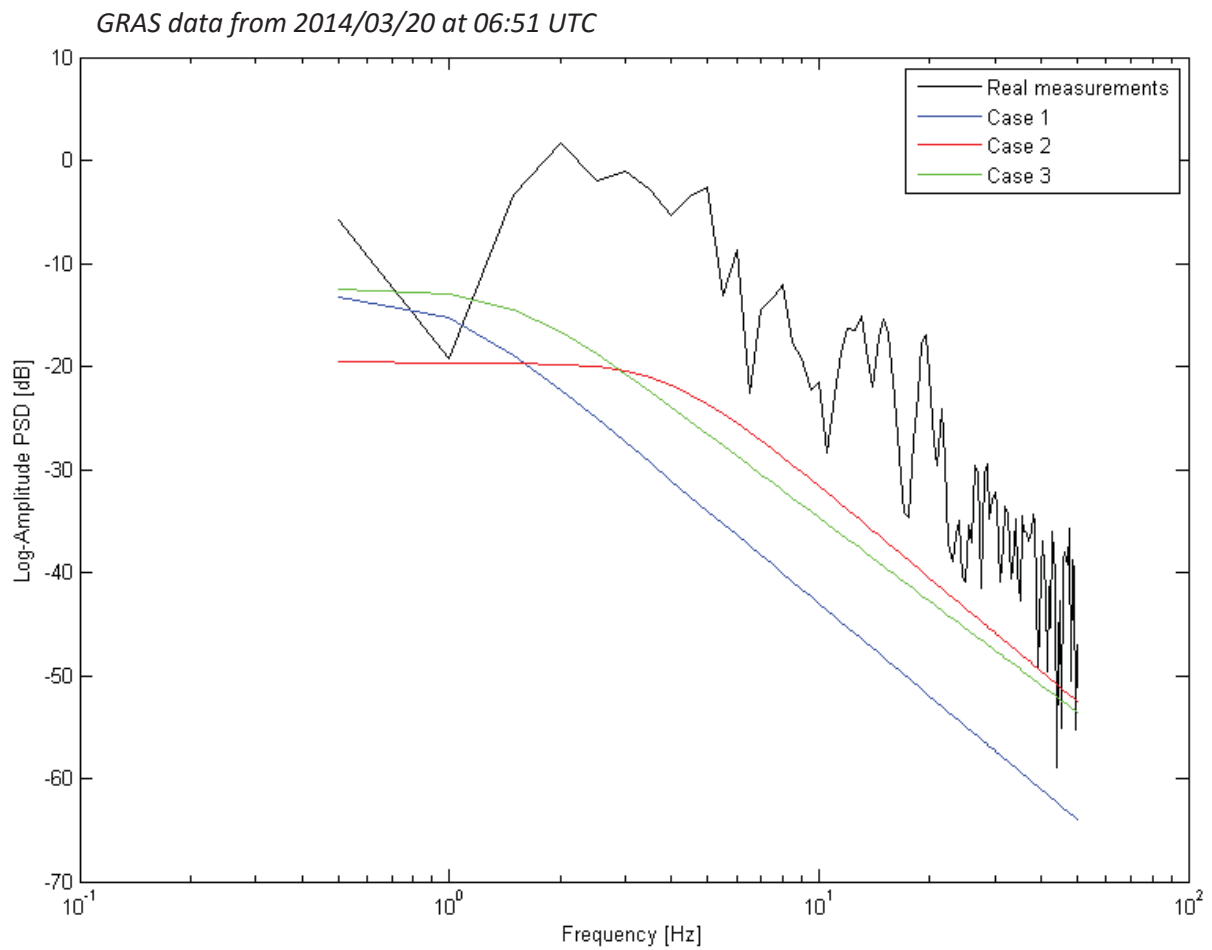


Figure 3.7. Amplitude third scintillation event [1300-1500] and model cases comparison

As it can be seen on the figures above, the models do not fit the scintillation in its whole duration. The third scintillation has the worst resemblance comparing to each model, while in the second scintillation the case 2 model matches quite good.

The results of the phase PSD are shown below (Fig. 3.8.-3.10).

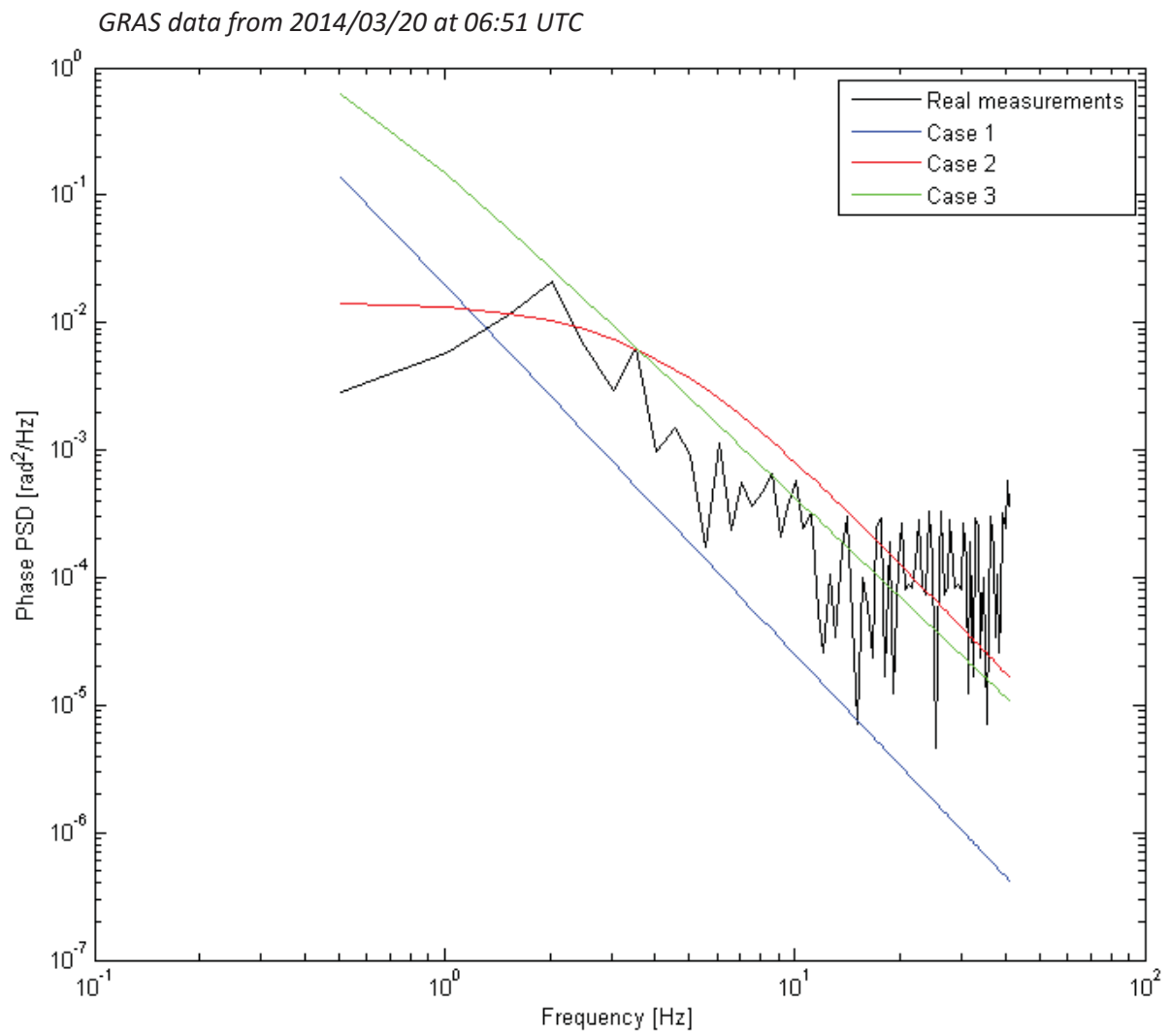


Figure 3.8. Phase first scintillation event [1-150] and model cases comparison

GRAS data from 2014/03/20 at 06:51 UTC

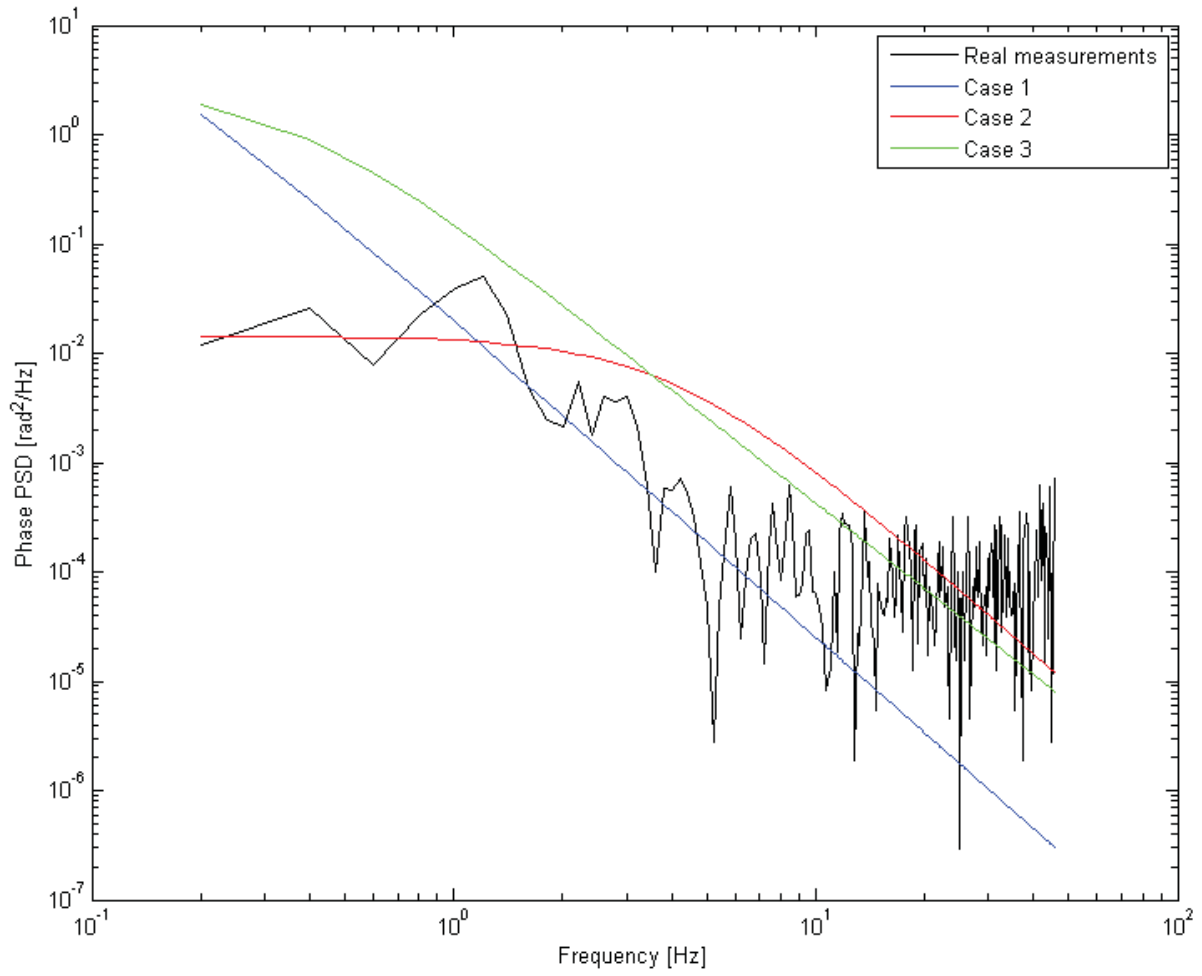


Figure 3.9. Phase second scintillation event [650-900] and model cases comparison

GRAS data from 2014/03/20 at 06:51 UTC

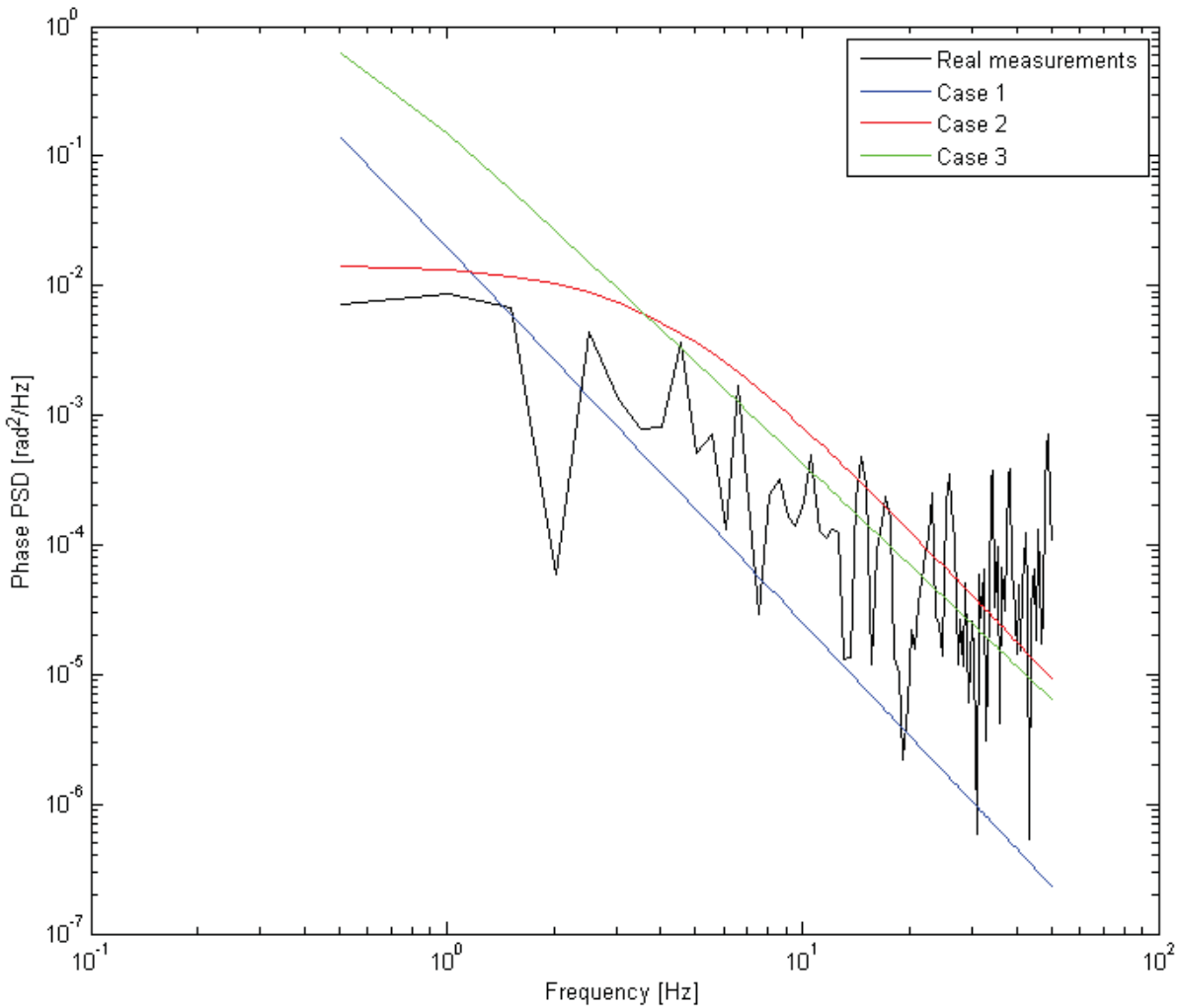


Figure 3.10. Phase third scintillation event [1300-1500] and model cases comparison

The figures above reveal differences between the model and measured scintillation events. However the case 2 characteristic matches the third scintillation quite well. For better description of the scintillation effect, model should resemble each particular scintillation event. To obtain more accurate results, an optimized model should be achieved.

In order to proceed with the optimization process, a proper starting point should be determined. Further analysis of the cases performance was conducted to obtain one of the parameters set, as a starting point for the optimization. To determine the best fitting among these cases, 15 data samples with scintillation events for both amplitude and phase were used. By comparing the Mean Square Error (MSE) between the real measurements and the models, the best case could be selected. The tables containing the MSE results are presented below.

GRAS data time (UTC)	MSE for Case 1 [dB ²]	MSE for Case 2 [dB ²]	MSE for Case 3 [dB ²]
2014-03-15, 14:21	436.4410	132.6377	156.9182
2014-03-17, 00:06	507.6462	162.1943	193.9576
2014-03-15, 04:15	401.0681	121.9034	144.6069
2014-03-16, 20:42	701.4453	259.8360	315.7227
2014-03-18, 18:18	320.6824	83.7924	105.2525
2014-03-19, 06:15	326.2058	89.5575	104.8518
2014-03-19, 06:15	368.5320	106.5323	124.6554
2014-03-19, 09:39	1017.5	456.2001	534.1493
2014-03-19, 21:21	674.7217	258.2823	299.7953
2014-03-19, 23:03	362.4111	107.5855	130.0454
2014-03-20, 22:42	499.5257	163.8500	193.9823
2014-03-21, 03:51	677.9732	246.7120	301.2491
2014-03-21, 22:21	362.4859	94.8693	115.3730
2014-03-24, 11:15	754.4338	288.1247	346.6114
2014-03-24, 16:15	663.4786	255.8493	303.0054

Table 3.2. MSE comparison of the amplitude models

GRAS data time (UTC)	MSE for Case 1 $\left[\left(\frac{\text{rad}^2}{\text{Hz}}\right)^2\right]$	MSE for Case 2 $\left[\left(\frac{\text{rad}^2}{\text{Hz}}\right)^2\right]$	MSE for Case 3 $\left[\left(\frac{\text{rad}^2}{\text{Hz}}\right)^2\right]$
2014-03-15, 14:21	2.1200	4.4143e-05	0.0723
2014-03-17, 00:06	0.9516	0.0024	0.0474
2014-03-15, 04:15	0.9530	0.0040	0.0497
2014-03-16, 20:42	1.6952	1.6389e-04	0.0628
2014-03-18, 18:18	0.7716	0.0102	0.0440
2014-03-19, 06:15	0.5860	0.0172	0.0441
2014-03-19, 06:15	0.9793	0.0333	0.0676
2014-03-19, 09:39	0.6719	0.0917	0.0854
2014-03-19, 21:21	2.5473	4.0701e-05	0.0833
2014-03-19, 23:03	0.8602	0.2009	0.2246
2014-03-20, 22:42	0.9825	0.0050	0.0516
2014-03-21, 03:51	1.4937	7.9729e-05	0.0582
2014-03-21, 22:21	1.1156	0.0111	0.0550
2014-03-24, 11:15	25.1175	24.8426	24.2207
2014-03-24, 16:15	2.546	1.9135e-04	0.0831

Table 3.3. MSE comparison of the phase models

As it can be seen in the table above, in most data samples the case 2 was superior to case 1 and 3. In only two occurrences MSE was a bit higher for the case 2, however the difference was very small. Based on the presented data analysis, case 2 was selected as a starting point for further optimization process.

4. Optimization of the scintillation model

The optimization process is used to improve the quality of engineering results, as well as achieve the optimal solution in many problems with given boundaries. Optimization is able to find the most suited compromise between two or more opposable conditions. In this project, optimization should result in minimizing the difference between the real data measurements and the model. As a result proper relations between the model parameters, T, f_0, p , separately for amplitude, as well as phase model, should be achieved. The objective function of this problem is a minimization of the mean square error, which is a mean square value of the subtraction of the model function values and the measurement data, collected from the satellite.

$$\min F = \frac{1}{n} \sum_{i=1}^n (\hat{X}_i - X_i)^2 \quad (4.1)$$

Where:

\hat{X} - GRAS data measurements,

X - model function values.

In this thesis few optimization functions were explored. Every function has a different algorithm, which calculates the minimum and concludes with different parameters of the model. The optimization was conducted separately for an amplitude, as well as a phase scintillation. As a starting point, case 2 parameters were used in each optimization process.

4.1 Optimization functions overview

The first optimization function, that was used in the thesis were *lsqcurvefit* and *lsqnonlin*. Both apply the same least square calculation algorithm. Difference between these functions lay in their purpose. *lsqcurvefit* is more appropriate for data fitting problems. Regardless of their purpose they give the same results in this specific problem. The least square method fits the nonlinear system with an linear function with every iteration [26]. The number of iterations and starting point depend on the complexity of the function.

Fminsearch is another function contained in a Matlab Optimization Toolbox. It is intended to minimize an unconstrained function of several variables, starting at declared, initial point. It refers to solving the problems over the real numbers and gives local solutions. *Fminsearch* uses the direct search algorithm and should indicate satisfactory results even for highly discontinuous problems [27].

Fminunc is a function, which similarly to *Fminsearch*, minimizes an unconstrained, multivariable function. To obtain results, it may use the 'quasi-newton' algorithm or the 'trust-

region' algorithm. In the second case, providing the gradient is necessary. *Fminunc* is more proficient than *Fminsearch*, however it is decidedly less effective for problems, which are highly discontinuous [28].

4.2 Obtained results

In this subchapter, the optimization process was performed on one particular real data file, which contained 3 visible scintillation events, described in the chapter 3.3. Following notation: first, second, third scintillation, corresponds to that description.

Subsequently to the implementation of the least square optimization function, the parameters of the model were calculated. The results for the first scintillation are shown below.

T_{χ}	$f_{0\chi}$	p_{χ}
3.3193	2.3854	2.9522

Table 4.1. Parameters for the amplitude model for the first scintillation using *lsqcurvefit*

Plotted model with the first scintillation measurement are displayed on the Figure 4.1.

GRAS data from 2014/03/20 at 06:51 UTC

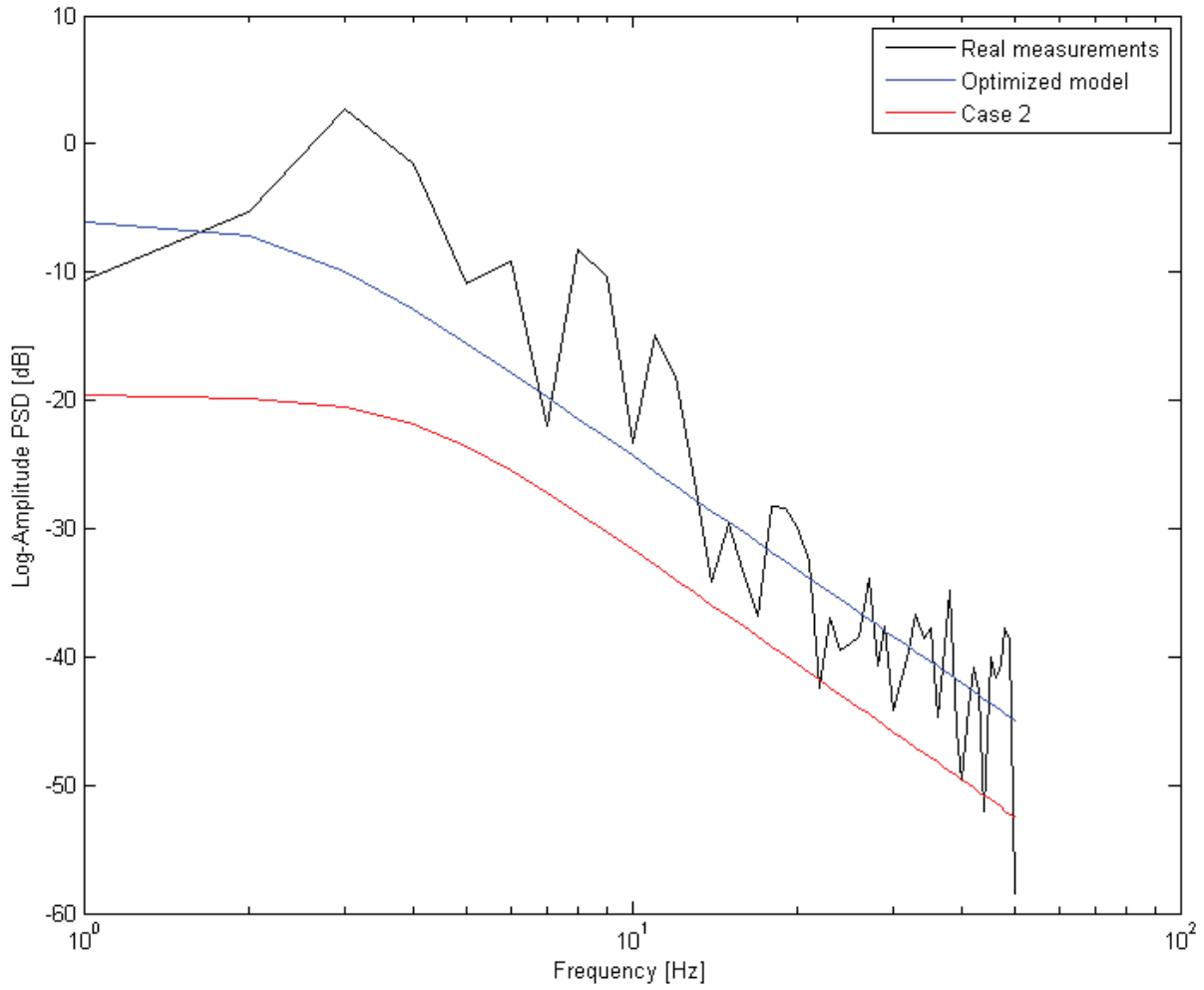


Figure 4.1. Optimization of the amplitude model for the first scintillation using *Isqcurvefit*

The retrieved, optimized model resembles the measurement better than in case 2 model. The fitting of the optimized model is more accurate. The characteristics match the scintillation event through the whole duration, while the magnitude of case 2 characteristic is lower than the scintillation measurements.

The optimization process was conducted for the phase of the first scintillation. The results are shown in the Table 4.2 and Figure 4.2.

T_ϕ	$f_{0\phi}$	p_ϕ
1.3461	4.8605	3.1626

Table 4.2. Parameters for the phase model for the first scintillation using *Isqcurvefit*

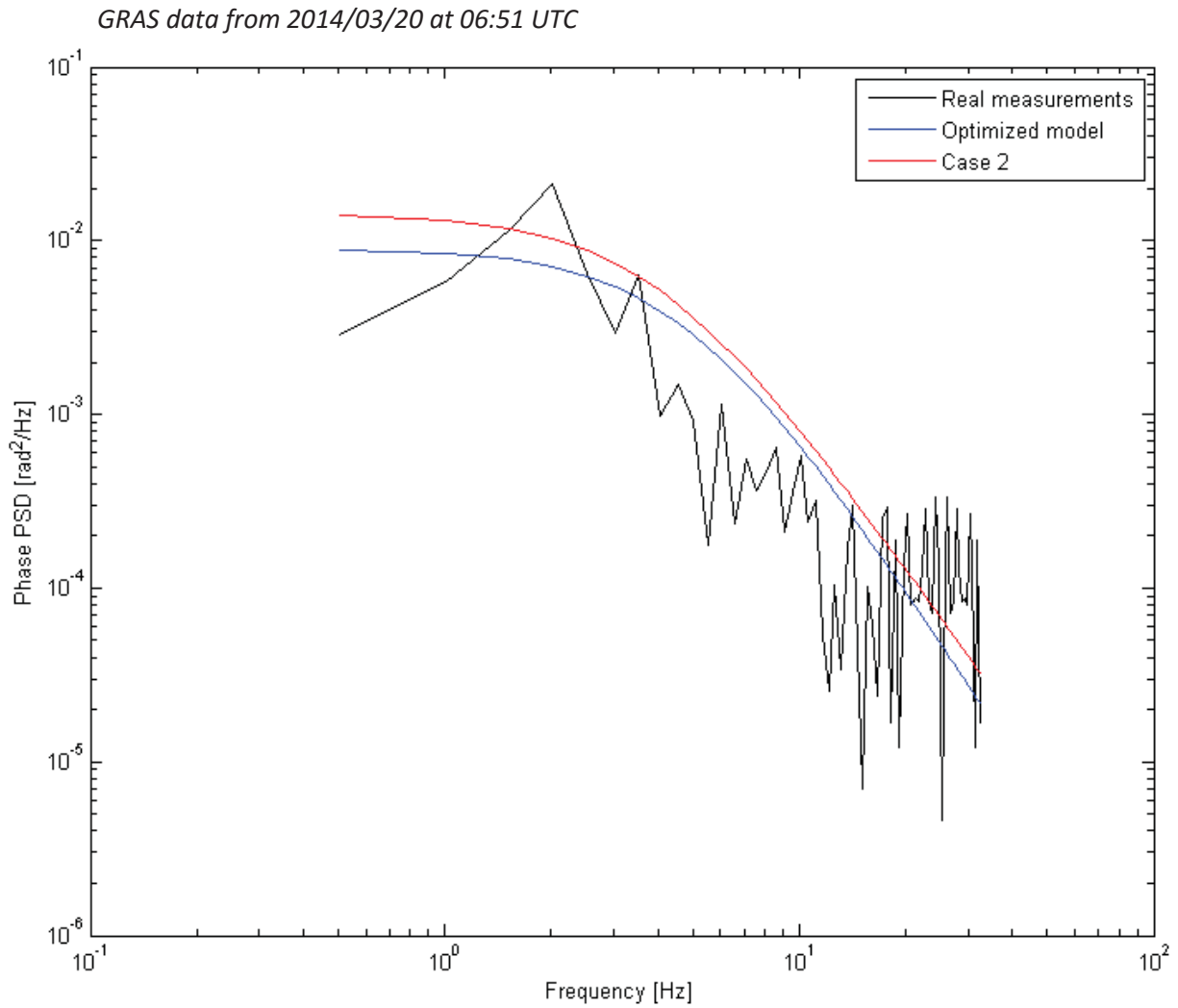


Figure 4.2. Optimization of the phase model for the first scintillation using *lsqcurvefit*

Comparing the optimized model with the case 2 model, it can be seen that it improved the resemblance of the measurements. Both characteristics descends around the same roll-off frequency, however the optimized characteristic is closer to the measurements than the case 2.

Furthermore, the optimization process was performed for the amplitude and the phase of the second scintillation event. Results for the amplitude model are displayed below.

T_{χ}	$f_{0\chi}$	p_{χ}
8.2428	4.0304	3.4493

Table 4.3. Parameters for the amplitude model for the second scintillation using *lsqcurvefit*

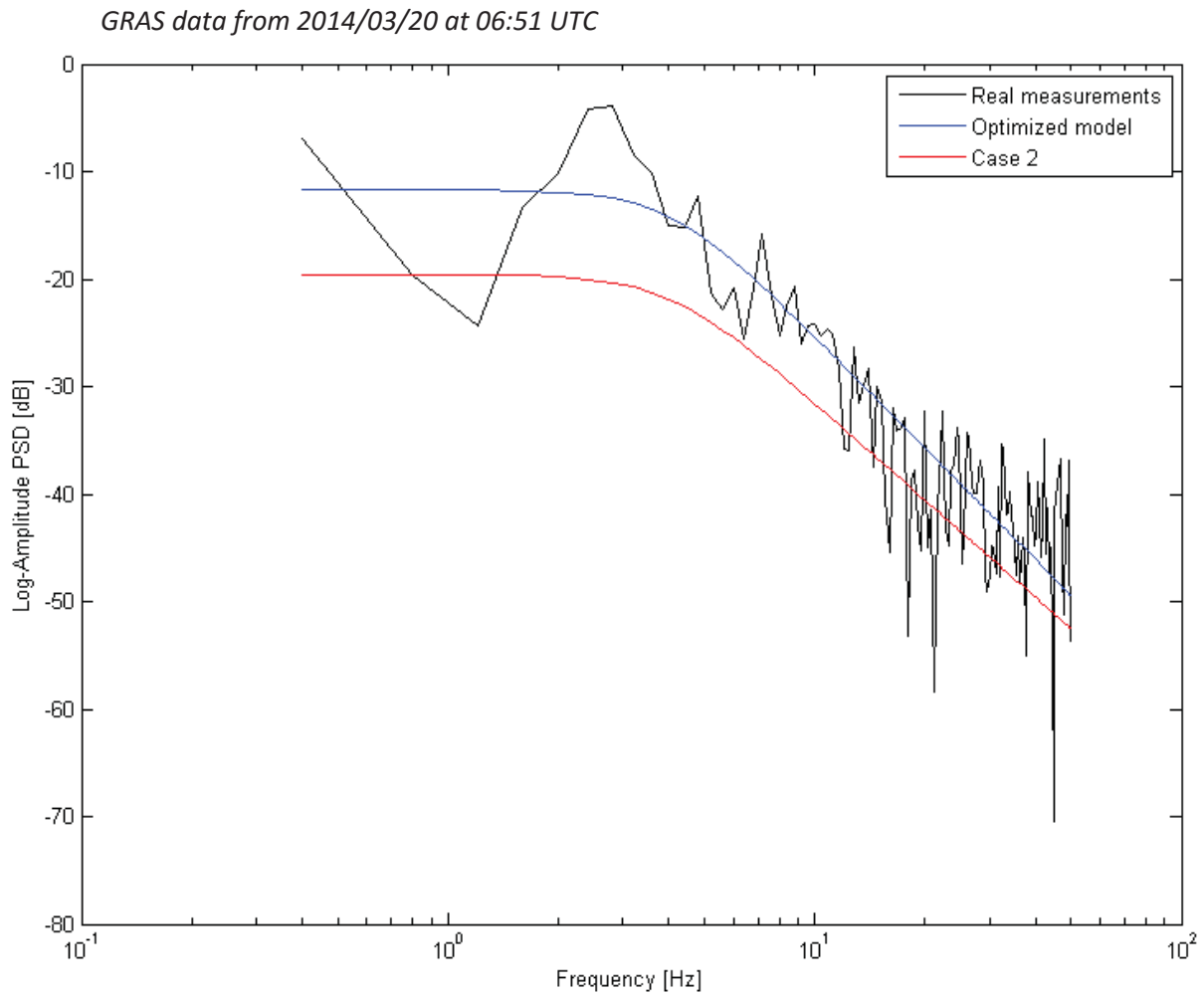


Figure 4.3. Optimization of the amplitude model for the second scintillation using *Isqcurvefit*

Despite of the calculated spectral strength, the model matches the scintillation event in every part of the characteristic. The roll-off frequency and slope of the PSD are also high but remain within their boundary values.

Results for the phase second scintillation are presented below (Table 4.4, Figure 4.4.).

T_{ϕ}	$f_{0\phi}$	p_{ϕ}
0.0136	0.9617	1.7986

Table 4.4. Parameters for the phase model for the second scintillation using *Isqcurvefit*

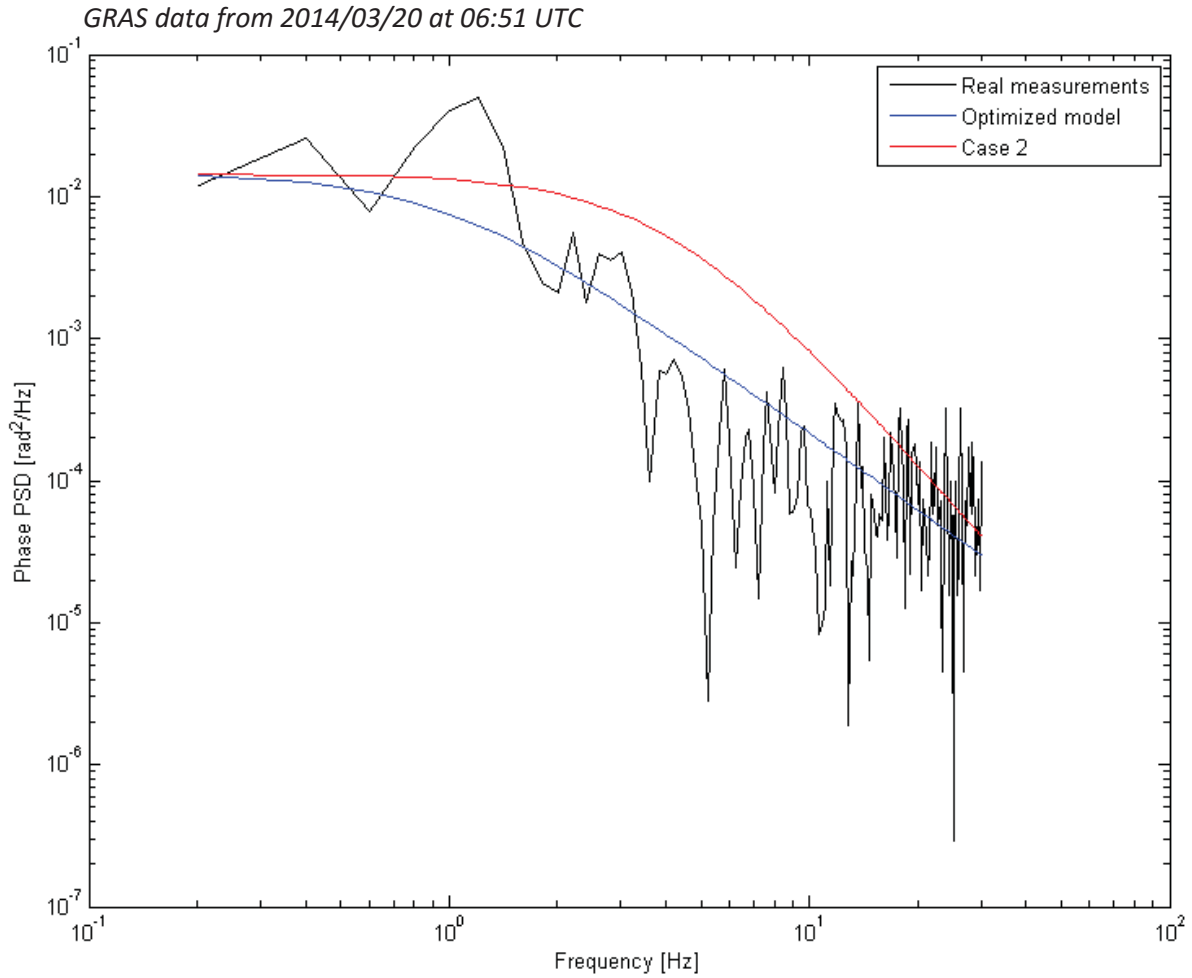


Figure 4.4. Optimization of the phase model for the second scintillation using *lsqcurvefit*

Values of the phase model for the second scintillation are lower than in the first case. The model fits in every part of the real characteristics and provides with better results than the model in the case 2.

Last results retrieved for the third amplitude scintillation are shown on Table 4.5. With those parameters Figure 4.5 were plotted.

T_χ	$f_{0\chi}$	p_χ
3.4329	6.0481	2.3377

Table 4.5. Parameters for the amplitude model for the third scintillation using *lsqcurvefit*

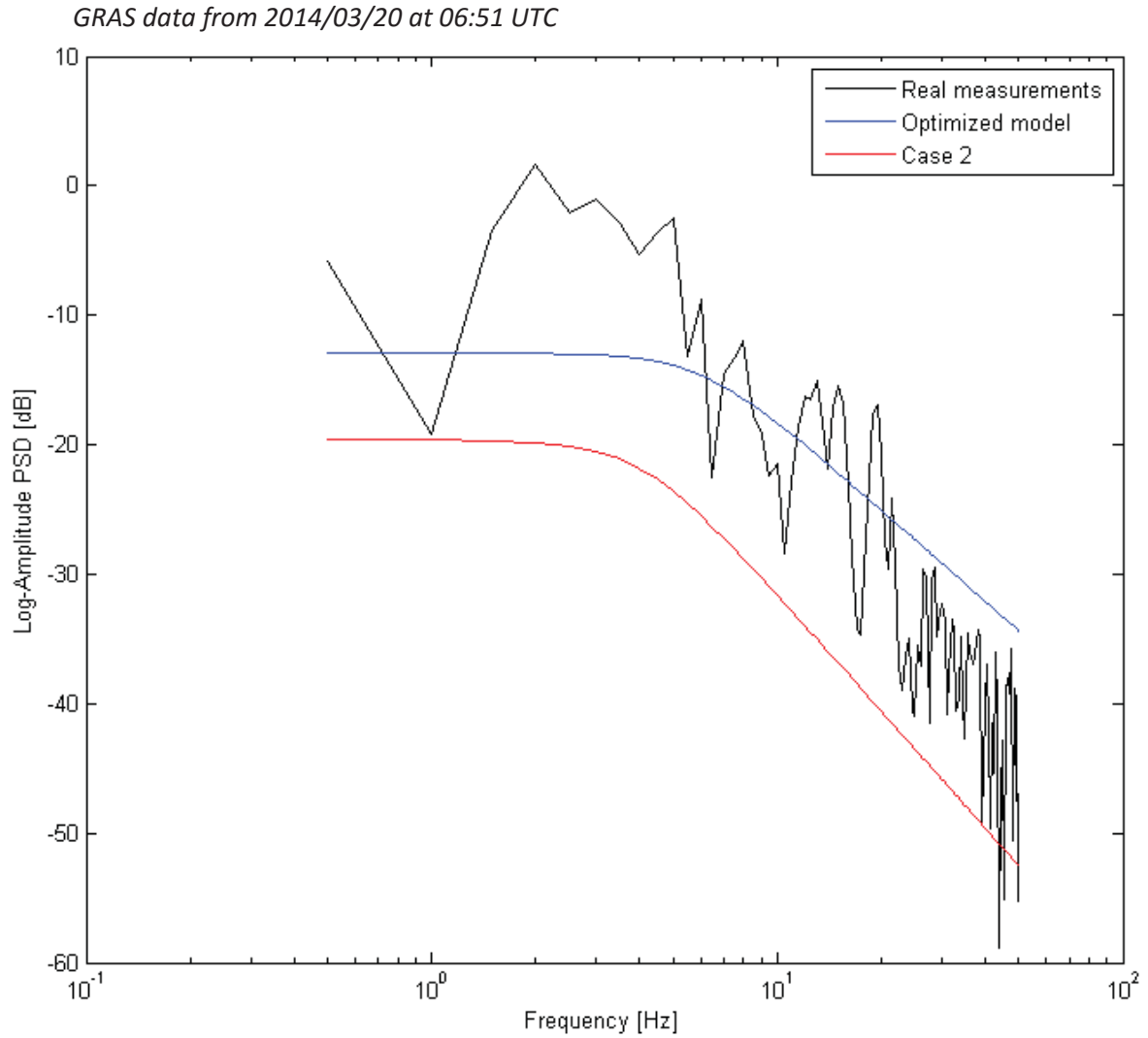


Figure 4.5. Optimization of the amplitude model for the third scintillation using *lsqcrvefit*

In this figure improvement can be seen in comparison with the model parameters given in case 2. Due to high variance of the PSD, the optimized model does not match the last part of the signal and consequently slope of the case 2 remains as more accurate. The results of the optimization process could be enhanced, however, as the project studies implied, the values of the parameters were highly above the boundaries. Within this boundaries the optimization function finds a comprise between the slope of the PSD and its magnitude, which is consequently presented in the thesis.

The optimised model characteristic for the amplitude and phase scintillation events using the *fminsearch* function are presented on the Figures 4.6 - 4.8. Calculated values of the model parameters are shown on Table 4.6.

T_x	f_{0x}	p_x
6.4464	4.1885	3.4135

Table 4.6. Parameters for the amplitude model for the second scintillation using fminsearch

Characteristic using the values in the table above are illustrated on the Figure 4.6.

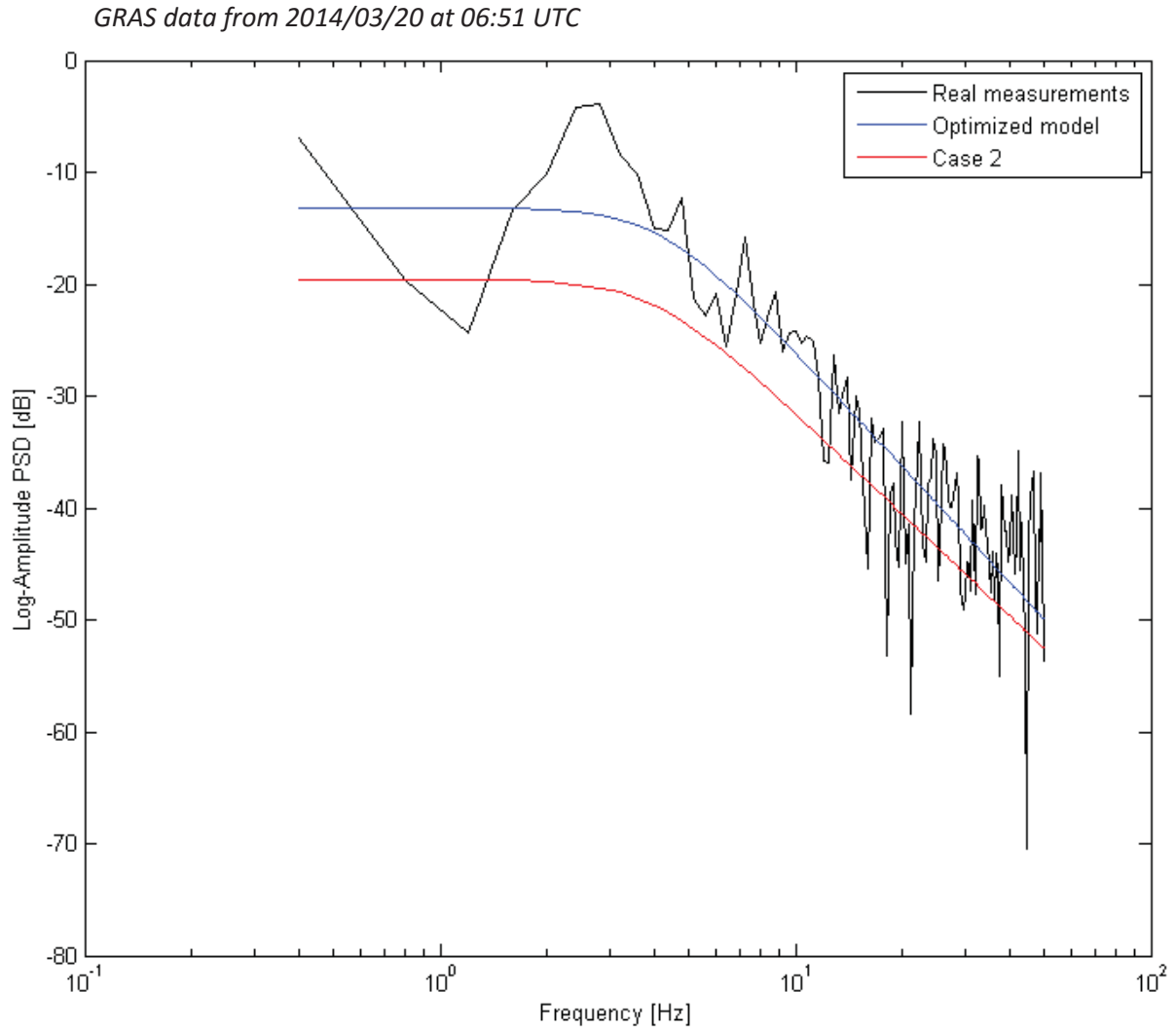


Figure 4.6. Optimization of the amplitude model for the second scintillation using fminsearch

As it can be seen in the figure above the fitting of the model for the second scintillation is almost perfect for the whole duration. The only problem lays in the value of the spectral magnitude, which is slightly above the average. It is connected to the high value of the amplitude in the first two peaks. The function finds the optimum fitting between them, which result in the spectral magnitude value.

Furthermore, the optimised parameters for the phase model third scintillation are presented in Table 4.7.

T_x	f_{0x}	p_x
2.1413	3.7531	2.0847

Table 4.7. Parameters for the amplitude model for the third scintillation using *fminsearch*

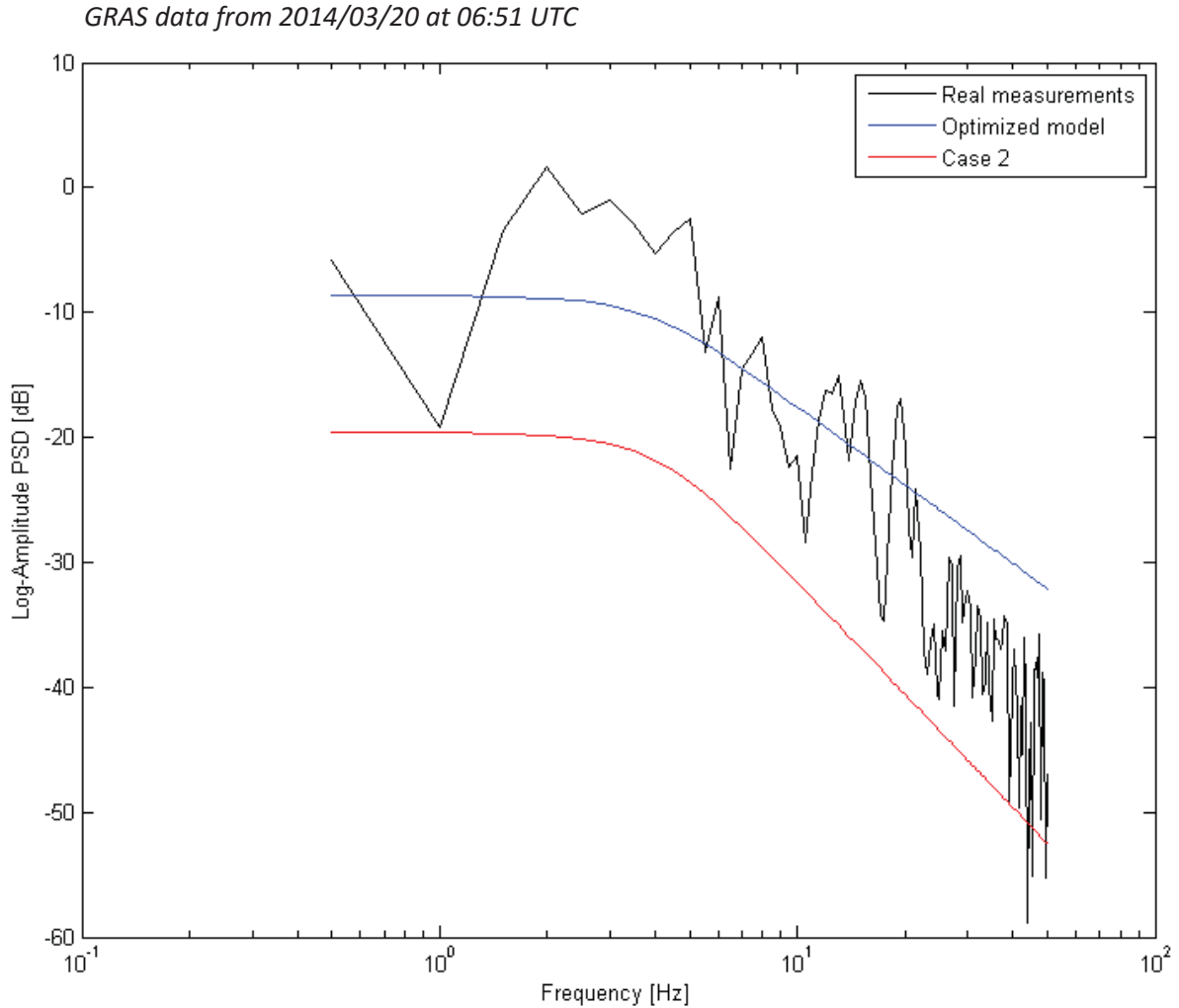


Figure 4.7. Optimization of the amplitude model for the third scintillation using *fminsearch*

The figure above reveal that the optimised model does not match the scintillation in its entire duration. The last part of the event is slightly under the model characteristics. The *fminsearch* function similarly to the previous function, calculated parameters which exceeded the boundary values. That is why it had to find a compromise in the parameters, when the boundaries were included. If the decreasing tendency of the scintillation was the same as the previous parts of the signal, it would result in very accurate slope value of the model.

The results of the phase model third scintillation optimization are presented on Table 4.8 and Figure 4.8.

T_ϕ	$f_{0\phi}$	p_ϕ
0.0061	0.8028	1.8974

Table 4.8. Parameters for the phase model for the third scintillation using *fminsearch*

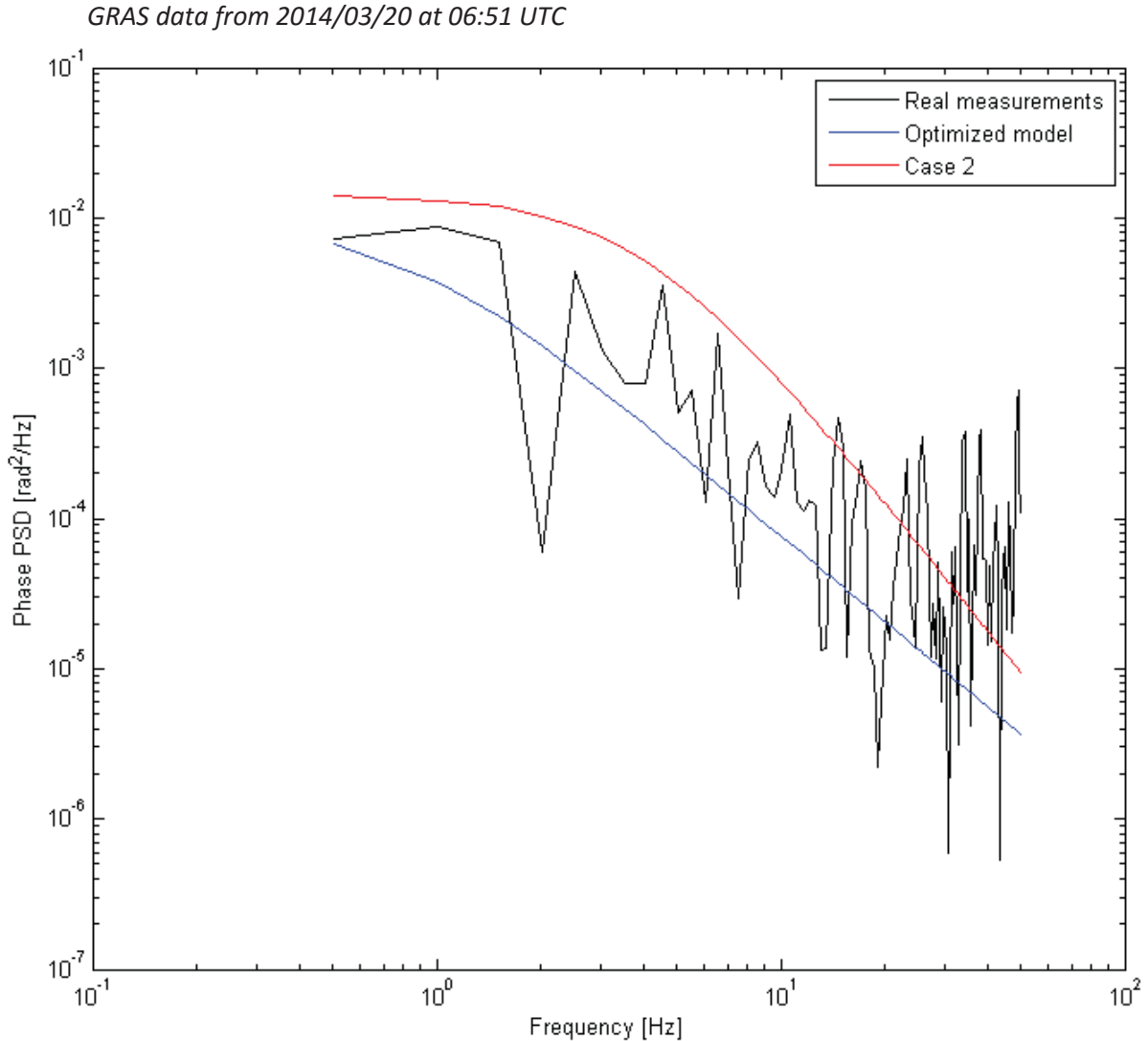


Figure 4.8. Optimization of the phase model for the third scintillation using *fminsearch*

The last optimization with the *fminsearch* function gave much better results than in case 2 scenario proposed by RUAG. The whole scintillation is correctly matched with the optimized phase.

Overall the optimization function *fminsearch* contributed with a set of reasonable results. Although in some cases the complexity of the signal was too high for the function to overcome. The number of iterations is few times greater than in the *lsqcurvefit* results. The reason of this huge difference lays in the sole purpose of this particular function. *Fminsearch* is not commonly used in data fitting problems.

The optimization process using *fminunc* was performed on each scintillation event. However, the best results were obtained for the phase scintillations whereas, the amplitude results were not satisfactory compared to previous optimization methods. Calculated values of the model for the first phase scintillation are presented in the Table 4.9.

T_ϕ	$f_{0\phi}$	p_ϕ
0.0236	1.412	1.7614

Table 4.9. Parameters for the phase model for the first scintillation using *fminunc*

Characteristics of this optimization are illustrated on the Figure 4.9.

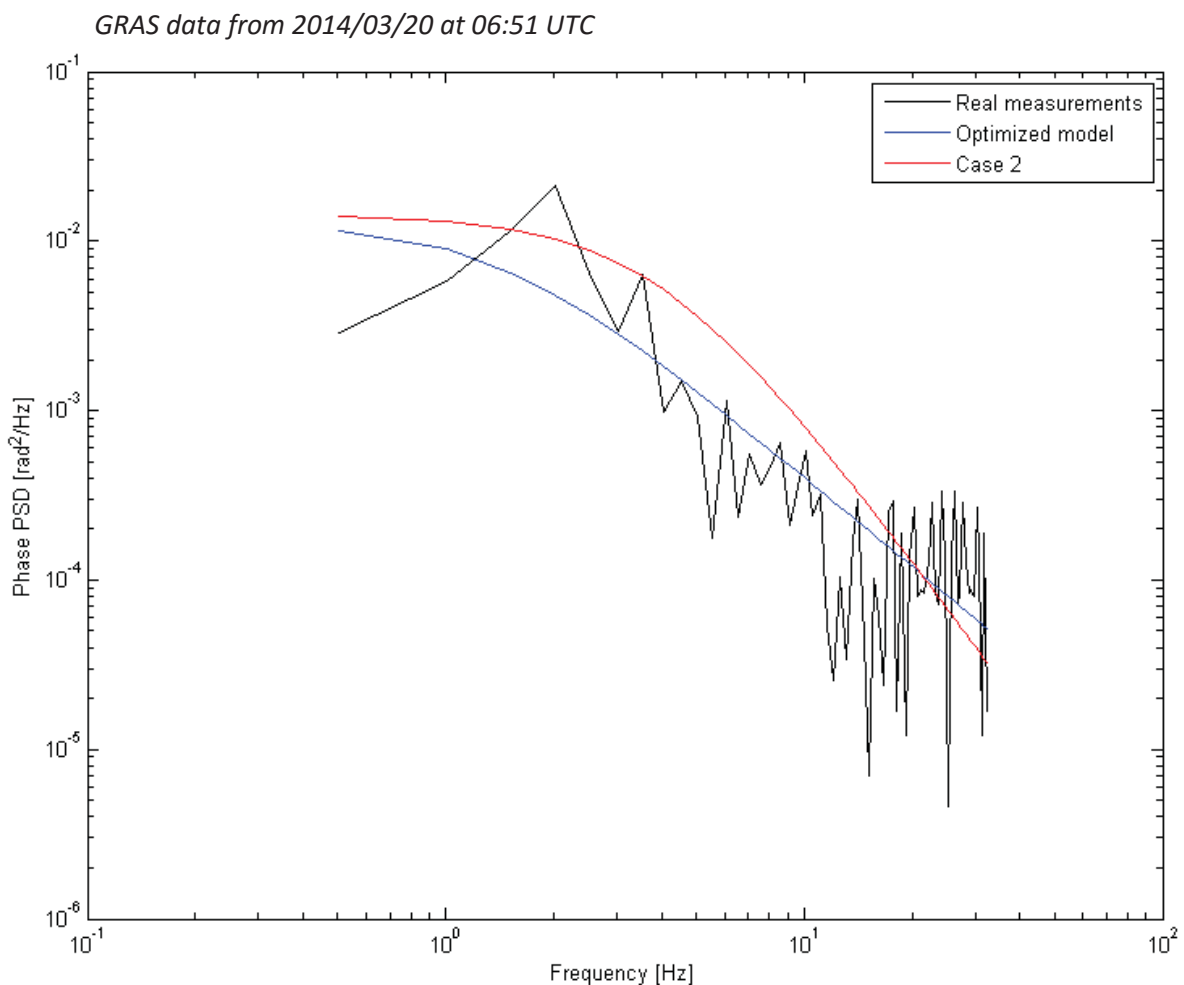


Figure 4.9. Optimization of the phase model for the first scintillation using *fminunc*

On the contrary, the optimization of the phase first scintillation gave satisfactory results. Due to less complex model than in the amplitude, the function was able to provide optimal values in few iterations. The characteristic resemble the scintillation event in its whole duration despite high level of variations.

The last optimization was performed for the third scintillation and the amplitude results are presented in Table 4.10 and Figure 4.10.

T_χ	$f_{0\chi}$	p_χ
1.5475	2.9784	1.9144

Table 4.10. Parameters for the amplitude model for the third scintillation using *fminunc*

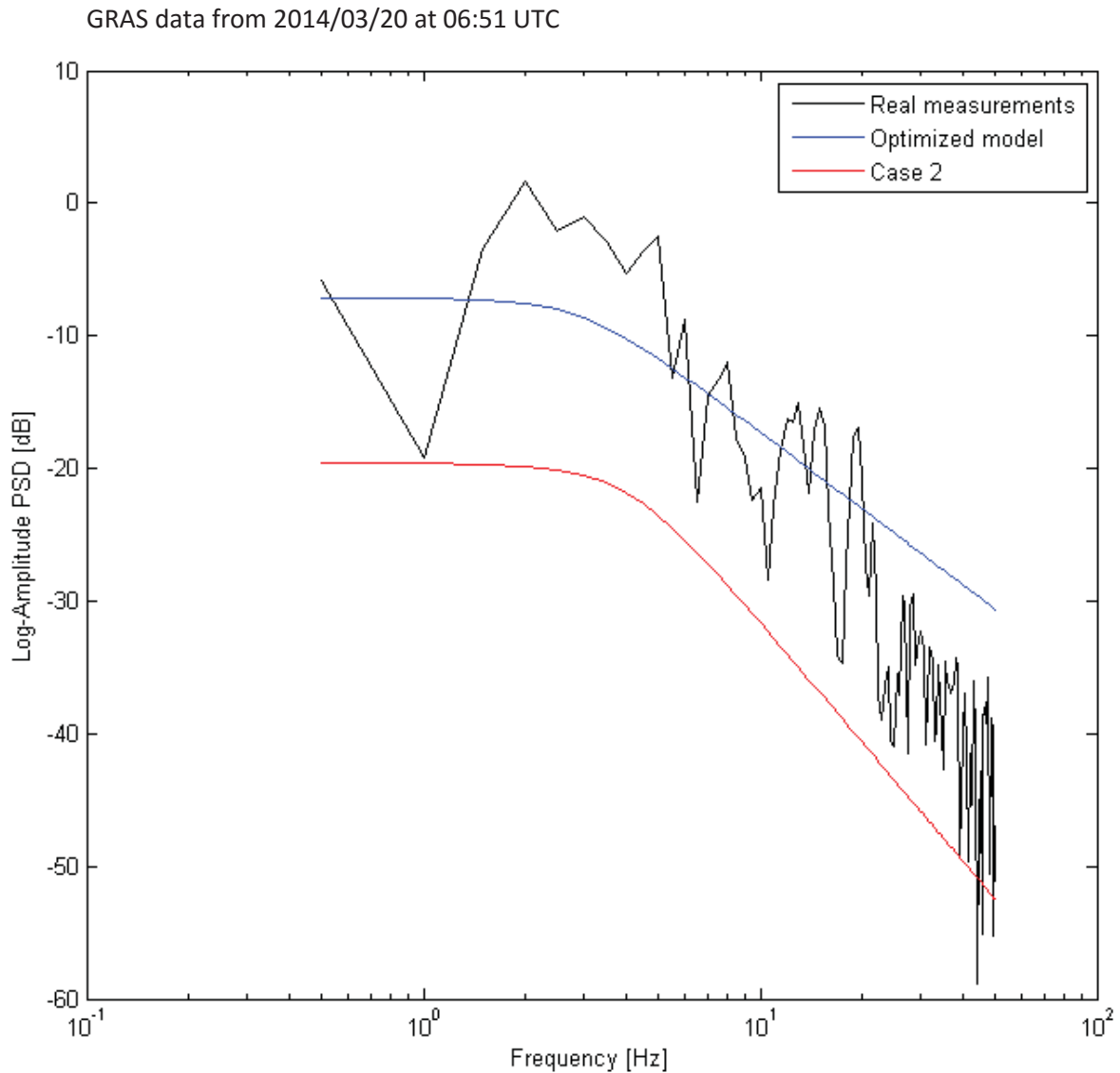


Figure 4.10. Optimization of the amplitude model for the third scintillation using *fminunc*

Figure above reveals similar problem, which occurred in previous optimization functions. It does not handle rapid changes in the decreasing tendency of the scintillation event, in the last part of the signal. Moreover, the slope could be more accurate, but the used algorithm

calculates coefficients, which values fairly exceed the boundaries. After applying boundaries it compromise the magnitude with the slope of the PSD.

The results of the last performed optimization can be seen on the Table 4.11 and the Figure 4.11.

T_ϕ	$f_{0\phi}$	p_ϕ
0.0091	1.543	1.5916

Table 4.11. Parameters for the phase model for the third scintillation using *fminunc*

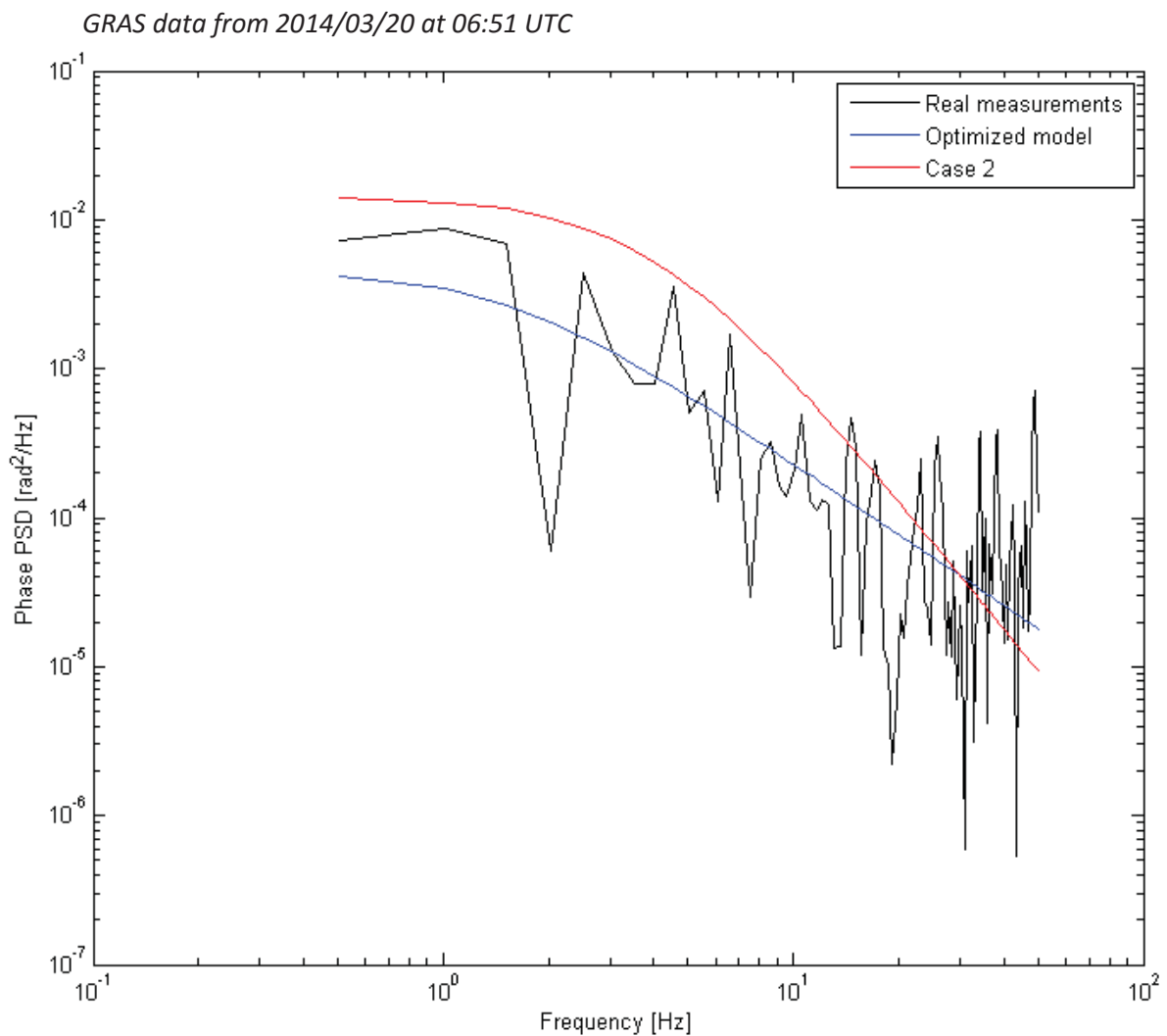


Figure 4.11. Optimization of the phase model for the third scintillation using *fminunc*

The last optimization achieved satisfactory results. As it can be seen in the figure above the characteristics match each other.

Overall the *fminunc* function gave solid results of optimization, but only for the phase model. Due to its less complexity, it was able to find the minimum of the function in few iterations.

Unfortunately the optimized amplitude model is barely acceptable. This optimization function is used for simple unconstrained problems and is not commonly used for data fitting solutions.

4.3 Comparative analysis of the results

To decide which approximation of the real data measurements is the most accurate, a MSE including different sets of the model parameters has been calculated. By comparing the MSE values retrieved from various optimization methods for each individual scintillation event, efficiency of these functions can be evaluated. The results for the first amplitude scintillation are shown in the table below.

MSE retrieved from case 2 [dB ²]	MSE retrieved from <i>lsqcurvefit</i> [dB ²]
116.8341	34.8029

Table 4.12. MSE obtained after optimization for the first amplitude scintillation event.

For the first amplitude scintillation, 34,8029 is the lowest value of an error, which has been derived from *lsqcurvefit* function. It indicated the best set of parameters among all the optimization functions and allowed to achieve more than three times less MSE value than the case 2 proposed by RUAG Space. Furthermore, the results for the second amplitude scintillation are presented in the Table 4.13.

MSE retrieved from case 2 [dB ²]	MSE retrieved from <i>fminsearch</i> [dB ²]	MSE retrieved from <i>lsqcurvefit</i> [dB ²]
60.0655	37,836	37,562

Table 4.13. MSE obtained after optimization for the second amplitude scintillation event.

In the second amplitude scintillation *lsqcurvefit* has also achieved the highest accuracy among all optimized models. Although, *fminsearch* gave very similar MSE values. The MSE values retrieved from both *lsqcurvefit* and *fminsearch* are almost twice lower than in case 2. Comparing their figures (Fig. 4.3 and 4.6), the similarity can be seen as well. The results for the last amplitude scintillation are displayed in the table below.

MSE retrieved from case 2 [dB ²]	MSE retrieved from <i>fminsearch</i> [dB ²]	MSE retrieved from <i>fminunc</i> [dB ²]	MSE retrieved from <i>lsqcurvefit</i> [dB ²]
164.3354	92,064	107,431	76.1281

Table 4.14. MSE obtained after optimization the third amplitude scintillation event.

On the other hand, one of the optimization method biggest flaws has been revealed in the third amplitude scintillation. Sudden changes in the decreasing tendency of the measurement, result in more thorough calculations in the algorithms, including *lsqcurvefit*. Due to these changes the optimization functions calculated magnitude, which highly exceeded the boundary values. It had to find a compromise between the magnitude and the slope of the characteristics within the boundaries of the parameter values. Nevertheless, the obtained results were better than the set of case 2 parameters in every optimizations process.

The first phase scintillation event MSE results are presented in the Table 4.15.

MSE retrieved from case 2 $\left[\left(\frac{\text{rad}^2}{\text{Hz}}\right)^2\right]$	MSE retrieved from <i>fminunc</i> $\left[\left(\frac{\text{rad}^2}{\text{Hz}}\right)^2\right]$	MSE retrieved from <i>lsqcurvefit</i> $\left[\left(\frac{\text{rad}^2}{\text{Hz}}\right)^2\right]$
1,284 x 10 ⁻⁵	1,272 x 10 ⁻⁵	1,085 x 10⁻⁵

Table 4.15. MSE obtained after optimization for the first phase scintillation event.

The phase model approximation has proceeded with accurate results as well. In the first phase scintillation, *fminunc* and *lsqcurvefit* have better fitting based on the MSE than case 2. Both functions matched the scintillation in its entire duration and were more precise. However, the *lsqcurvefit* provided with the most optimal set of parameters, since the MSE was the lowest among all. Further MSE results for the second scintillation event are displayed in the table below.

MSE retrieved from case 2 $\left[\left(\frac{\text{rad}^2}{\text{Hz}}\right)^2\right]$	MSE retrieved from <i>lsqcurvefit</i> $\left[\left(\frac{\text{rad}^2}{\text{Hz}}\right)^2\right]$
3.7034 x 10 ⁻⁵	3,6396 x 10⁻⁵

Table 4.16. MSE obtained after optimization for the second phase scintillation event.

In the second phase scintillation similar situation occurs as in the first phase scintillation. However, the case 2 matched the scintillation more accurately than in the previous scintillation. Nonetheless, the *lsqcurvefit* calculated more optimized values for the scintillation model and achieved lesser MSE than case 2. The third phase scintillation results are presented in the Table 4.17.

MSE retrieved from case 2 $\left[\left(\frac{\text{rad}^2}{\text{Hz}}\right)^2\right]$	MSE retrieved from <i>fminsearch</i> $\left[\left(\frac{\text{rad}^2}{\text{Hz}}\right)^2\right]$	MSE retrieved from <i>fminunc</i> $\left[\left(\frac{\text{rad}^2}{\text{Hz}}\right)^2\right]$	MSE retrieved from <i>lsqcurvefit</i> $\left[\left(\frac{\text{rad}^2}{\text{Hz}}\right)^2\right]$
$5,408 \times 10^{-6}$	$1,583 \times 10^{-6}$	$0,969 \times 10^{-6}$	$1,634 \times 10^{-6}$

Table 4.17. MSE obtained after optimization for the third phase scintillation event.

The last comparison of the MSE values confirmed the usability of the optimization process. Among all optimization methods the lowest MSE was achieved by *fminunc* and reached over 5 times lower values than the case 2 model.

To sum up, the approximation process performed in this project revealed a lot of advantages of using Matlab optimization toolbox. First of all, it allowed to solve the problem of model fitting to data measurements. Furthermore, it allowed to obtain proper sets of parameters, which can be furtherly used. Considering the fitting capability and values of MSE, *lsqcurvefit* function calculated the most accurate parameters of the model, surpassing previous case 2 model, thus the RUAG case 1 and 3 as well. The only flaw of this function appeared in the third amplitude scintillation, where it had more difficulties in finding the compromise between the parameters due to high irregularity of the measurement. Moreover, function *fminsearch*, due to the complexity of the problem, gave slightly worse results than *lsqcurvefit*. *Fminunc* was also overwhelmed by the nonlinearity of the model, especially in the amplitude. The phase results were satisfying in terms of the MSE value as well as the data fitting.

Consequently to this section, further data analysis with different GRAS data samples will be conducted using the *lsqcurvefit* optimization function, since it gave the best results among other functions

4.4 Optimization based on further GRAS data

In this subchapter further GRAS data analysis was performed. Among over 2000 data files, which have been analyzed, 15 occurrences of strong scintillations were found. The optimization process using *lsqcurvefit* was conducted for each individual scintillation event. Table containing results of the optimization and MSE value, retrieved between the model and measurements are shown in the Tables 4.18 and 4.19.

GRAS data time (UTC)	T_x	f_{0x}	p_x	MSE [dB ²]	Case 2 MSE [dB ²]
2014-03-20 06:51	3.3193	2.3854	2.9522	34.8029	116.8341
2014-03-20 06:51	8.2428	4.0304	3.4493	37,562	60.0655
2014-03-20 06:51	3.4329	6.0481	2.3377	76.1281	164.3354

2014-03-15, 14:21	11.8643	8.9087	2.9555	72.8414	132.6377
2014-03-17, 00:06	3.1625	1.0575	2.3468	55.3875	162.1943
2014-03-15, 04:15	2.403	0.7266	2.4645	74.5040	121.9034
2014-03-16, 20:42	3.5235	1.3437	1.9198	98.2420	259.8360
2014-03-18, 18:18	3.0155	1.5397	2.8510	59.5718	83.7924
2014-03-19, 06:15	1.3598	0.842	2.5387	61.8181	89.5575
2014-03-19, 06:15	7.0682	2.6707	2.8789	66.6680	106.5323
2014-03-19, 09:39	2.4202	1.4932	1.4458	103.8089	456.2001
2014-03-19, 21:21	1.1504	0.4052	2.0078	45.6418	258.2823
2014-03-19, 23:03	3.2195	2.9187	2.6775	77.4674	107.5855
2014-03-20, 22:42	1.2929	0.8920	2.0959	63.0091	163.8500
2014-03-21, 03:51	1.1706	5.444	1.9585	50.3146	246.7120
2014-03-21, 22:21	0.9884	1.4983	2.4096	39.1306	94.8693
2014-03-24, 11:15	2.2559	1.4691	1.8541	58.5909	288.1247
2014-03-24, 16:15	1.2457	2.8464	1.873	106.6140	255.8493

Table 4.18. Optimization results using *lsqcurvefit* for further amplitude scintillation events

GRAS data time (UTC)	T_ϕ	$f_{0\phi}$	p_ϕ	MSE $\left[\left(\frac{\text{rad}^2}{\text{Hz}}\right)^2\right]$	Case 2 MSE $\left[\left(\frac{\text{rad}^2}{\text{Hz}}\right)^2\right]$
2014-03-20 06:51	1.3461	4.8605	3.1626	1,085e-05	1,284e-05
2014-03-20 06:51	0.0136	0.9617	1.7986	3,6396e-05	3.7034e-05
2014-03-20 06:51	0.0091	1.543	1.5916	0,969e-06	5,408e-05
2014-03-15, 14:21	0.006	0.8958	1.4687	2.5481e-05	4.4143e-05
2014-03-17, 00:06	0.0306	5.04	1.9195	0.0016	0.0024
2014-03-15, 04:15	0.1413	3.0242	2.7169	0.0021	0.0040
2014-03-16, 20:42	0.1359	2.2552	2.4224	1.6189e-04	1.6389e-04
2014-03-18, 18:18	0.0343	2.1765	2.2311	0.0088	0.0102
2014-03-19, 06:15	0.0124	0.124	1.6718	0.0136	0.0172
2014-03-19, 06:15	0.067	1.71	2.7293	0.0203	0.0333
2014-03-19, 09:39	0.5698	0.4203	1.4365	0.0710	0.0917
2014-03-19, 21:21	0.3685	3.3734	3.1485	2.7503e-05	4.0701e-05
2014-03-19, 23:03	0.1485	0.6062	1.9178	0.1931	0.2009
2014-03-20, 22:42	1.6932	6.8713	3.0961	0.0035	0.0050
2014-03-21, 03:51	0.6606	3.5667	2.9063	7.8125e-05	7.9729e-05
2014-03-21, 22:21	0.0898	2.6243	2.6211	0.0080	0.0111
2014-03-24, 11:15	2.2979	0.5503	3.7597	21.2350	24.8426
2014-03-24, 16:15	3.6419	5.0852	3.3920	1.8883e-04	1.9135e-04

Table 4.19. Optimization results using *lsqcurvefit* for further phase scintillation events

As it can be seen in the results above, for each scintillation event, the model has been optimized, giving a better sets of model parameters in the terms of data fitting and MSE. The difference of optimization performance vary, among all conducted calculations. Some of the examples indicate much better results, whereas other gave slightly corrected parameters. In the case of phase optimization, the changes of mean square errors are very minor. It is due to the fact that the values of the phase are small in compare to the values of amplitude. However, even small changes in the MSE are very visible on the plots. Few examples of the results are presented in the figures below.

One of the resulting set of parameters for an amplitude scintillation are shown in the Table 4.20.

T_{χ}	$f_{0\chi}$	p_{χ}	MSE [dB^2]	Case 2 MSE [dB^2]
3.1625	1.0575	2.3468	55.3875	162.1943

Table 4.20. Optimization results for the amplitude from 2014/03/17 at 00:06 UTC

The respective characteristics for this set of parameters are presented in the Figure 4.12.

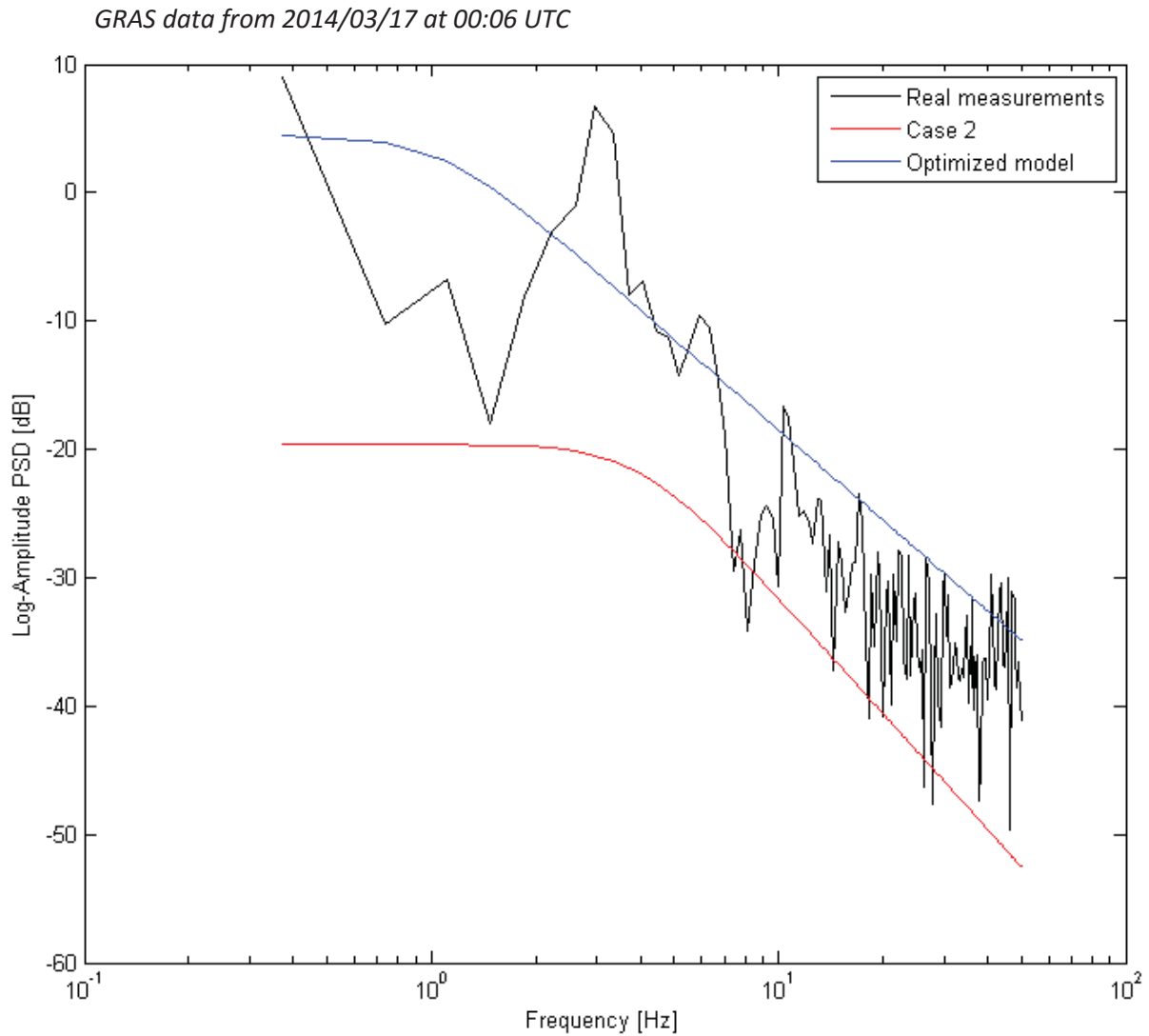


Figure 4.12. Optimization of the amplitude model from 2014/03/17 at 00:06 UTC

The figure above reveals a large difference between the optimized model and the case 2 model. The magnitude of the model proposed by RUAG is much lower and does not match the scintillation. Level of the optimized model magnitude fits the real scintillation and results in more than 3 times lower MSE value.

The next set of parameters and corresponding MSE values are displayed in the Table 4.21.

T_{ϕ}	$f_{0\phi}$	p_{ϕ}	$\text{MSE}\left[\left(\frac{\text{rad}^2}{\text{Hz}}\right)^2\right]$	Case 2 $\text{MSE}\left[\left(\frac{\text{rad}^2}{\text{Hz}}\right)^2\right]$
0.1413	3.0242	2.7169	0.0021	0.0040

Table 4.21. Optimization results for the phase from 2014/03/15 at 04:15 UTC

The characteristics for this set of parameters are presented in the Figure 4.13.

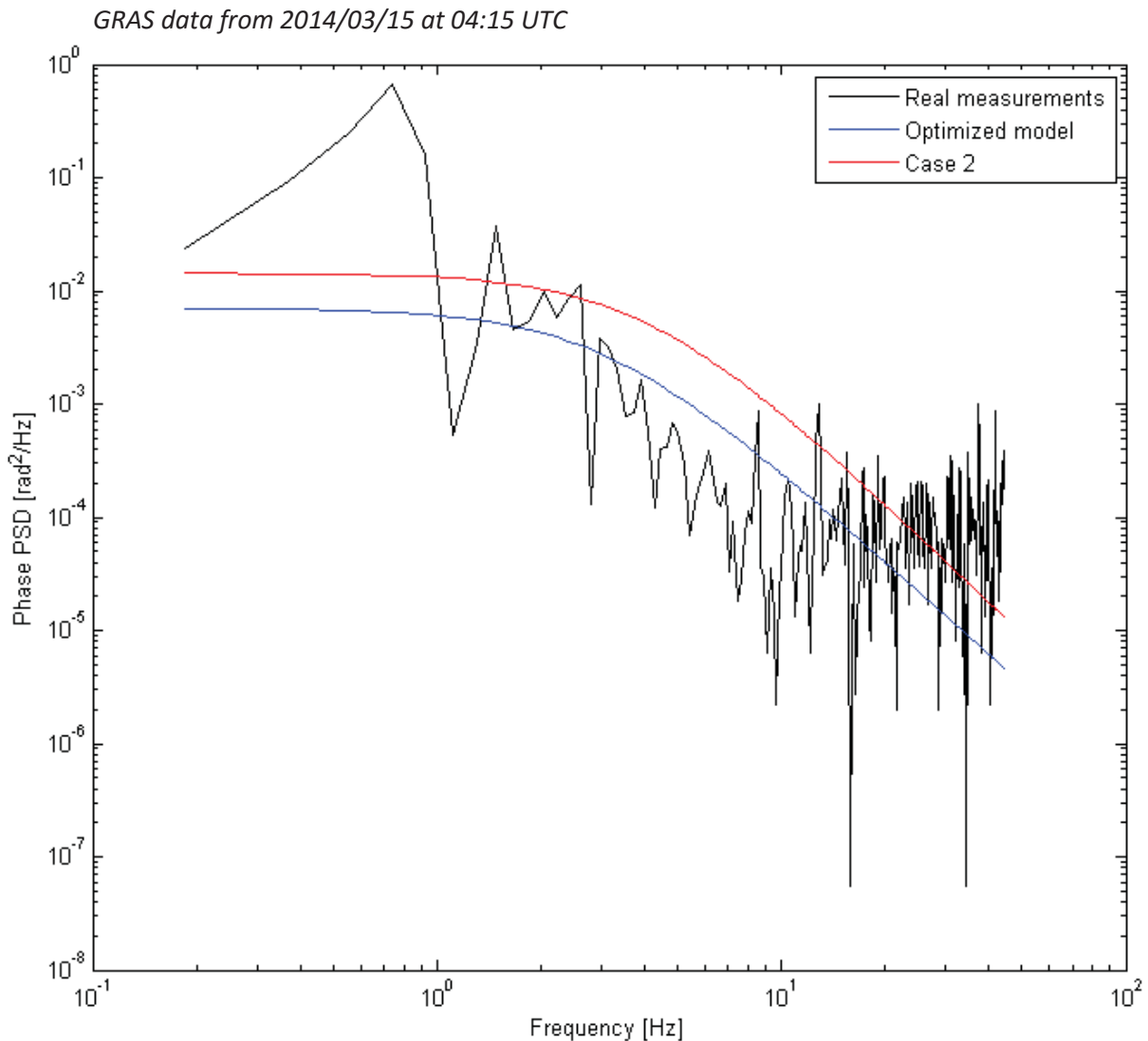


Figure 4.13. Optimization of the phase model from 2014/03/15 at 04:15 UTC

In this particular plot, slight improved can be seen. The case 2 models magnitude is higher than in the optimized model. Even though, both characteristics look quite similar, the one obtained from the optimization process provides a better fitting. The roll-off frequency, as well as the slope of the PSD are well positioned. The MSE also proves that the model matches the scintillation event. Its value is almost twice smaller than the case 2 MSE.

Furthermore, another set of parameters and their plots are presented in the Table 4.22 and Figure 4.14.

T_ϕ	$f_{0\phi}$	p_ϕ	$\text{MSE}\left[\left(\frac{\text{rad}^2}{\text{Hz}}\right)^2\right]$	Case 2 $\text{MSE}\left[\left(\frac{\text{rad}^2}{\text{Hz}}\right)^2\right]$
0.1359	2.2552	2.4224	1.6189e-04	1.6389e-04

Table 4.22. Optimization results for the phase from 2014/03/16 at 20:42 UTC

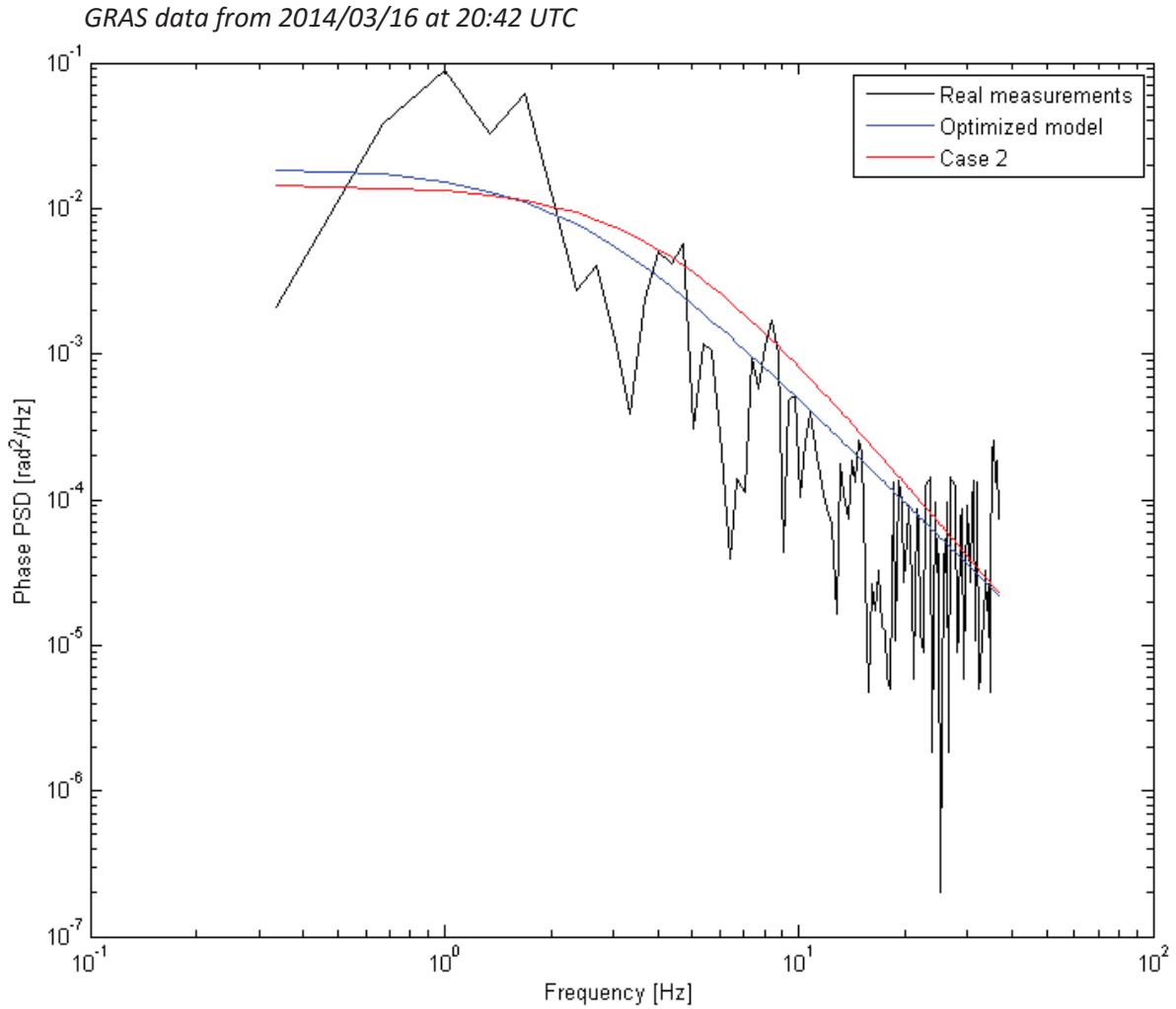


Figure 4.14. Optimization of the phase model from 2014/03/16 at 20:42 UTC

This is another example of a successful optimization. While the MSE of the optimized model slightly differs from the case 2 model, the plots reveal differences. The slope of the PSD is well preserved and matches the scintillation in its whole duration, whereas, the roll-off frequency is in the same position as the descend of the scintillation event. The magnitude of both characteristics are on very similar level.

The next optimization process was performed in the amplitude of the signal and its results are shown in the table below.

T_x	f_{0x}	p_x	MSE [dB ²]	Case 2 MSE [dB ²]
7.0682	2.6707	2.8789	66.6680	106.5323

Table 4.23. Optimization results for the amplitude from 2014/03/19 at 06:15 UTC

The characteristic for this set is presented in the Figure 4.15.

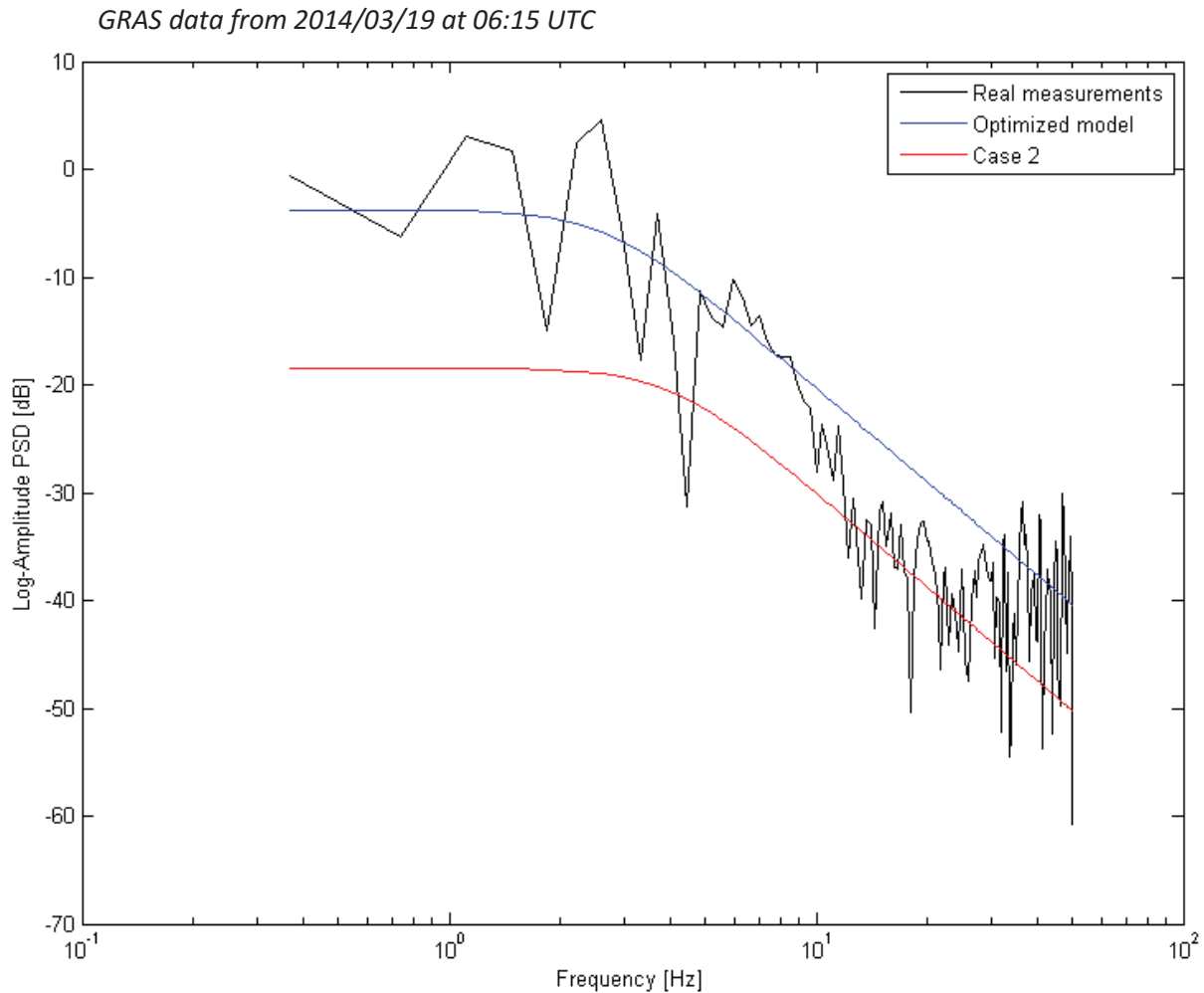


Figure 4.15. Optimization of the amplitude model from 2014/03/19 at 06:15 UTC

The scintillation event, which can be seen above, is quite irregular. Due to a sudden change of its amplitude in the last part of the signal, the optimized model does not fully match the scintillation in that part of characteristic. On the other hand, every coefficient of the model is well optimized. The magnitude is on the correct level and the roll-off frequency as well. The slope of the PSD descends similarly to the measurement data. It results in a much lower MSE value than in the case 2 model.

Further data analysis was conducted and its results are presented in Table 4.24.

T_ϕ	$f_{0\phi}$	p_ϕ	MSE $\left[\left(\frac{\text{rad}^2}{\text{Hz}}\right)^2\right]$	Case 2 MSE $\left[\left(\frac{\text{rad}^2}{\text{Hz}}\right)^2\right]$
0.3685	3.3734	3.1485	2.7503e-05	4.0701e-05

Table 4.24. Optimization results for the phase from 2014/03/19 at 21:21 UTC

GRAS data from 2014/03/19 at 21:21 UTC

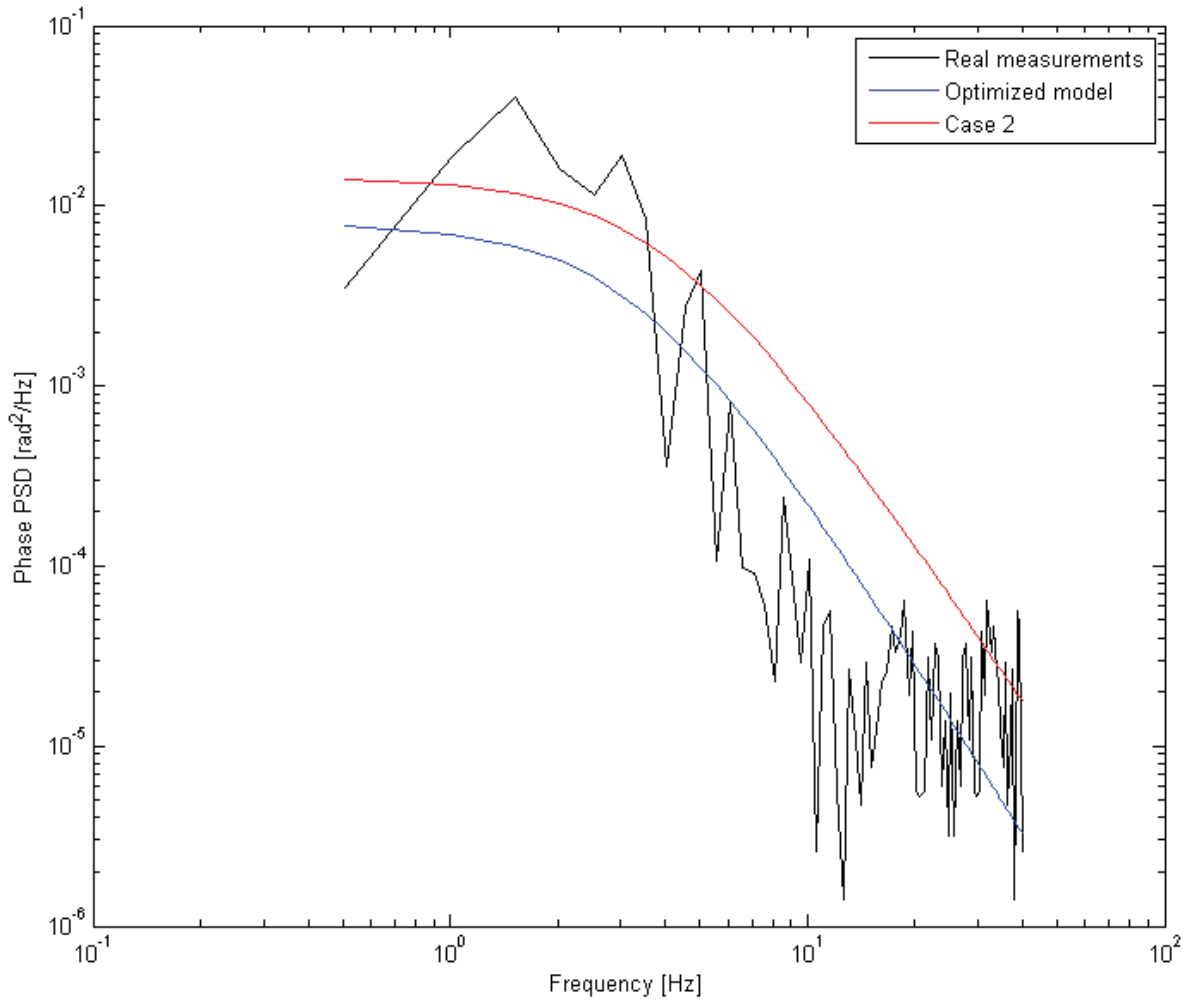


Figure 4.16. Optimization of the phase model from 2014/03/19 at 21:21 UTC

As it can be seen in the figure above, this optimization process was successful as well. The optimized model has the proper magnitude and roll-off frequency causing the characteristic match the scintillation event. The case 2 model is positioned slightly higher, resulting in a poorly fitted PSD slope, while the slope of the optimized model descends with the measurement data.

The next calculated values of the coefficients are presented in the table below. The results are shown in the Fig. 4.17.

T_{χ}	$f_{0\chi}$	p_{χ}	MSE [dB^2]	Case 2 MSE [dB^2]
1.1706	5.444	1.9585	50.3146	246.7120

Table 4.25. Optimization results for the amplitude from 2014/03/21 at 03:51 UTC

GRAS data from 2014/03/21 at 03:51 UTC

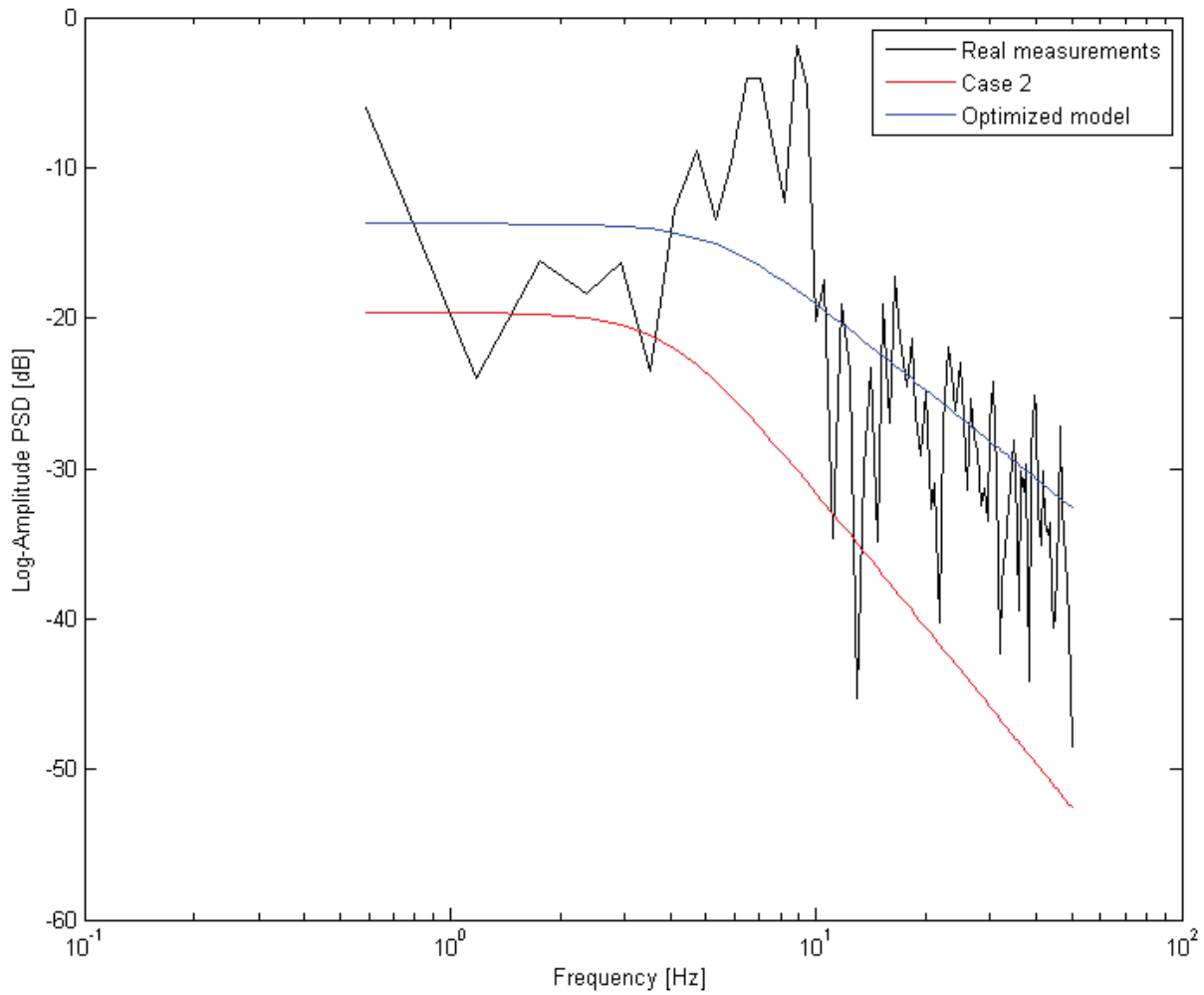


Figure 4.17. Optimization of the amplitude model from 2014/03/21 at 03:51 UTC

This calculation is most likely the best example of the superiority of optimization over stiff parameter selection. Optimization handled the scintillation almost perfectly. It found a satisfactory compromise between all the parameters. As a result, the magnitude, roll-off frequency and PSD slope matches the scintillation during the whole length of the signal. Whereas, the case 2 model does not fit the scintillation in any terms. The difference can also be seen in the MSE of the characteristics. The optimized model's MSE is almost 5 times lower than case 2, which proves its dominance.

The results for the phase optimization for the same scintillation sample are shown in the Table 4.26 and in the Fig. 4.18.

T_ϕ	$f_{0\phi}$	p_ϕ	$\text{MSE} \left[\left(\frac{\text{rad}^2}{\text{Hz}} \right)^2 \right]$	Case 2 $\text{MSE} \left[\left(\frac{\text{rad}^2}{\text{Hz}} \right)^2 \right]$
0.6606	3.5667	2.9063	7.8125e-05	7.9729e-05

Table 4.26. Optimization results for the phase from 2014/03/21 at 03:51 UTC

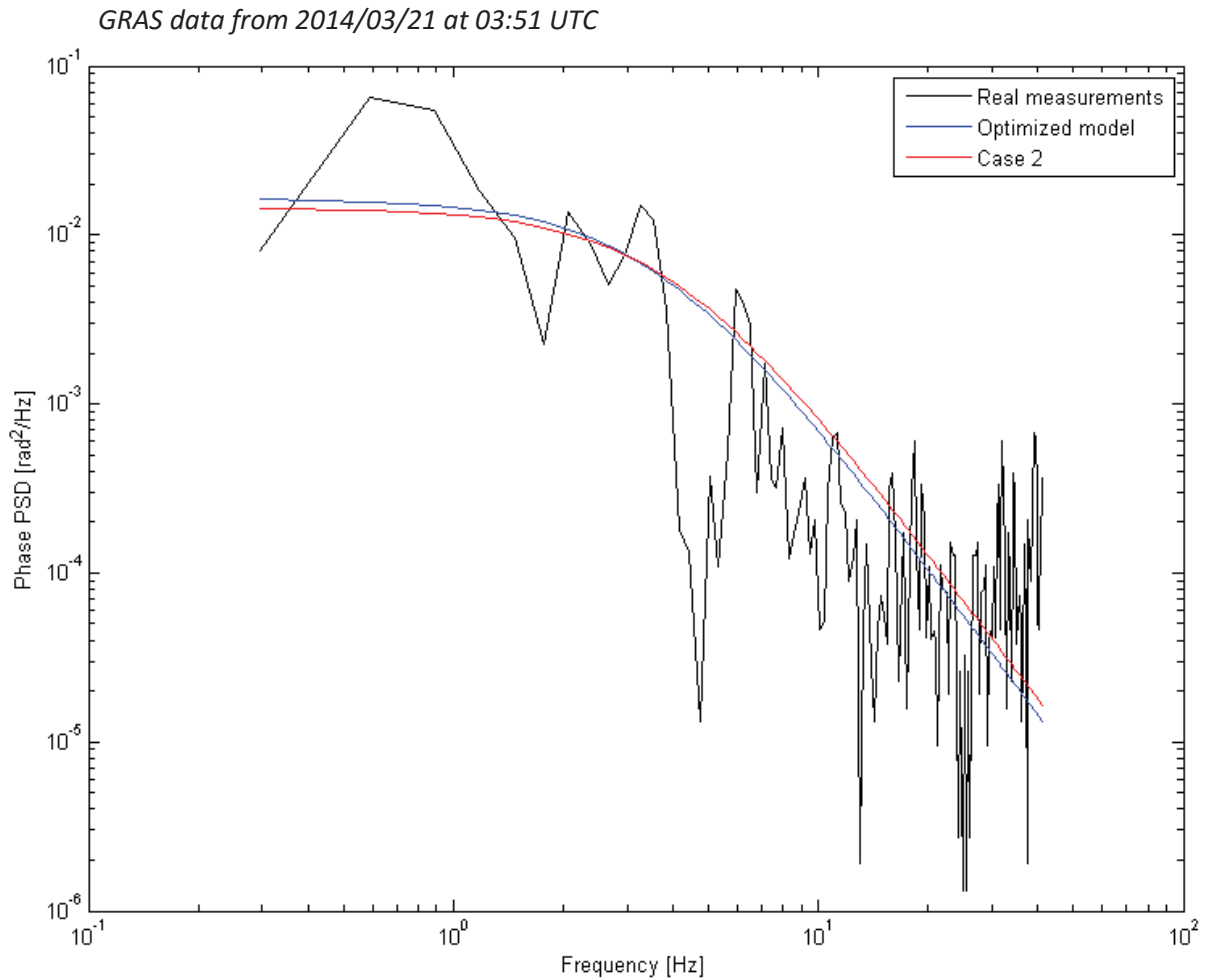


Figure 4.18. Optimization of the phase model from *2014/03/21 at 03:51 UTC*

On the other hand, in the phase, the optimization slightly improved the model for this particular scintillation. The magnitude and the roll-off frequency is very similar to the one in case 2 characteristic. However, the difference lays in the slope of the PSD. In the optimized plot, the slope is closer to the measurement data. This concludes that the case 2 model was not far from being optimal for this particular scintillation event.

The next amplitude results are displayed in the Table 4.27. The plots are shown in the Figure 4.19.

T_{χ}	$f_{0\chi}$	p_{χ}	MSE [dB^2]	Case 2 MSE [dB^2]
0.9884	1.4983	2.4096	39.1306	94.8693

Table 4.27. Optimization results for the amplitude from *2014/03/21 at 22:21 UTC*

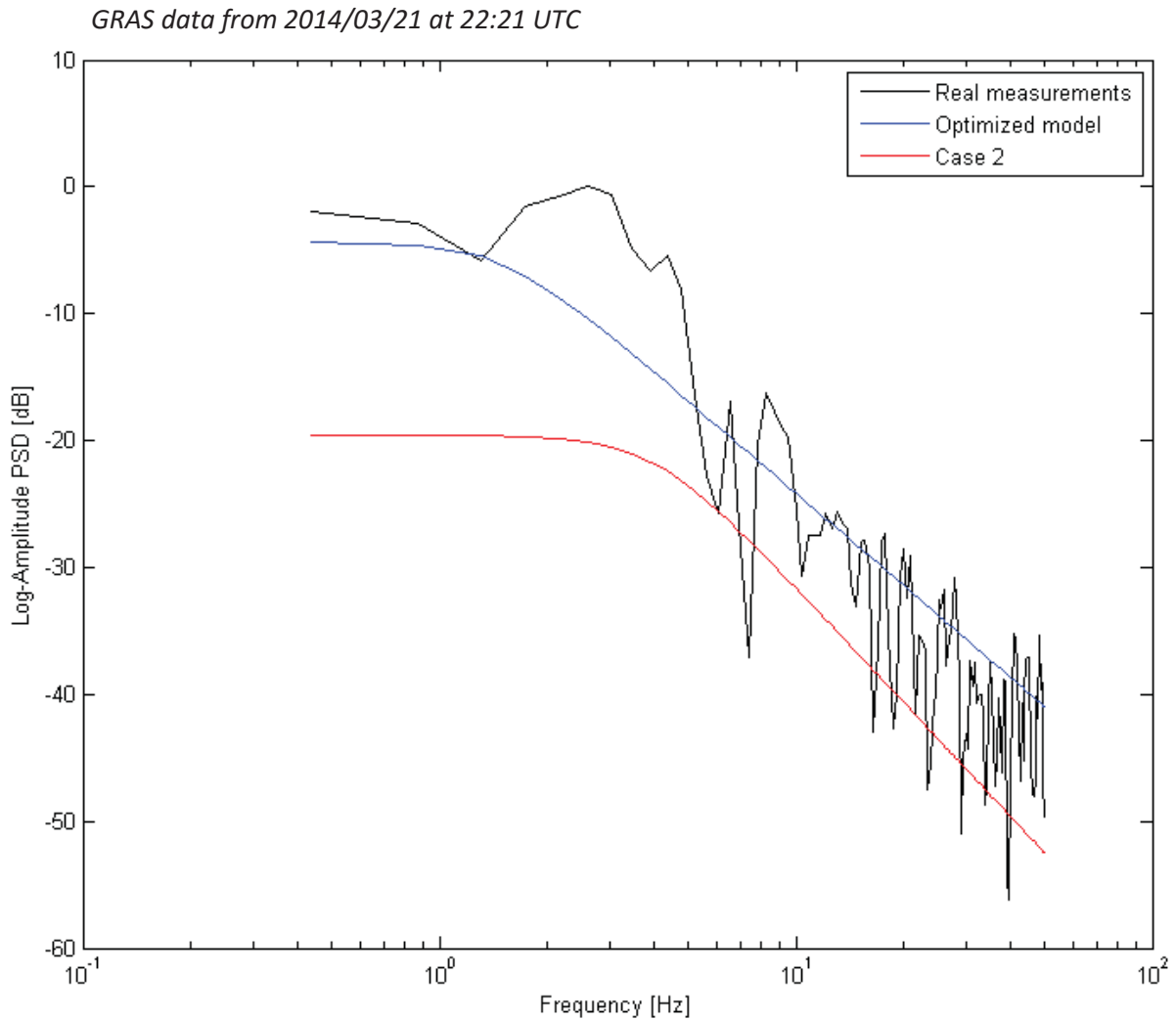


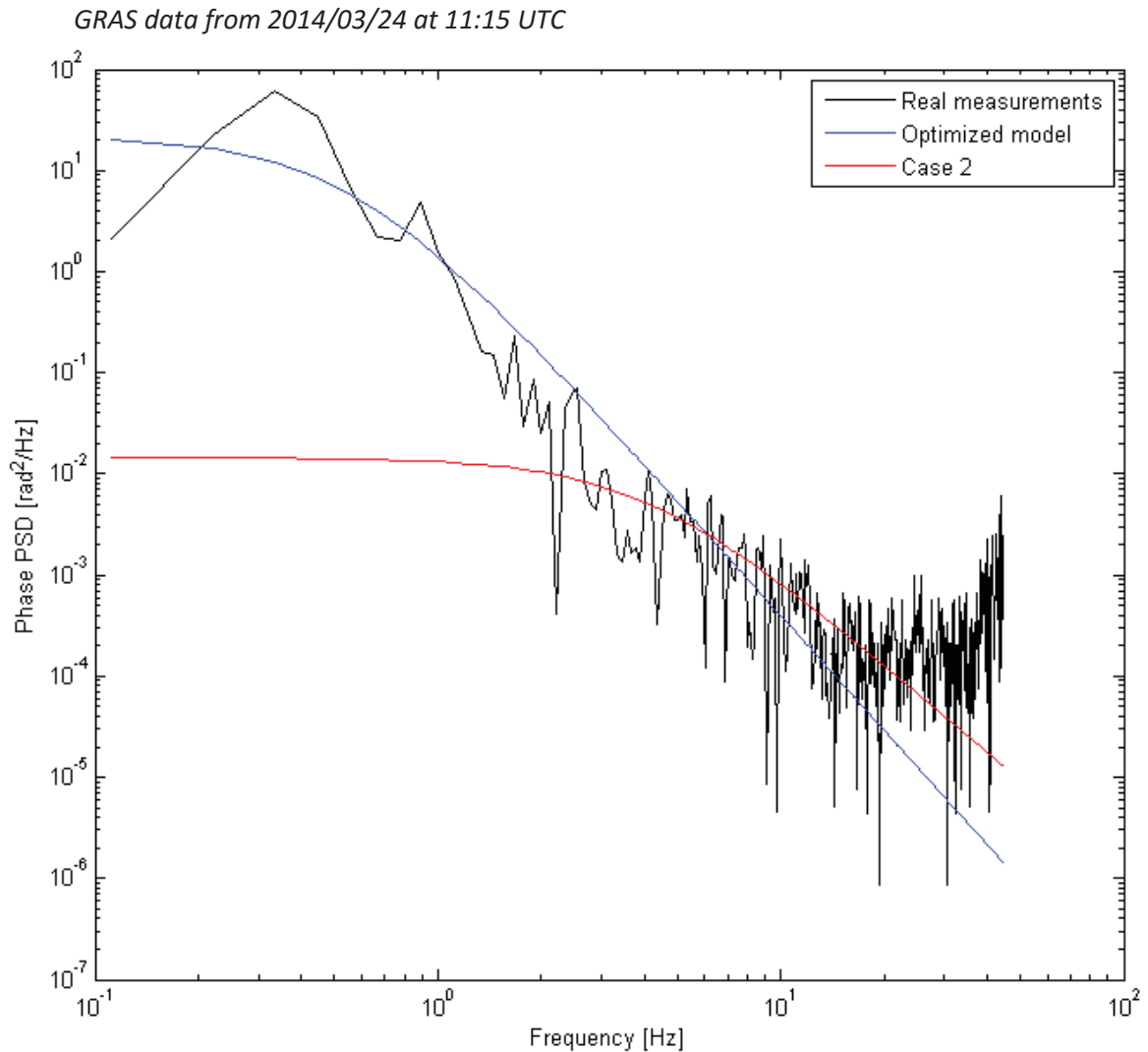
Figure 4.19. Optimization of the amplitude model from 2014/03/21 at 22:21 UTC

Above a good example of a well optimized scintillation model can be seen. Its MSE is almost 3 times lower than case 2. The magnitude is well preserved as well as the slope of the PSD. The characteristic fits entirely the data measurements, significant Improvement is visible.

The last example results of the optimization process are presented in the Table 4.28, while their plots are shown in the Figure 4.20.

T_ϕ	$f_{0\phi}$	p_ϕ	$\text{MSE}\left[\left(\frac{\text{rad}^2}{\text{Hz}}\right)^2\right]$	Case 2 $\text{MSE}\left[\left(\frac{\text{rad}^2}{\text{Hz}}\right)^2\right]$
2.2979	0.5503	3.7597	21.2350	24.8426

Table 4.28. Optimization results for the phase from 2014/03/24 at 11:15 UTC



This is an unusual example, since the phase scintillation event has a high magnitude at the beginning of the signal and much lower at the end. The case 2 model characteristic is far too low to fit this scintillation. After calculating the optimal coefficients of the model, the characteristic is well fitted in terms of the magnitude, roll-off frequency and the PSD slope as well. However it does not reflect the last part of the signal properly.

4.4.1 Distinction of the final parameters

In this section, selection of the final parameters was conducted, in order to conclude with one preferable set of parameters for both amplitude and phase scintillation model. Firstly, histograms were used to reveal the distribution of values for each parameter. The histograms are based on 18 different values of each parameter, obtained in the optimization process, described in the previous section. Each of these coefficients has a particular set of values which ranged between 0.001 to 6. By analyzing its distribution, the dominant range of values

occurrence could be distinguished. Additionally, the normal density function was included to determine how the obtained values are located in reference to the mean value.

Amplitude histograms for each of the coefficient are shown in the Figures 4.21-4.23.

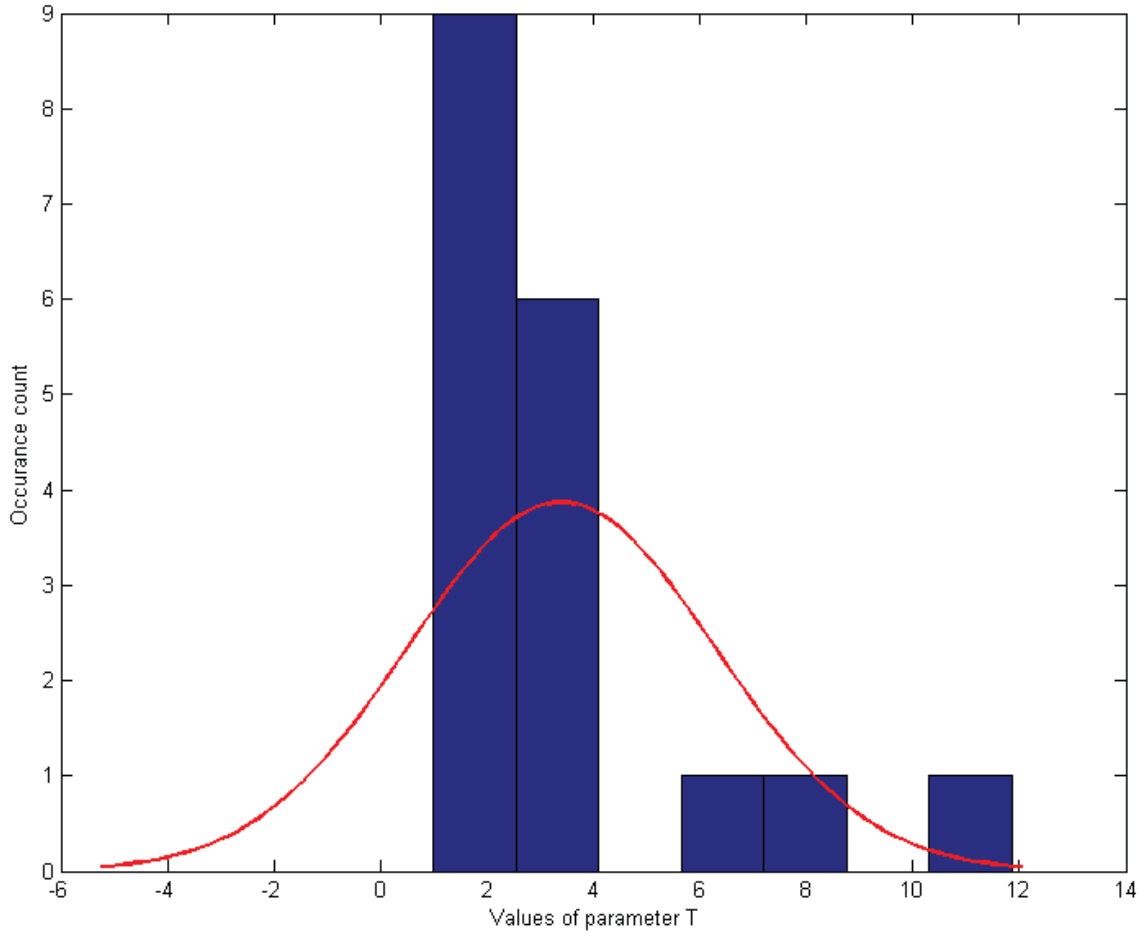


Figure 4.21. T_χ parameter histogram and normal density function for amplitude

The figure above indicates the dominant range of values, which lays in between 0.9 and 2.5. Half of the calculated coefficients are positioned in that interval. Wide distribution of the values can be seen in the plot. Moreover, the standard deviation for this particular histogram is equal to 2.88, which also implicates the widespread distribution. Thus, the final value of the T_χ parameter was calculated by mean value of the dominant range and is equal to 1.59.

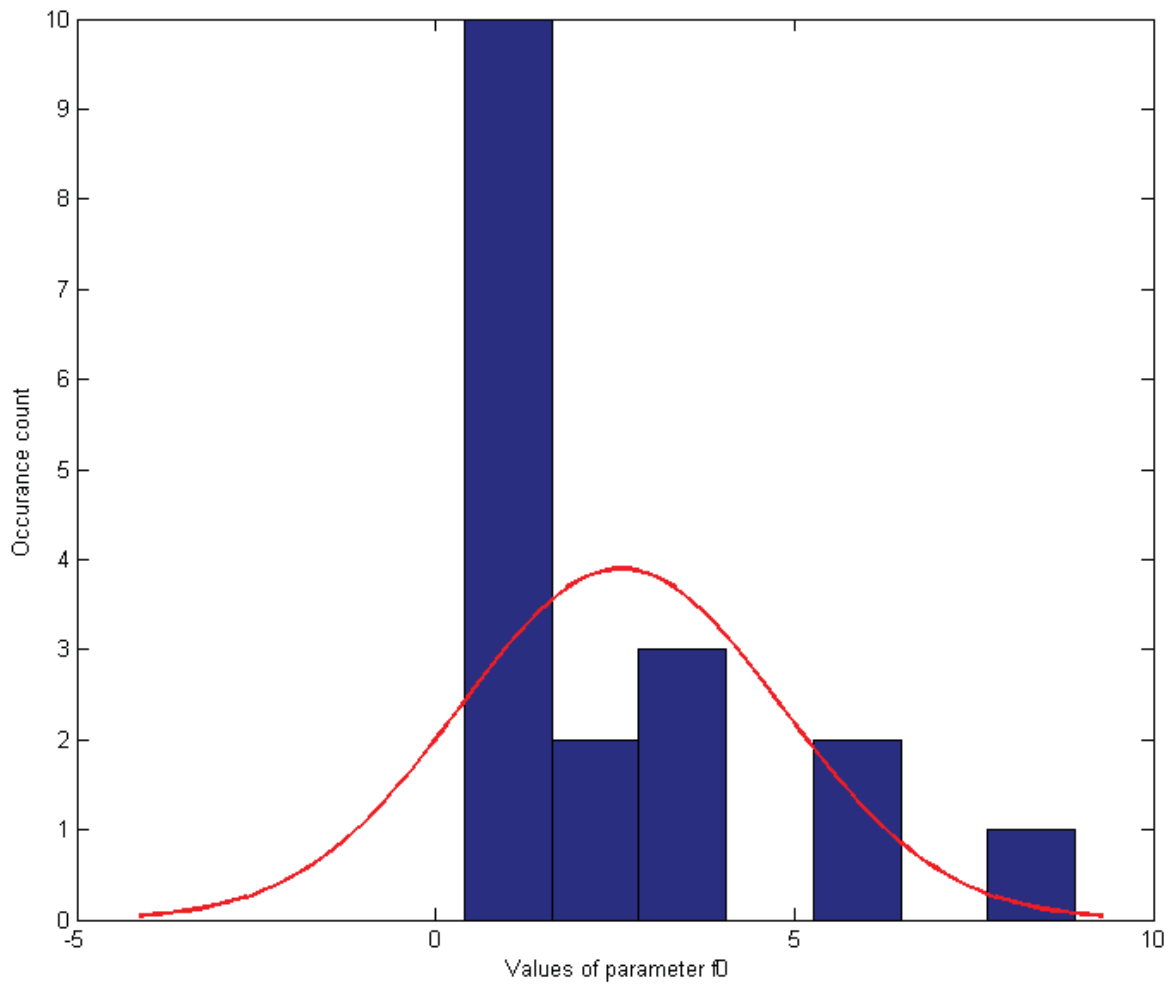


Figure 4.22. $f_{0\chi}$ parameter histogram and normal density function for amplitude

Similarly to the previous parameter, a dominant interval can be distinguished. Its values occur between 0.7 and 1.6 and the standard deviation in this case is equal to 2.24. Therefore, the calculation process (mean value) was conducted for the highest bar and gave the result of 1.13.

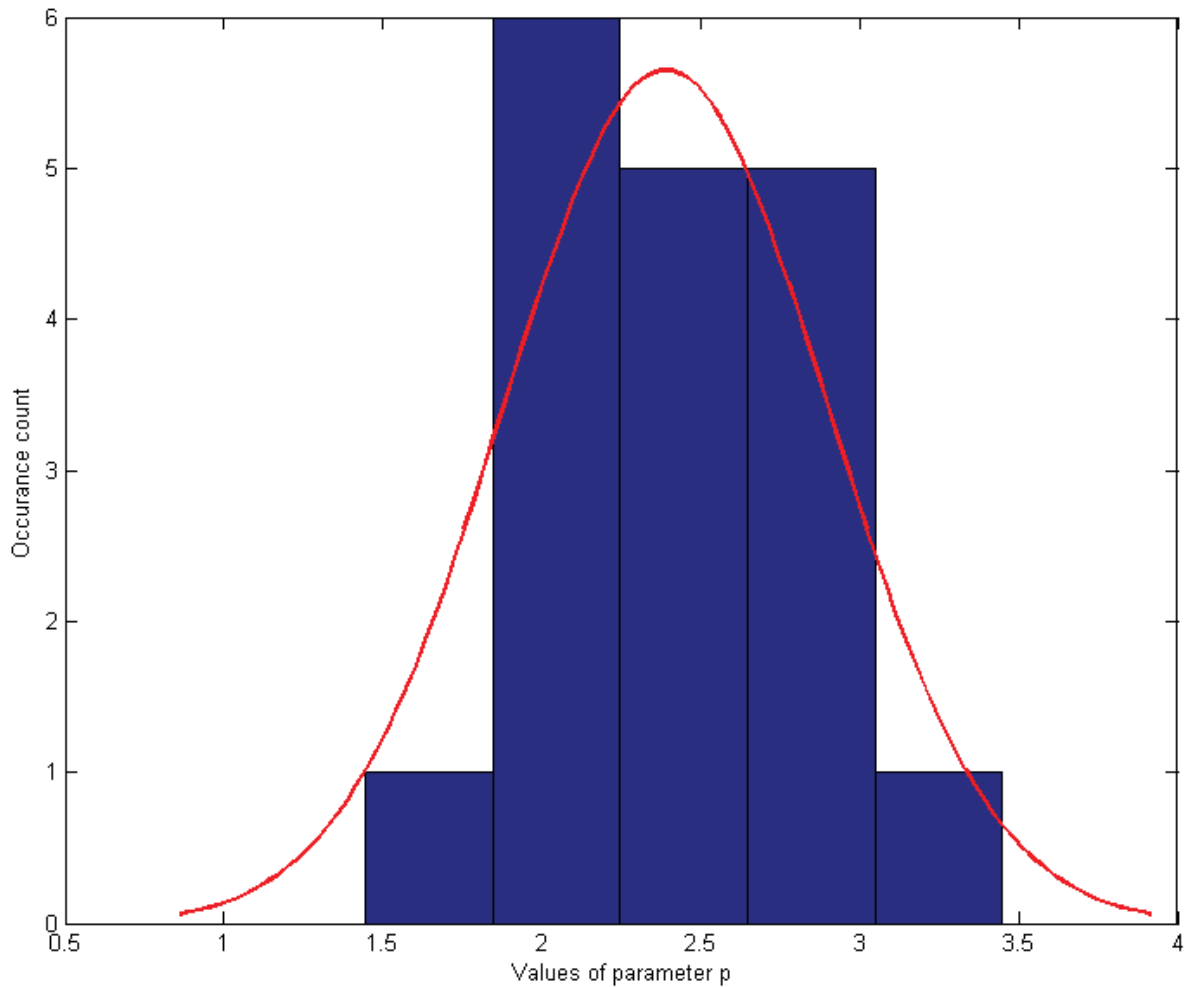


Figure 4.23. p_χ parameter histogram and normal density function for amplitude

In the last parameter of the amplitude, the values are equally distributed, which is shown on the histogram. Same number of results occurred for few different intervals. In this case the standard deviation was equal to 0.51, which confirms narrow distribution of coefficients. In order to choose the final value of the p_χ parameter, the mean value was calculated using all of the 18 coefficients, as there was no dominant range in this particular situation. Resulted value is equal to 2.39.

Phase histograms are presented in the Figures 4.24-4.26.

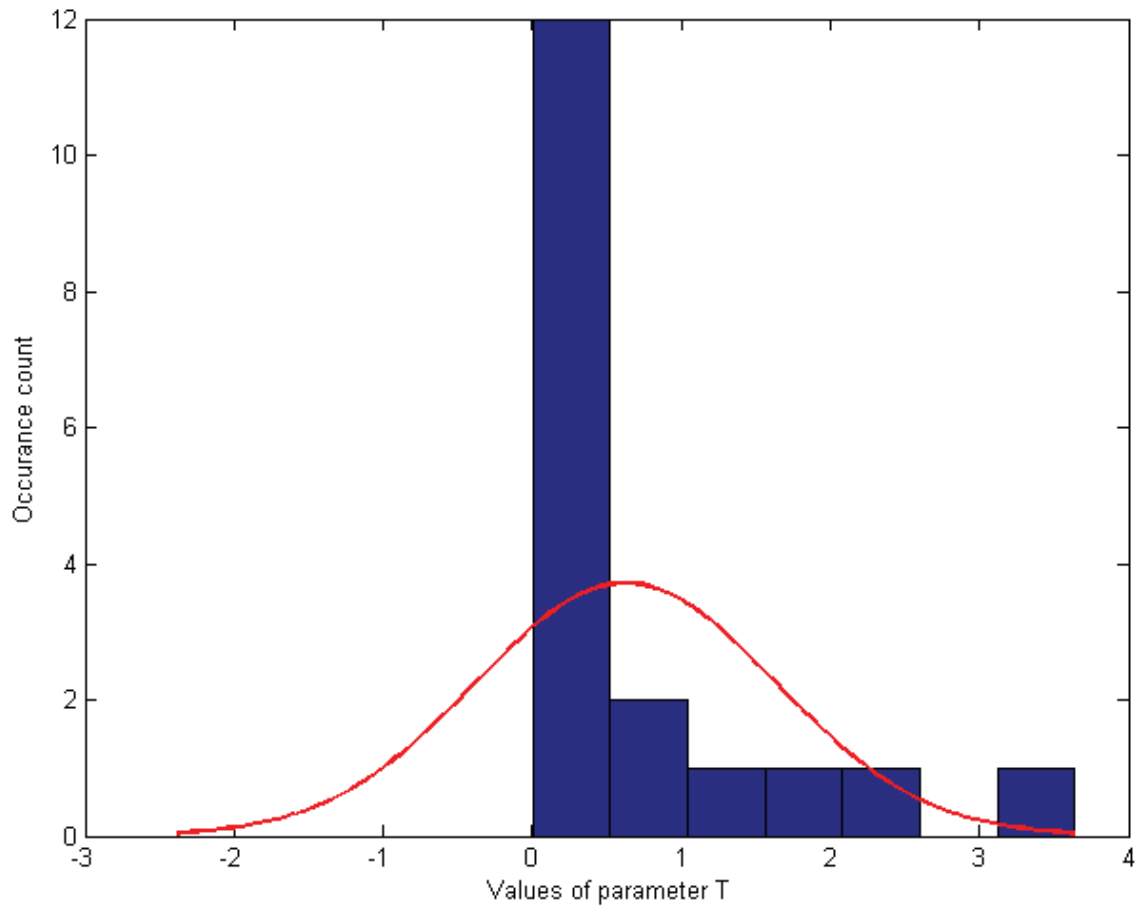


Figure 4.24. T_ϕ parameter histogram and normal density function for phase

For the T_ϕ parameter of the phase model, dominant interval can be easily distinguished. It contains 12 calculated coefficients and ranges between 0.001 - 0.5. Standard deviation is equal to 1.004. Since most of the results are located in the mentioned interval, the mean value was calculated of those results and was equal to 0.088.

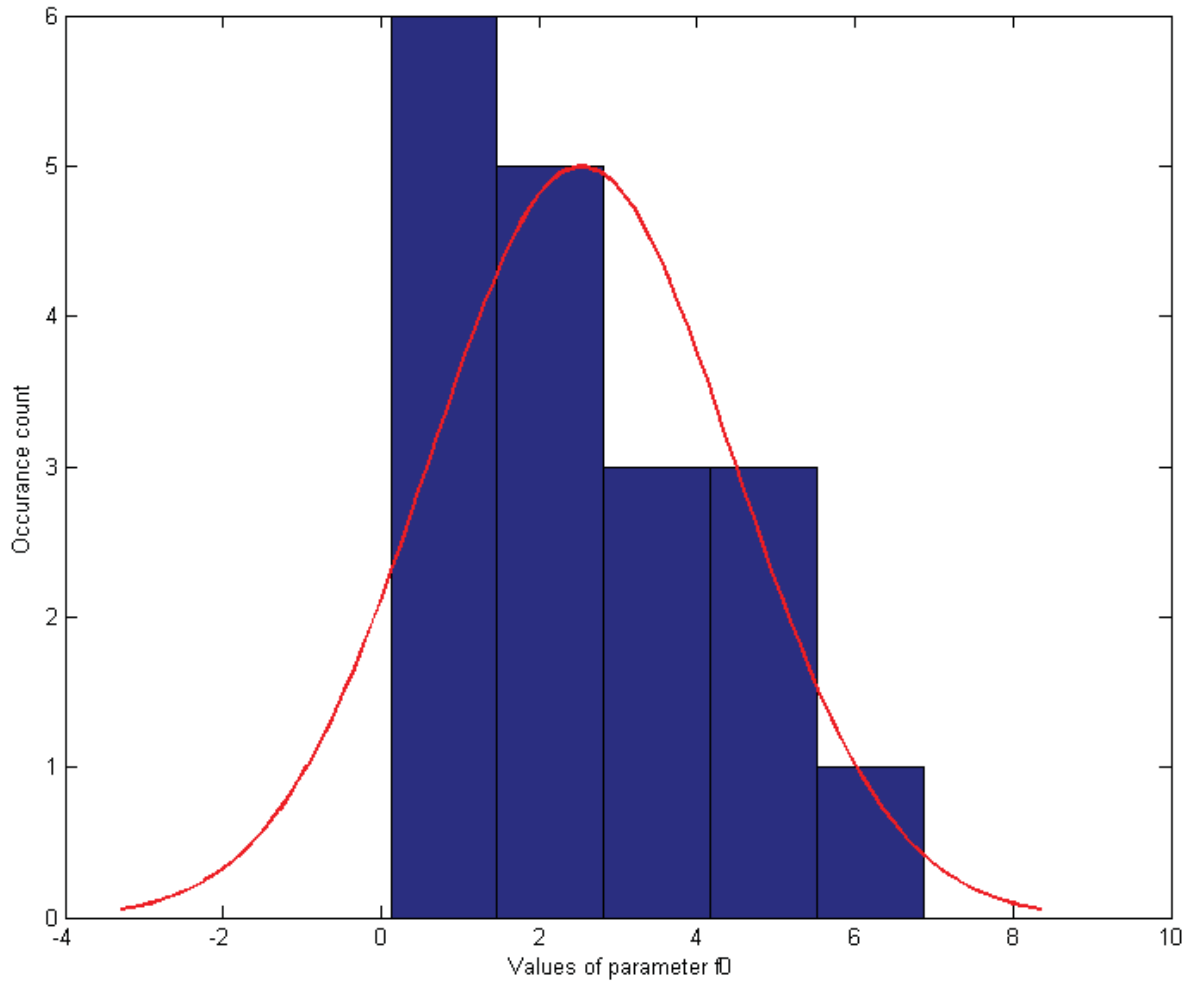


Figure 4.25. $f_{0\phi}$ parameter histogram and normal density function for phase

As it can be seen in the figure above, there is no range, which dominate significantly among others. Even though the standard deviation was equal to 1.94, the same number of coefficients occurred in few different intervals. Thus, the mean value was calculated using 18 parameters and resulted in the value of 2.54.

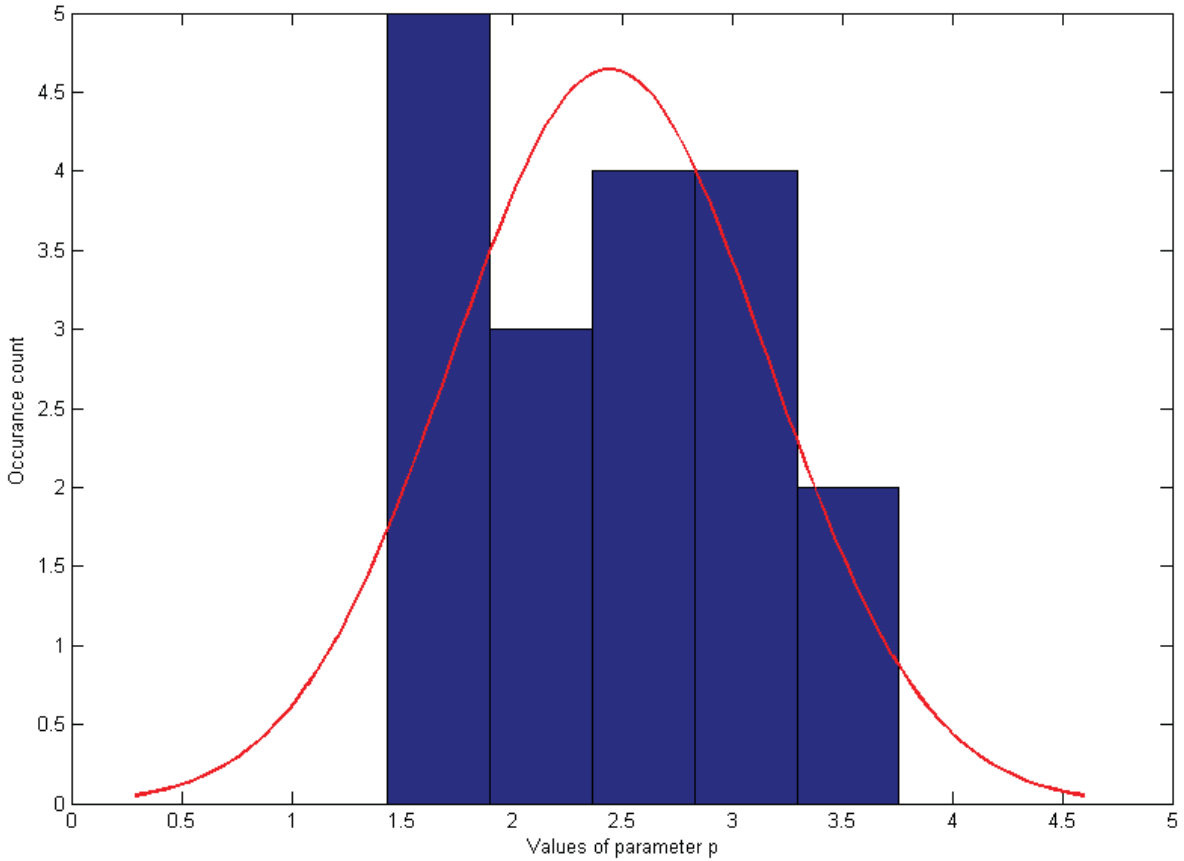


Figure 4.26. p_ϕ parameter histogram and normal density function for phase

In the last histogram another equally distributed range of parameters can be seen with standard deviation equal to 0.718. Consequently the mean value was deducted from all the coefficients and gave the result of 2.44.

Furthermore, performance of the amplitude and phase model with obtained parameters was verified. Verification was performed based on 18 scintillation events, which have been used in previous section. Resulted MSE compared to RUAG model cases of the amplitude are shown in the Table 4.29.

GRAS data time (UTC)	MSE for Case 1 [dB^2]	MSE for Case 2 [dB^2]	MSE for Case 3 [dB^2]	MSE for final param. [dB^2]
2014-03-20 06:51	419.6769	116.8341	148.7221	58.0629
2014-03-20 06:51	277.8616	60.0655	77.4798	94.9862
2014-03-20 06:51	524.7358	165.3354	208.6672	51.1659
2014-03-15, 14:21	436.4410	132.6377	156.9182	44.2531
2014-03-17, 00:06	507.6462	162.1943	193.9576	34.4204
2014-03-15, 04:15	401.0681	121.9034	144.6069	68.1659
2014-03-16, 20:42	701.4453	259.8360	315.7227	53.3116

2014-03-18, 18:18	320.6824	83.7924	105.2525	97.168
2014-03-19, 06:15	326.2058	89.5575	104.8518	86.7848
2014-03-19, 06:15	368.5320	106.5323	124.6554	68.3480
2014-03-19, 09:39	1017.5	456.2001	534.1493	129.2002
2014-03-19, 21:21	674.7217	258.2823	299.7953	40.7136
2014-03-19, 23:03	362.4111	107.5855	130.0454	90.7519
2014-03-20, 22:42	499.5257	163.8500	193.9823	40.3469
2014-03-21, 03:51	677.9732	246.7120	301.2491	57.2424
2014-03-21, 22:21	362.4859	94.8693	115.3730	55.0697
2014-03-24, 11:15	754.4338	288.1247	346.6114	52.3651
2014-03-24, 16:15	663.4786	255.8493	303.0054	69.3154

Table 4.29. Verification process of the final results for the amplitude

The table above shows that the selected parameters for amplitude model are correct and improved mathematical description of the scintillation. Significant progression can be seen, comparing to the cases obtained before. In most of the examples, the MSE values are few times smaller.

Results for the verification process of the phase are presented in the Table 4.30.

GRAS data time (UTC)	MSE for Case 1 $\left[\left(\frac{\text{rad}^2}{\text{Hz}}\right)^2\right]$	MSE for Case 2 $\left[\left(\frac{\text{rad}^2}{\text{Hz}}\right)^2\right]$	MSE for Case 3 $\left[\left(\frac{\text{rad}^2}{\text{Hz}}\right)^2\right]$	MSE for final param. $\left[\left(\frac{\text{rad}^2}{\text{Hz}}\right)^2\right]$
2014-03-20 06:51	2.5493	1.2846e-05	0.0837	1.1419e-05
2014-03-20 06:51	1.0200	3.7034e-05	0.0497	3.7023e-05
2014-03-20 06:51	2.5494	5.4088e-06	0.0837	1.2317e-06
2014-03-15, 14:21	2.1200	4.4143e-05	0.0723	1.9711e-05
2014-03-17, 00:06	0.9516	0.0024	0.0474	0.0015
2014-03-15, 04:15	0.9530	0.0040	0.0497	0.0021
2014-03-16, 20:42	1.6952	1.6389e-04	0.0628	1.1359e-04
2014-03-18, 18:18	0.7716	0.0102	0.0440	0.0094
2014-03-19, 06:15	0.5860	0.0172	0.0441	0.0140
2014-03-19, 06:15	0.9793	0.0333	0.0676	0.0204
2014-03-19, 09:39	0.6719	0.0917	0.0854	0.0678
2014-03-19, 21:21	2.5473	4.0701e-05	0.0833	2.7347e-05
2014-03-19, 23:03	0.8602	0.2009	0.2246	0.1913
2014-03-20, 22:42	0.9825	0.0050	0.0516	0.0026
2014-03-21, 03:51	1.4937	7.9729e-05	0.0582	6.1647e-05
2014-03-21, 22:21	1.1156	0.0111	0.0550	0.0062
2014-03-24, 11:15	25.1175	24.8426	24.2207	23.7516

2014-03-24, 16:15	2.546	1.9135e-04	0.0831	1.4505e-04
-------------------	-------	------------	--------	------------

Table 4.30. Verification process of the final results for the phase

The optimized model implemented in all the examples gave better results than other cases. MSE values are lower, which can be considered as improved results. Obtained parameters for the phase model can be acknowledged as appropriate.

5. Conclusions

The optimization method presented in this paper, allowed to obtain more accurate sets of parameters for scintillation model, comparing to the ones used as a starting point, provided by RUAG Space company. According to the statistical analysis conducted after optimization process, distinction of preferable set for the amplitude and phase model was possible.

In order to distinguish the most accurate set of parameters, distribution of the parameters was analyzed. Afterwards, mean value was calculated for each of selected dataset, which is thoroughly described in section 4.4.1 of the thesis. Results were obtained separately for amplitude and phase model, for each model coefficient.

The resulting sets for amplitude and phase are presented in the Table 5.1 and 5.2.

T_χ	$f_{0\chi}$	p_χ
1.59	1.13	2.39

Table 5.1. Resulting set of parameters for the amplitude

T_ϕ	$f_{0\phi}$	p_ϕ
0.088	2.54	2.44

Table 5.2. Resulting set of parameters for the phase

The main goal of this project was to provide as precise as possible mathematical model, in order to improve the retrieval of atmospheric profiles in RO. It is shown in the paper, that the model has been successfully optimized, which improved its accuracy.

6. Future work

Performed optimization, has precipitated to increased model accuracy, thus it is adequate and refined. However, data measurements may still contain noises other than ionospheric scintillations, which also affects the GPS signal dynamics. To discover this phenomena, a further research is required.

Moreover, in the thesis only L1 signal has been studied. In the future work, other frequencies of the GPS signal can be investigated for scintillation occurrence. It might also be examined, how the data obtained from equatorial regions differs from the ones at polar latitudes and how the model behaves.

Furthermore, the optimization process can be performed using different attempts. Worth of considering would be solving this problem with neural network or genetic algorithms. These methods are widely used in linear, as well as nonlinear problems. As a result pareto efficiency may be indicated.

Reference list

- [1] Paul M. Kintner, Jr. (2008, Feb. 21) *A Beginner's Guide to Space Weather and GPS* [Online]. Available: https://gps.ece.cornell.edu/SpaceWeatherIntro_ed2_10-31-06_ed.pdf
- [2] RUAG Space AB, "Simulating scintillation data," P-GOS-NOT-0115-SE, Issue 1, May 2001.
- [3] K. C. Yeh and C.-H. Liu, "Radio wave scintillations in the ionosphere," *Proc. IEEE*, vol. 70, no. 4, pp. 324–360, Apr. 1982.
- [4] RUAG Space AB, "Scintillation effects on signal dynamics," P-GOS-NOT-0077-SE, Issue 2, 15 Nov. 2001.
- [5] Satellite navigation. *Wikipedia*. Available: https://en.wikipedia.org/wiki/Satellite_navigation. Accessed Feb. 17, 2016.
- [6] J. J. Spilker Jr., Bradford W. Parkinson, "Overview Of GPS Operation And Design," *Global Positioning System: Theory and Applications*, Vol. 1. American Institute of Aeronautics and Astronautics, 1996.
- [7] E. R. Kursinski, G. A. Hajj, J. T. Schofield, R. P. Linfield, and K. R. Hardy, "Observing Earth's atmosphere with radio occultation measurements using the Global Positioning System," *J. Geophys. Res. Atmospheres*, vol. 102, no. D19, pp. 23429–23465, Oct. 1997.
- [8] *GPS Radio Occultation*. [Online]. Available: <http://www.cosmic.ucar.edu/ro.html>. Accessed: Oct. 22, 2015.
- [9] *An Introduction to GPS Radio Occultation and Surface Reflection*. [Online]. Available: <http://www.geooptics.com/GeoOptics/RO.html>. Accessed: Oct. 22, 2015.
- [10] C. Rocken, Y.-H. Kuo, S. V. Sokolovskiy, and R. A. Anthes, "The ROCSAT-3/COSMIC mission and applications of GPS radio occultation data to weather and climate," *Proceedings of SPIE - The International Society for Optical Engineering, Remote Sensing Applications of the Global Positioning System*, Vol. 5661, pp. 1-12 (2004).
- [11] L. Cucurull, J. C. Derber, R. Treadon, and R. J. Purser, "Assimilation of Global Positioning System Radio Occultation Observations into NCEP's Global Data Assimilation System," *Mon. Weather Rev.*, vol. 135, no. 9, pp. 3174–3193, Sep. 2007.
- [12] "Effect of Ionospheric Scintillations on GNSS - A White Paper," SBAS Ionospheric Working Group, Nov. 2010. Available: http://waas.stanford.edu/papers/IWG/sbas_iono_scintillations_exec_summ.pdf
- [13] Strangeways, H. J., Y.-H. Ho, M. H. O. Aquino, Z. G. Elmas, H. A. Marques, J. F. G. Monico, and H. A. Silva (2011), On determining spectral parameters, tracking jitter, and GPS positioning improvement by scintillation mitigation, *Radio Sci.*, 46, RS0D15, doi:10.1029/2010RS004575.
- [14] S. Priyadarshi, "A Review of Ionospheric Scintillation Models," *Surv. Geophys.*, vol. 36, no. 2, pp. 295–324, 2015.
- [15] Y. Béniguel, B. Forte, S. M. Radicella, H. J. Strangeways, V. E. Gherm, and N. N. Zernov, "Scintillations effects on satellite to Earth links for telecommunication and navigation purposes," *Ann. Geophys.*, vol. 47, no. 2–3 Sup., Dec. 2004.

- [16] C. L. Rino, "A power law phase screen model for ionospheric scintillation: 1. Weak scatter," *Radio Sci.*, vol. 14, no. 6, pp. 1135–1145, Nov. 1979.
- [17] M. B. R. Bagge, "Spaceborne GNSS Radio Occultation Instrumentation for Operational Applications," *Proc. ION GPS 2000*, 2000.
- [18] M. Bonnedal, J. Christensen, A. Carlström, and A. Berg, "Metop-GRAS in-orbit instrument performance," *GPS Solut.*, vol. 14, no. 1, pp. 109–120, Sep. 2009.
- [19] "MetOp overview," *European Space Agency*. [Online]. Available: http://www.esa.int/Our_Activities/Observing_the_Earth/MetOp_overview. Accessed: Oct. 22, 2015.
- [20] RUAG Space AB, "Description of GRAS Level 1, 2 and 3 Formats," U-GNSS-NOT-1091200-RSE, Issue 2, Apr. 2015.
- [21] "Power spectra." [Online]. Available: <https://www.wavemetrics.com/products/igorpro/dataanalysis/signalprocessing/powerspectra.htm>. Accessed: May 26, 2016.
- [22] "Understanding FFTs and Windowing", National Instruments [Online]. Available: <http://www.ni.com/white-paper/4844/en/>. Accessed: Oct. 26, 2015.
- [23] Beniguel, Yannick, "Characterisation of equatorial scintillations For transionospheric links," Proceedings of the 13th International Technical Meeting of the Satellite Division of The Institute of Navigation (ION GPS 2000), Salt Lake City, UT, September 2000, pp. 688-695
- [24] Y. Jiao, Y. T. Morton, S. Taylor, and W. Pelgrum, "Characterization of high-latitude ionospheric scintillation of GPS signals," *Radio Sci.*, vol. 48, no. 6, p. 2013RS005259, Nov. 2013.
- [25] M. van de Kamp, P. S. Cannon, and M. Terkildsen, "Effect of the ionosphere on defocusing of space-based radars: IONOSPHERIC DEFOCUSING OF SBR," *Radio Sci.*, vol. 44, no. 1, Feb. 2009.
- [26] Least squares. Wikipedia. Available: https://en.wikipedia.org/wiki/Least_squares. Accessed Oct. 3, 2015.
- [27] *Find minimum of unconstrained multivariable function using derivative-free method - MATLAB fminsearch*. MathWorks documentation. [Online]. Available: <http://www.mathworks.com/help/matlab/ref/fminsearch.html>. Accessed: Nov. 6, 2015.
- [28] *Find minimum of unconstrained multivariable function - MATLAB fminunc*. MathWorks documentation. [Online]. Available: <http://www.mathworks.com/help/optim/ug/fminunc.html>. Accessed: Nov. 6, 2015.